Development, Production, and Characterization of Plastic Hypodermic Needles

A Thesis
Presented to
The Academic Faculty

By

Jeffrey Taylor Stellman

In Partial Fulfillment
Of the Requirements for the Degree
Master of Science in Mechanical Engineering

Georgia Institute of Technology

August, 2009

Development, Production, and Characterization of Plastic Hypodermic Needles

Approved by:

Dr. Jonathan S. Colton
George W. Woodruff School of Mechanical Engineering
Georgia Institute of Technology

Dr. Rudolph L. Gleason
George W. Woodruff School of Mechanical Engineering
Georgia Institute of Technology

Dr. Mark R. Prausnitz
School of Chemical and Biomolecular Engineering
Georgia Institute of Technology

Date Approved: May 7, 2009

"You know my methods. Apply them."

Sir Arthur Conan Doyle

The Sign of Four (1890), Chapter 6

ACKNOWLEDGMENTS

I would like to thank my advisor, Dr. Colton, and all the support staff at Georgia Tech for the guidance and support they provided during my research. In addition, I would like to thank both Dr. Prausnitz and Dr. Gleason for taking the time to serve on my thesis committee.

In addition, this project was funded in part by U.S. Centers for Disease Control and Prevention SBIR Contract 2000-2008-M-26726 to Tribofilm Research Inc. with Dr. Mark Papania of the CDC as project contact. Also thanks to Vinay Sahkrani of TriboFilm Research Inc. for coating a portion of the needles with their TriboGlide coating, and Trevor Nye and Andreas Aeschlimann of SSB Technology PTY LTD for providing their plastic needles. Their assistance is greatly appreciated.

Finally, I would like to thank all of my friends and family, who gave me support and encouragement during my time at Georgia Tech.

TABLE OF CONTENTS

LIST OF TABLES

LIST OF FIGURES

LIST OF SYMBOLS

A	Cross Sectional Area
A_c	Crack Surface Area
A_t	Tip Contact Area
A_n	Needle Cross Sectional Area
d	Outer Needle Diameter
E	Modulus of Elasticity
E_f	Modulus of Elasticity of Film
F_c	Cutting Force
F_f	Frictional Force
F_i	Force to Initiate Crack
F_p	Force to Propagate Crack
F_s	Stiffness Force
F_{total}	Total penetration force
G_p	Puncture Resistance
G_c	Tear Resistance
I	Moment of Inertia
K	Effective Length Factor
L	Length
N	Normal Force
P_{cr}	Critical Buckling Load
r	Radius of Gyration
r_i	Inner Radius
r_o	Outer Radius
r_t	Tip Radius
t_f	Thickness of Film
t_{field}	Numerical Field Thickness Constant
α	Tip Angle
δW	Work Input
δA	Change in Surface Area
μ	Coefficient of Friction
σ_y	Compressive Yield Strength

SUMMARY

Every year billions of injections are given worldwide. A significant portion of these injections are considered to be unsafe, particularly in developing countries. Needles are used for injections into multiple patients without proper sterilization. This reuse results in the spread of blood born pathogens, such as Hepatitis A, Hepatitis B, and HIV. Most reuse can be attributed to unsafe disposal practices, as many regions in developing countries lack the equipment necessary to properly dispose of hypodermic needles. One viable solution to this problem is a plastic hypodermic needle. Reuse of a plastic needle could easily be prevented by something as common as a match ($600°C < T < 800°C$), as the melting point of most polymers is below 300°C.

This thesis describes the injection molding process used to fabricate plastic hypodermic needles. The fabrication of the molds that are used to make the needles is a key issue, as the complexity and small scale of the details of a hypodermic tip are difficult to replicate. It was found that a forging process using a copper wire as the material being forged produces the best replication of a hypodermic needle. The copper insert is malleable enough to conform to the tip of a hypodermic needle. Copper also is able to withstand the pressures and temperatures that occur within a mold during the injection molding process.

In order to determine the effectiveness of plastic needles, testing is conducted to measure needle properties and to compare steel and plastic hypodermic needles. Penetration tests are conducted through a thin polyurethane film. Eight types of needles are used including five steel varieties and three plastic varieties. Four gages of needles

are tested to determine the importance of needle diameter in penetration force. The eight types of needles are coated with four types of lubricant as well as tested without any lubricant to determine the role that coefficient of friction has in penetration force. In addition, the tip radii of the needles are measured to determine the importance tip radius has on penetration force.

In addition to penetration testing, buckling tests are conducted. The results of the buckling tests are used to determine a suitable range of material properties for plastic hypodermic needles. Multiple penetration tests also are conducted to represent the withdrawal of medicine from a vial before injection. For these tests a single needle is penetrated into the polyurethane film three times in succession. These tests determine the resistance that both the needle nips and needle lubrication have to multiple penetrations.

The results show that tip radius, needle diameter, tip angle, and coefficient of friction have a direct effect on the penetration force. Lower penetration forces are achieved through minimizing all three parameters. The results of the penetration tests are used to develop an equation that predicts the penetration force of a hypodermic needle through the polyurethane film based on the following variables - coefficient of friction, tip radius, and needle diameter. The result of the buckling tests show that a minimum value for the elastic modulus of a hypodermic needle material is 8 GPa, which provides insight for material selection of the plastic hypodermic needles. The multiple penetration tests show that a needle is more likely damaged by mishandling than by penetration through polyurethane film.

The end result of the work done in this thesis is a 22 gage plastic needle which has a tip design that is created from a steel hypodermic needle. The needle is molded

using Vectra A130 liquid crystal polymer resin, and when lubricated using MDX4-4159 dispersion solution is capable of penetrating polyurethane film at an average penetration force of 1.62 N. This is lower than the penetration force of an uncoated 22 gage steel hypodermic needle (1.76 N), but remains higher than a factory lubricated steel hypodermic needle which is 0.60 N. With the progress made in this thesis, the parameters that affect penetration are better understood and can be optimized to create a plastic needle that is capable of penetration at levels that are comparable to lubricated steel needles.

CHAPTER 1

INTRODUCTION

This thesis studies the development and capabilities of plastic hypodermic needles to serve as replacements for steel hypodermic needles. The penetration of steel control and plastic hypodermic needles through skin mimics is studied experimentally to determine the effects of factors such as tip radius, needle diameter, tip angle and lubrication.

1.1 Background of hypodermic needles

It is estimated that annually over 12 billion injections are given worldwide using steel hypodermic needles [1]. Steel hypodermic needles are an excellent means of transdermal drug delivery because of their high strength, low cost, and ease of manufacture. There are problems, however, with the spread of blood-borne pathogens as a result of needle reuse. It has been estimated that in many developing countries unsafe injection practices (a single syringe and needle are used on multiple patients without proper sterilization) exceed 50% of all injections given [2]. While these numbers are staggering, the primary reason for needle reuse in developing countries is the cost of injections. In reality the cost of reuse of syringes is much more significant than the cost of sterile syringes. One model predicts 8-16 million hepatitis B virus, 2.3-4.7 million hepatitis C virus, and 80,000-160,000 human immunodeficiency virus infections result from unsafe injections every year [3], and accounted for 32%, 40%, and 5%, respectively, of new infections in 2000 [4]. The cost of these new infections is estimated to be $535

million per year in direct medical expenditures which translates to an additional $0.125 per injection for the estimated 4.3 billion injections given in developing countries [5]. This figure more than doubles the estimated cost of a new single-use needle and syringe.

Several devices are currently available that are intended to reduce the likelihood of needle reuse [6]. Manual-shielding needle and syringe combinations retract the needle into the syringe after use, which is effective at reducing reuse. An example of this is the Inviro Snap Safety Syringe, Inviro Medical Devices, Inc, Duluth, GA. These needle-syringe combinations do have a premium, however, as they are estimated to cost $0.54 per injection where as a conventional disposable needle and syringe is estimated to cost over 80% less at $0.10 per injection [7].

Another issue with steel needles is safe disposal practices. In order to be properly destroyed, medical waste must be incinerated at temperatures around 1500°C [8]. Many countries and regions lack the means necessary to produce and operate these incinerators, so the medical waste ends up in landfills. In one region of Pakistan a report showed that 26 out of 44 clinics studied were found to dump medical waste into local landfills instead of using incineration to destroy the waste. This leads to scavengers sifting through the landfills seeking medical waste. They collect the waste and resell it to clinics where it is reused [9]. These practices lead to both direct exposures to harmful waste and less obvious environmental contamination [10].

One viable solution to this problem is a plastic hypodermic needle. Plastic has the same advantages as steel in that it is low cost, easily manufactured on a large scale, and has the rigidity necessary to withstand the forces of an injection. It also has advantages that steel needles are not able to offer. A plastic needle can be blunted and sealed with

heat from a common match (600°C < T < 800°C) because most plastics have melting points below 300°C. The blunted needles easily could be collected and disposed of or recycled with virtually no risk of reuse or contamination. Previous studies [11-13] showed that plastic needles can be manufactured that are capable of penetration. The primary focus of this thesis is to expand upon previous efforts to characterize hypodermic needle penetrations, explore the influence that different lubricants have on both steel and plastic needles' ability to penetrate, develop a needle that is capable of penetration on levels comparable to steel needles, and create guidelines for future needle and lubrication developments.

1.2 Description of needles and lubricants tested

This study involves the use of steel needles from two different manufacturers. Steel needles from Inviro Medical Devices, Inc., Lawrenceville, GA, are tested in three gages: 18, 22, and 30. Steel needles from Myco Medical, Cary, NC, are tested in two gages: 22 and 26. The 18 gage needles have a nominal outer diameter of 1.27 mm, an inner diameter of 0.8382 mm, and a cannula length of 38.1 mm. The 22 gage needles have a nominal outer diameter of 0.7112 mm, an inner diameter of 0.3937 mm, and a cannula length of 25.4 mm. The 26 gage needles have a nominal outer diameter of 0.4572 mm, an inner diameter of 0.2413 mm, and a cannula length of 12.7 mm. The 30 gage needles have a nominal outer diameter of 0.3048 mm, an inner diameter of 0.1524 mm, and a cannula length of 12.7 mm [14].

Two varieties of plastic needles are tested. One is manufactured by SS&B Technology Ltd., Australia. They are tested in both 25.4 mm and 16 mm cannula lengths and have outer and inner diameters corresponding to a standard 22 gage hypodermic

needle. These needles are made out of Ticona Vectra MT1300, Germany, (USP class VI) and include an integrated hub. The other variety of plastic needle is made at Georgia Institute of Technology. Their dimensions also correspond to a standard 25.4 mm length 22 gage hypodermic needle. These needles are made from Ticona Vectra A130. Vectra A130 is not a medical grade plastic; however there is a version, MT1310, which is mechanically and thermally similar to A130 and is USP Class VI compliant. Vectra A130 was used because of its availability. The manufacturing process of these needles is described at length later in this thesis. Both varieties of plastic are liquid crystal polymers. MT 1300 is unfilled whereas A130 is 30% glass filled. All needles used in experimentation are shown in Figure 1.

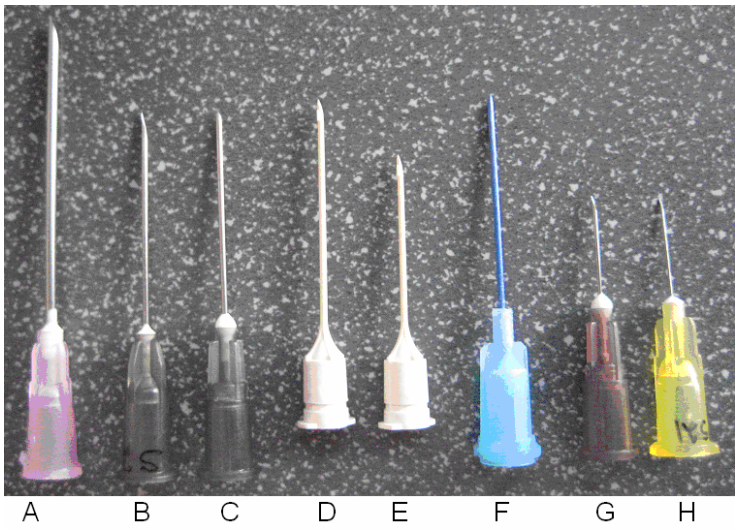

Figure 1 – Needles used during experimentation

A - 18 gage Inviro Medical, Steel

B - 22 gage Inviro Medical, Steel

C - 22 gage Myco Medical, Steel

D - 22 gage SS&B 25.4 mm, Vectra MT1300

E - 22 gage SS&B 16 mm, Vectra MT1300

F - 22 gage Georgia Tech, Vectra A130

G - 26 gage Myco Medical, Steel

H - 30 gage Inviro Medical, Steel

Three types of lubricant are tested in this study. The first lubricant is Dow Corning (Midland, Michigan) MDX4-4159, 50% silicone medical grade. This lubricant is used commercially on needles [15]. Needles are tested "as-received" directly from the two needle manufacturers with this lubricant. In addition to the "as-received" tests, MDX4-4159 was applied to bare needles in-house. The solution is reduced to a silicone concentration of <5% by means of dilution in 70% mineral spirits and 30% isopropyl alcohol, applied to the needles, and cured for three days at 70 C. This process was optimized in previous studies [11] and the application process is outlined in Appendix A. The second lubricant used is Dow Corning 360 Medical Fluid 1000 CST, which is silicone oil with a viscosity of 1000 cSt. The oil is simply wiped onto the needles before penetration. This procedure is outlined in Appendix A. The third lubricant tested is an experimental silicone-free immobilized lubricant system based on perfluoropolyether (PFPE) chemistry and using atmospheric plasma technology referred to as TriboGlide [16]. TriboGlide is developed by TriboFilm Research, Inc., Raleigh, NC. In addition to the three types of lubricant, needles are tested without any treatment, i.e. bare.

1.3 Objective

The purpose of this thesis is to further explore the abilities of plastic hypodermic needles. Steel and plastic needles are studied by both penetration tests through polyurethane film and by buckling tests. Penetration factors, such as frictional forces, cutting forces and penetration forces, are analyzed and conclusions are drawn as to the effect of needle parameters on these factors. The parameters studied are needle material, diameter, tip angle, tip radius, and lubricant. Upon conclusion of the tests, the findings

are developed into a model relating all of the needle characteristics to the force of penetration necessary for the combinations of needle types and lubricants. In addition a plastic needle that is able to penetrate with low forces is produced, as are recommendations for design improvements.

1.4 Thesis outline

Chapter 2 explains the fabrication of the plastic hypodermic needles. The mold fabrication process is outlined including mold design, mold manufacture, tip insert design, and tip insert manufacture. The injection molding of the needles is described, including the material selection and moldability of various resins.

Chapter 3 describes the experimental setup and test methods used for both the penetration and the buckling tests. In addition, methods for estimating tip characteristics of the needles and coefficients of friction of the various lubricants are described. The different characteristics of the needles that are studied are discussed.

Chapter 4 presents the results from the experimentation including physical penetration and buckling tests, finite element models of needle buckling, analysis of buckling equations, tip characteristic estimation, and coefficient of friction tests.

Chapter 5 interprets the results of the experiments. Needle penetration is broken down into stages and analyzed. A model relating tip radius, diameter, material, and lubrication is developed and the importance of these characteristics on separate stages of penetration is discussed.

Chapter 6 presents a summary of work done, conclusions developed during the course of experimentation, and recommendations for future work.

CHAPTER 2

FABRICATION OF PLASTIC HYPODERMIC NEEDLE

Chapter 2 describes the development and fabrication of the plastic needles made at Georgia Tech. In addition, an alternate technique used by SS&B Technologies is described.

2.1 Needle mold housing

The needle mold is designed for a Sumitomo 75-ton injection-molding machine, located in the hibay of the MARC building on Georgia Tech's Atlanta campus. This machine is shown in Figure 2.

Figure 2 - Sumitomo 75-ton injection molding machine

The mold must fit within the existing mold's housings, which have approximate dimensions of 5.6 inches by 6.8 inches. A mold is designed to fit within the housing and is shown in Figure 3.

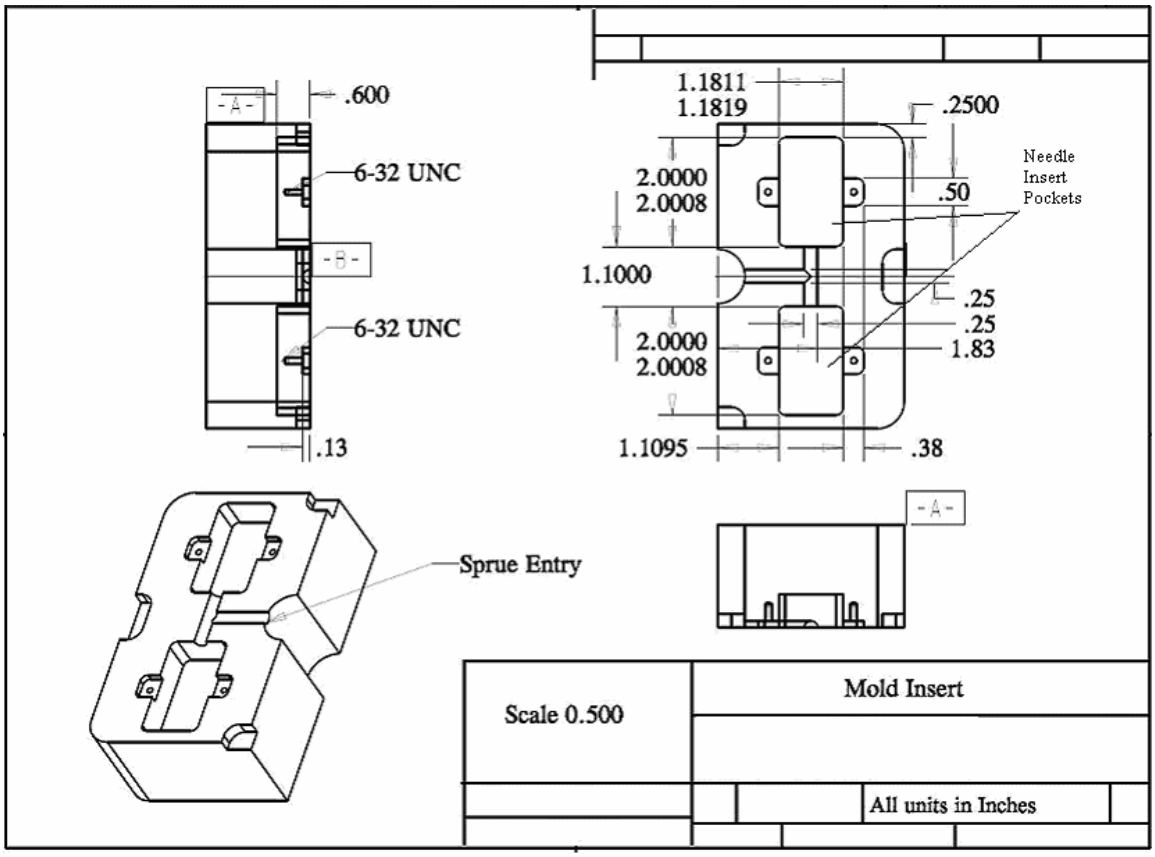

Figure 3 - Large mold insert

As shown in Figure 3, the large mold insert does not have any of the geometries necessary to make the needles themselves. The large insert has smaller pockets that house the molds for the needles. The portion of the mold that contains the needle geometry is easily interchangeable so that only a small portion of the entire mold need be modified to change the needle design. It is also important to note that four "portions" are necessary to fill the mold housing. Two "portions" are made following the design specified in Figure 3. These "portions" are positioned so that the faces with the pockets for the needle mold inserts are in contact and all edges are aligned when they are within

the injection-molding machine. Two more "portions" are made without the pockets for the needle mold inserts. These solid blocks act as fillers to occupy the void in the bottom half of the provided housing. The sprue enters at the center of the mold located at the 1.1 inch diameter cut-out seen in the bottom of the mold half.

2.2 Needle cannula mold insert design

2.2.1 Needle cannula mold description

A 22-gauge hypodermic needle with a nominal outside diameter of 0.7112 mm is produced. At the current stage of development the needles do not have hollow cores. While this does not allow for fluid flow testing to be conducted on the needles, it does allow for easier alterations of the needle design. As the central portion of the needle is structurally insignificant in comparison to its outer walls, its presence will not have a significant effect on the penetration force or the buckling load. Calculations shown in Chapter 4 show the difference in critical buckling load between a hollow and solid needle is around 20%. This is not enough to bring the needles tested buckling strength below the average penetration forces of those needles, so it is not considered significant. Methods exist to add a hollow core to injection molded devices, such as needles, using Gas Assisted Injection Molding [17]. These methods can be included in later stages of design. Modifications would require a gas inlet at the hub end of the needle then an exit channel at the tip of the needle. The mold also would require the proper fixtures for the gas connection.

The mold for the needle has two parts. The needle cavity is split equally in half along the length of the shaft. The depth of the channel is 0.3556 mm, or the outer radius of the needle. This channel is created in both parts of the mold so that when they are

aligned in the injection molding machine a cylindrical cavity with a 0.7112 mm diameter and a 50.8 mm length is created. This forms the shaft (cannula) of the needle. The mold maintains alignment by two 6.35 mm dowel pins.

2.2.2 Needle cannula mold manufacturing process

The key component to the needle cannula mold is the 0.7112 mm channel that runs down the length of each half. The alignment of one channel with the other is essential to produce a round needle. To ensure proper alignment the following steps were taken during the machining of the molds.

First, a single piece of steel, which is slightly larger than the two halves of the mold when they are aligned lengthwise, is clamped into the milling machine with the bottom face parallel to the table of the mill. The top surface is faced off to a proper thickness of 15.24 mm. This ensures that the top plane of the piece is perfectly parallel with the cutting plane of the machine. The channel, which forms the needle cannula, then is cut down the length of the piece using a 0.7112 mm ball end mill. The channel is cut to a depth of 0.3556 mm, which is equivalent to the radius of the needle being manufactures.

With the channel in place, the single long piece is cut in half perpendicular to the channel. A piece of 0.7112 mm diameter steel wire is set into one of the channels and the other mold half is placed on top of the mold with the wire such that both channels and the wire are concentric. This ensures proper alignment. The two pieces then are clamped together with the wire still in place, and the final outer dimensions of the molds are machined. The holes for the alignment pins are drilled and reamed with the wire still in position. Finally, threaded holes are added to each half so that the molds can be removed

easily from the larger mold insert. Detailed drawings of the mold halves, including units in inches, are shown in Figures 4, 5, 6, 7, and 8 below.

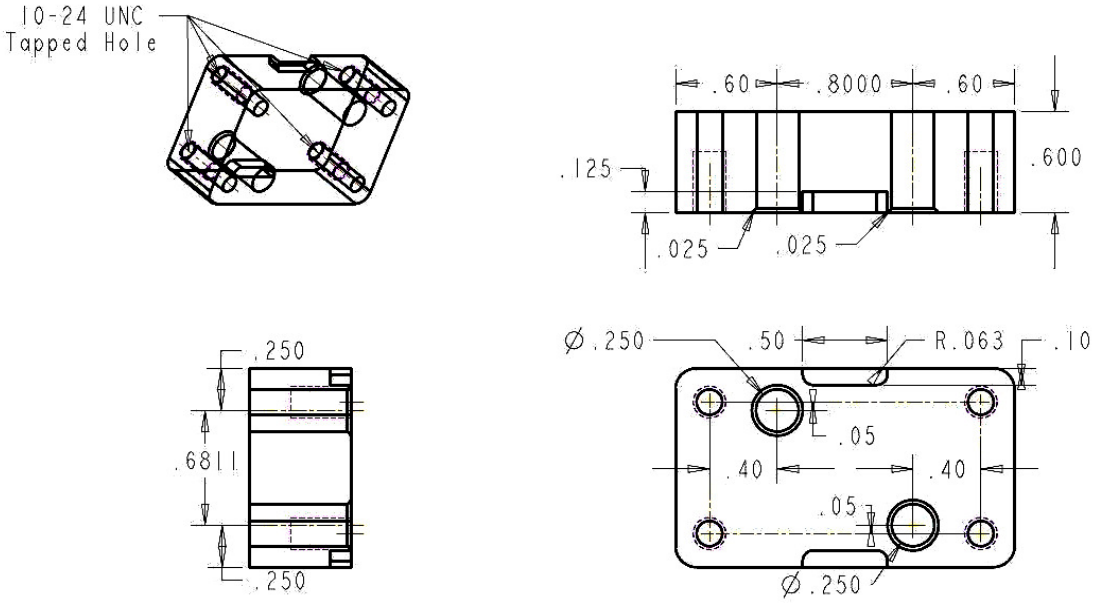

Figure 4 - Needle mold drawing left half

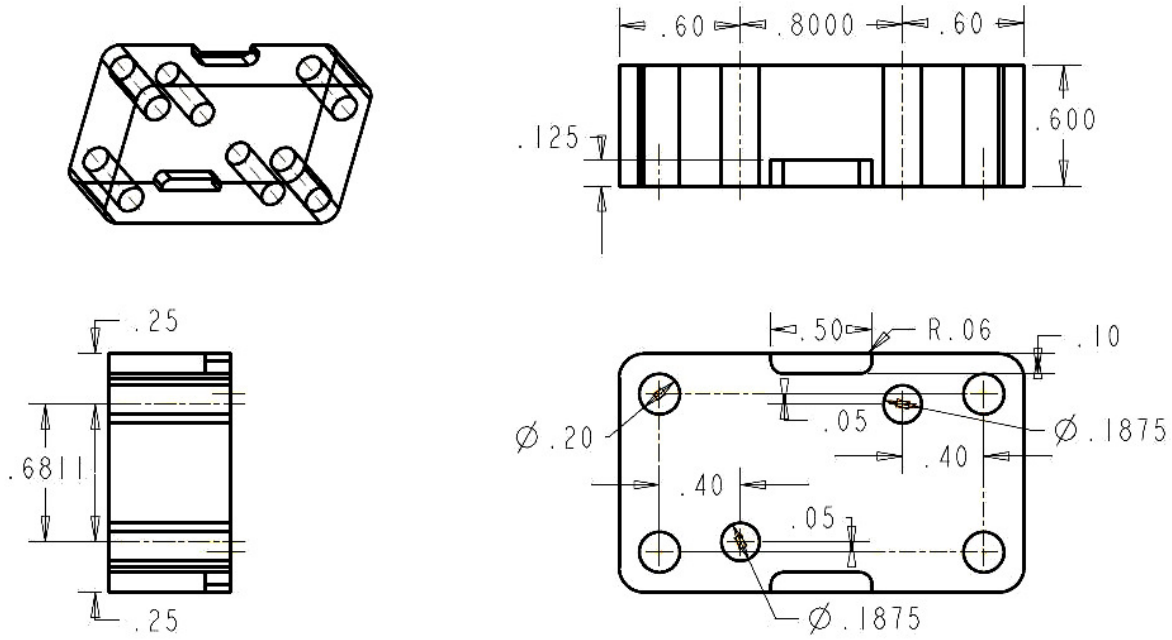

Figure 5 - Needle mold drawing right half

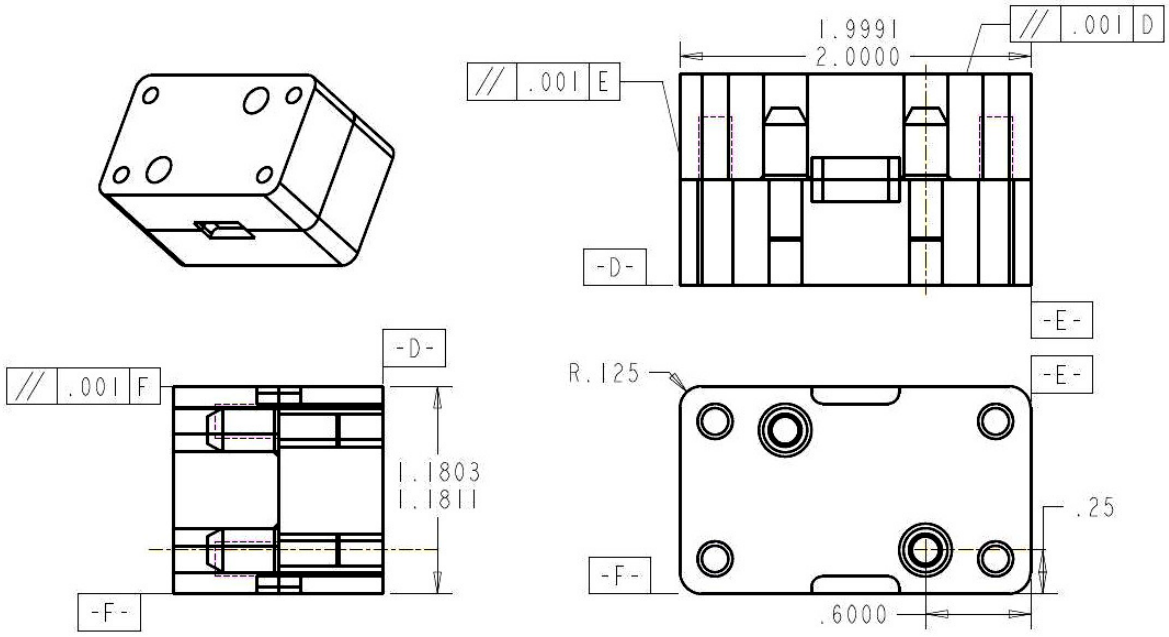

Figure 6 - Needle mold assembly drawing

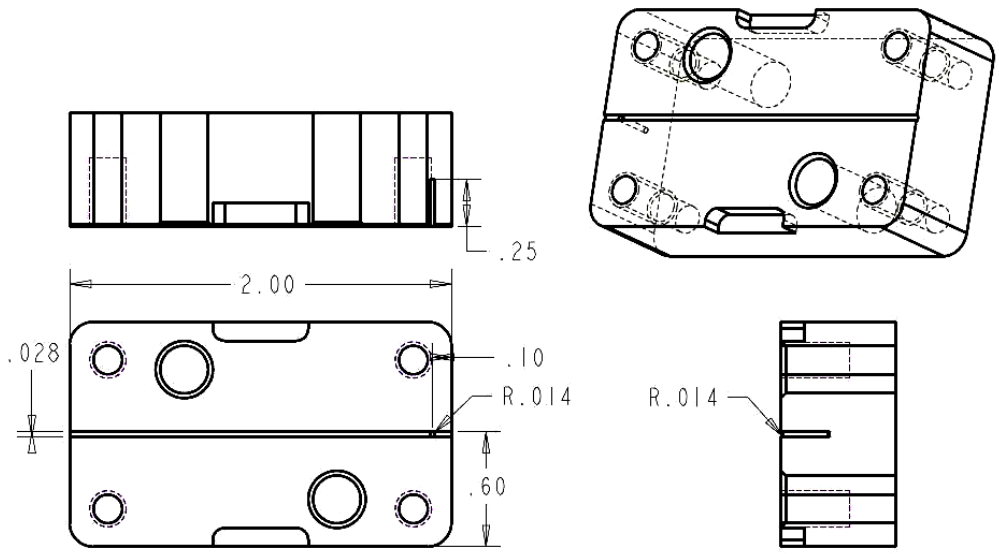

Figure 7 - Left mold channel

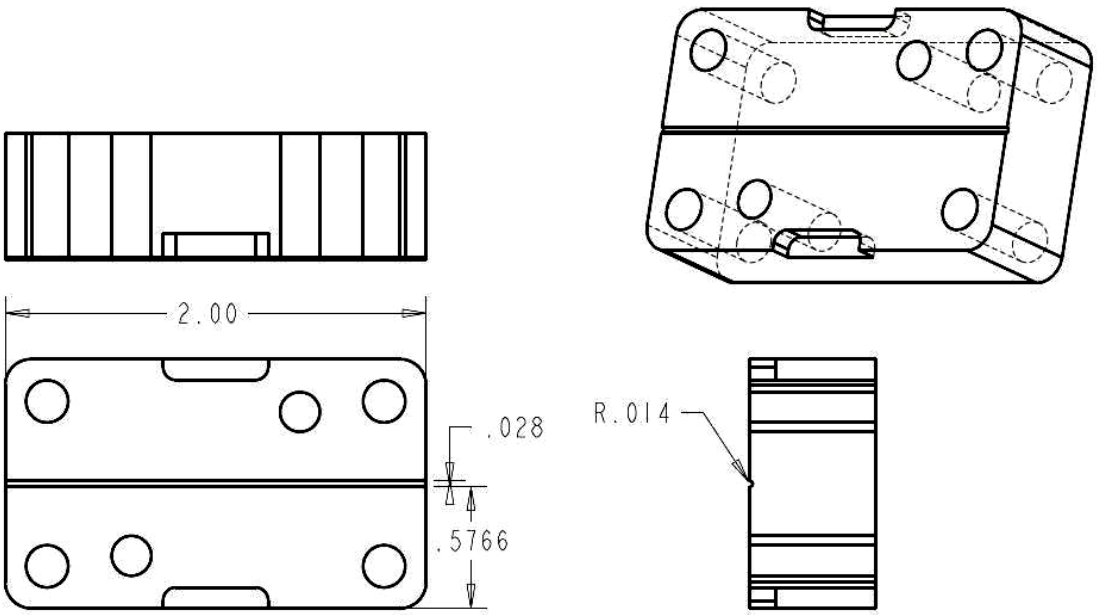

Figure 8 - Right mold channel

The mold inserts nest in the pockets of the large mold insert, which is positioned in the mold housing. When in place, this assembly forms the cannula of the plastic hypodermic needle. The total assembly loaded in the injection-molding machine is shown in Figure 9 below.

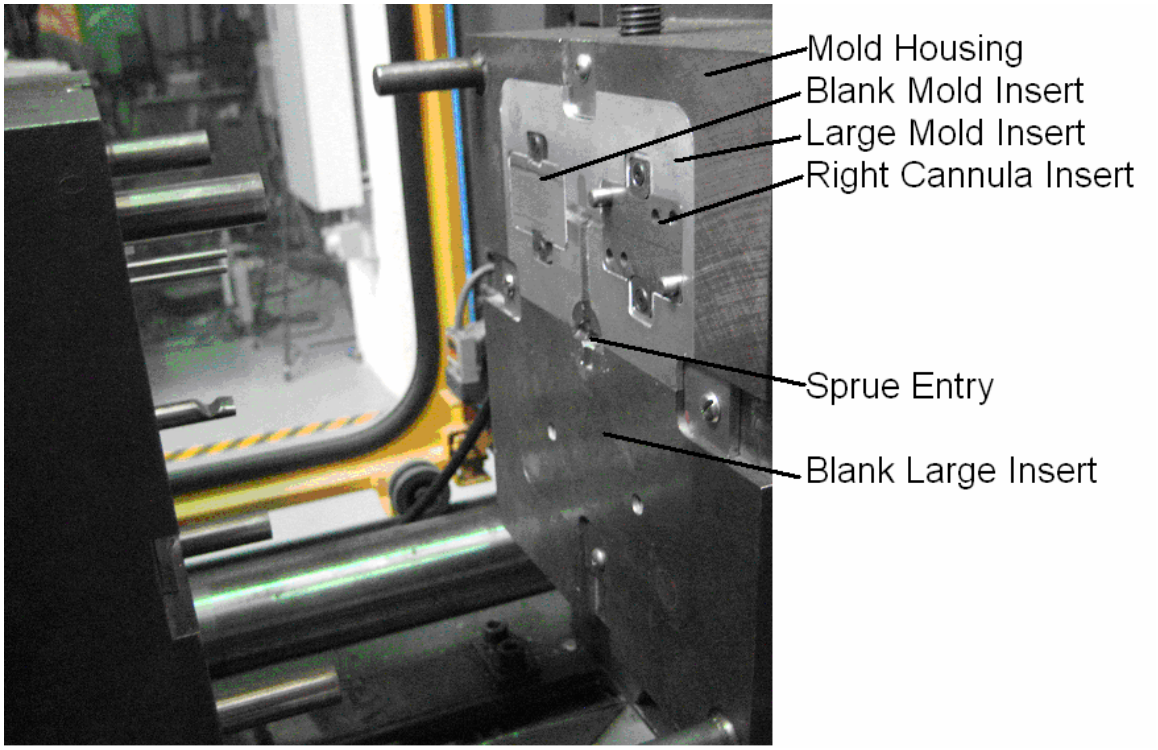

Figure 9 - Needle mold assembly

2.2.3 Alternate cannula mold insert manufacturing considerations

Ball end mills were the best choice for this stage of development because of their low cost and ease of manufacturing the molds. At only $14.15 per tool [18], the expense is small compared to the other methods explored. Before the final design was developed, however, several alternative methods of fabrication were considered. The first of these is sink electrical discharge machining (EDM), which is a very accurate method of machining and would be a viable application for machining the small intricacies present in the needle molds. This method, however, is quite costly. A single mold was estimated to cost around $1,000, which does not include the cost of the tip insert fabrication discussed in section 2.3. In addition, it proved difficult to find a machine shop able to make the molds within the desired time frame. Wire EDM also was considered, however it is also a costly process. One mold was estimated to cost approximately $400. In

addition, due to the small size and length of the hole required, it was likely that the wire used in the machining process would stray off center and produce a cavity that was not straight, which in turn would produce crooked needles. The idea of casting the molds based on a machined steel replicate of the needle design also was explored; however it proved to be very difficult to achieve the level of replication desired.

2.3 Needle tip insert fabrication

2.3.1 Needle tip insert description

The needle tip insert is designed to rest in the 0.7112 mm channel. It contains the details that produce the plastic needle tip. For this study, needles of the same tip geometry are compared, so the tip insert is an inverse replication of a 22 gage Inviro Medical steel hypodermic needle. The tip insert is the most crucial portion of the needle mold. It controls the sharpness of the needle, which directly affects the penetration force.

The insert is made out of 0.8636 mm copper wire and has a length of approximately 12.7 mm. It contains an impression of a 22 gage Inviro Medical steel hypodermic needle. It is bonded to the needle cannula mold using ethyl cyanoacrylate glue. An image of a needle tip insert magnified 60 times is shown in Figure 10.

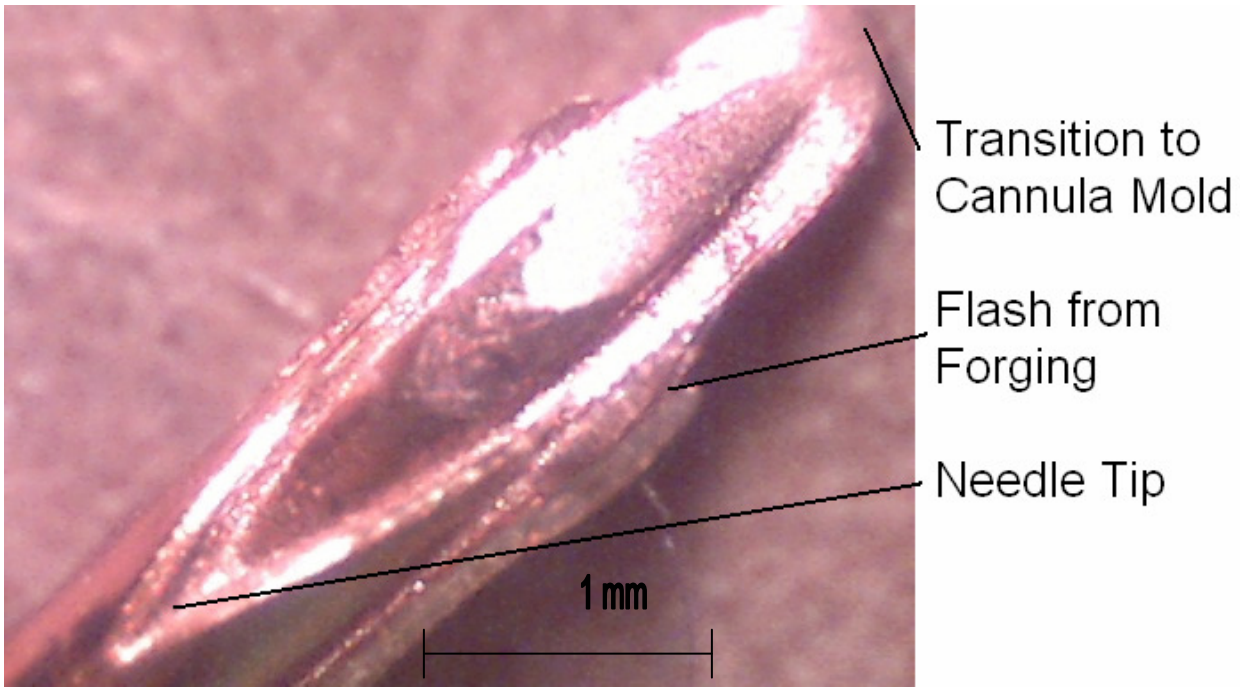

Figure 10 - Copper needle tip insert, 60x magnification

2.3.2 Needle tip insert fabrication

The needle tip insert fabrication is a forging process that begins with a piece of copper wire with a length around 12.7 mm and a diameter of 0.8636 mm. Wire with a slightly larger diameter than that of the mold is chosen so that the insert will completely conform to the channel of the needle cannula mold. This ensures there are no gaps between the surfaces of the cannula mold and the copper tip insert, thus eliminating flash around the tips of the needles during injection molding. Using a larger diameter wire than the diameter of the cannula channel also increases the pressure on the copper insert during the forging process and improves the detail of the impression. Wire of the same diameter was tried; however problems arose with accurately replicating the machined surfaces of the cannula mold in the copper insert.

The first step is to grind the wire to an angle of approximately 30°. Several angles were tested and it was found that cutting the wire to 30° allows for best replication

of all portions of the needle. Shallower angles allow excellent replication of the tip, however many of the other details of the needle are not replicated. Also, a significant amount of waste material from the copper insert is left in the needle cannula mold, which produces unwanted voids in the plastic needles. The waste material is difficult to remove without affecting the quality of the rest of the tip insert. Cutting the wire at a steeper angle does not allow replication of the entire length of the needle tip. It typically produces a gap in the mold where the tip insert blends into the cannula, which creates a lip on the plastic needle where a smooth transition should occur. This lip greatly increases penetration force of the plastic needles.

Once the wire is ground to a 30° angle, it is cut to a length of 12.7 mm and glued to the cannula mold using a drop of ethyl cyanoacrylate glue. The positioning of the tip insert is such that the 30° face of the insert forms a 150° angle with the lowest plane of the cannula channel. The insert and the channel are also concentric. An image of the insert placed in the channel is shown in Figure 11.

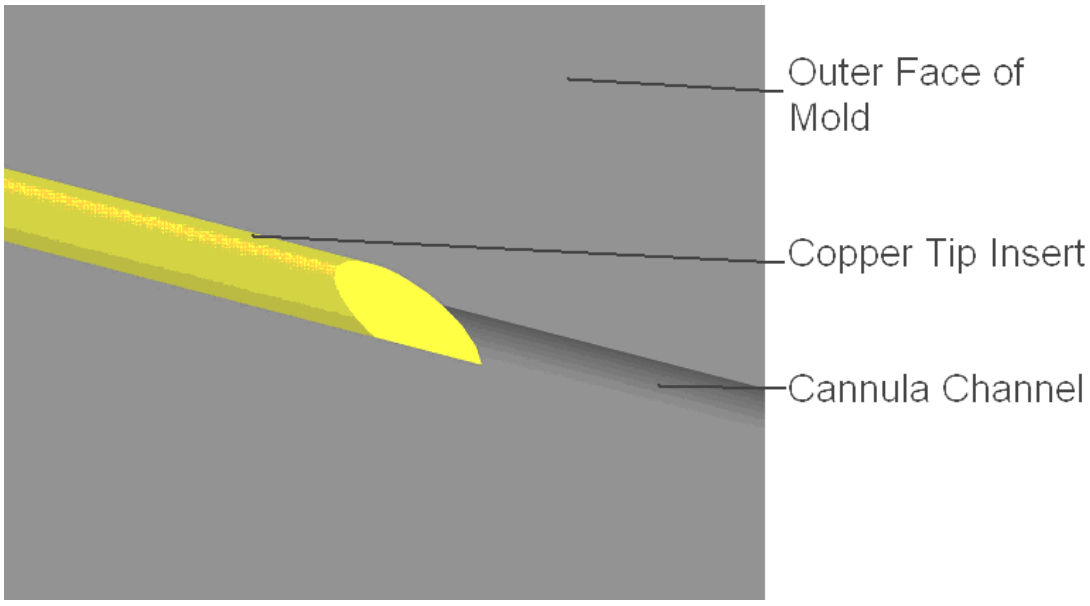

Figure 11 - Positioning of tip insert in cannula mold

Once the tip is in place on the cannula mold, the impression of the steel needle can be made into the copper insert. This forging process is conducted by positioning the steel needle on top of the copper insert. The two angled faces of the insert and the needle are in contact and roughly parallel. The transition point from the tip to the cannula on the needle is positioned directly above the same point on the mold assembly with the two points facing one another. The two points will not contact each other at this stage of the setup due to the geometry of the needle and mold. A cutaway view displaying the positioning is shown in Figure 12.

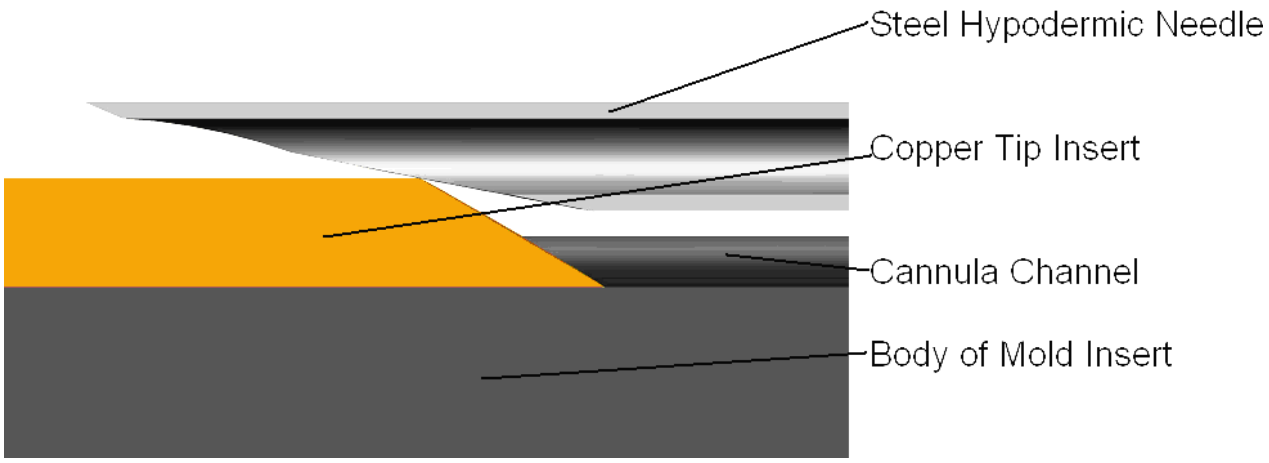

Figure 12 - Positioning of needle in cannula insert prior to forging

The needle pattern can now be replicated in the copper insert. To do this the other half of the cannula mold is aligned with the half containing the copper tip insert and the two halves are pressed together to the point of complete interfacial contact. A bench vice was used to compress the two mold halves, however any type of press would be acceptable as long as the pressure is not enough to deform the steel mold inserts. Once the halves are separated, the needle is removed and the impression of the needle is left in the copper insert. An image representing the forging of the copper insert is shown in

Figure 13. It is important to note that attempting to forge the same tip insert twice is very difficult and typically results in multiple impressions of the steel needle in the insert. This is an undesirable characteristic because the double impression will be replicated in the plastic needles which can cause reduced strength of the needles and increased penetration forces. All successful tip inserts were produced by the first forging. It is also important to note that this manufacturing method could be applied to virtually any tip design. The scope of this study was limited to manufacturing the needles successfully; however future studies could explore tip design optimization.

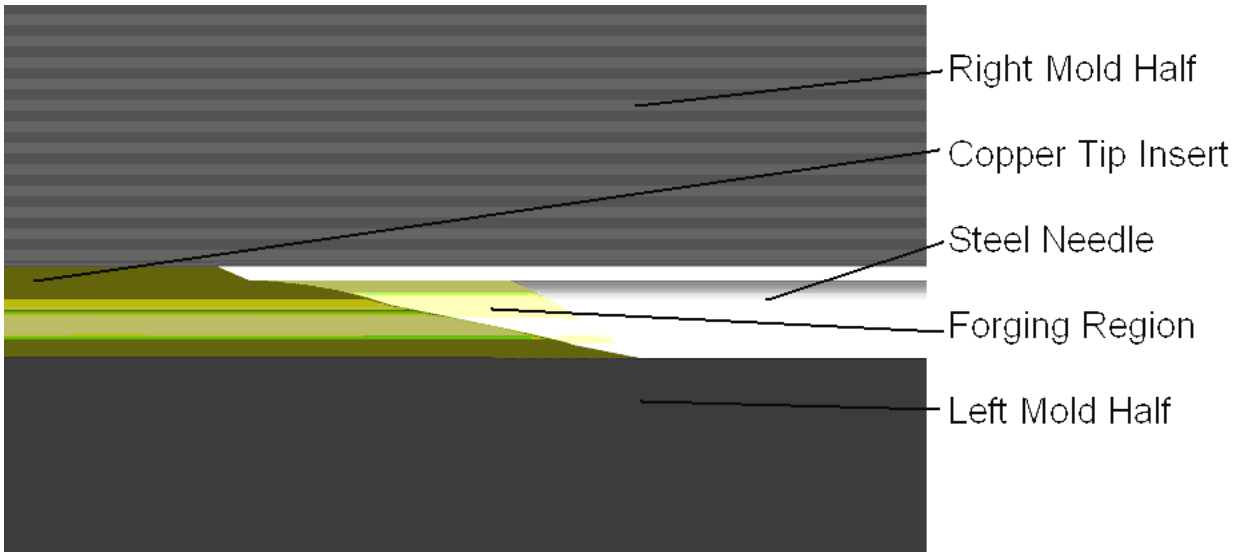

Figure 13 - Cutaway image of tip insert forging

2.3.3 Alternate tip insert manufacturing considerations

Many methods of manufacturing the tip insert were attempted before the final process was determined. Forging the tip insert proved to be the best method of producing a mold that was capable of producing sharp needles. It is inexpensive, easily done, and the materials necessary are readily available. Copper was chosen as the material for the insert because it is malleable enough to produce high quality likenesses of the object

being replicated. In addition it has a high enough melting temperature and strength to not be affected by the high temperatures and pressures that occur during injection molding. It is also known not to be hazardous to human health, so there are no concerns that arise from using it to make molds for hypodermic needles.

Forging the tip insert was attempted with other materials. Silver-, tin-, and lead-based solders were tried at one stage of design. They did prove to produce accurate replicates of the steel needle. These materials did not however prove to be able to withstand the environment within the mold during injection molding. Most began to melt and deform after a limited number of needles were made, which adversely affected the quality of the needle. There were also concerns about using lead to mold a device intended for human injections.

In addition to forging, casting of the tip insert was attempted. A steel casting mold was manufactured containing a 0.7112 mm channel, similar to the cannula mold insert. A steel needle was inserted into the channel to complete the mold for the tip insert. Various types of metal were used to determine which would produce the best replication however none of the trials proved successful. Upon multiple failed attempts, casting of the tip insert was not explored further.

Machining the tip insert is another fabrication method that was tested. Stainless steel and mild steel wires with diameters of 0.7112 mm were machined using micro end mills. Multiple tools of diameters ranging from 0.0254 mm to 0.127 mm were used to machine the wire. Many problems arose with the machining because it was very difficult to visualize what was occurring during the machining. It was difficult to determine the precise location of the material which leads to breakage of the tooling. With tooling of

that size, even slight variations in surface finish or flatness could cause the tool to break. In addition, the minimum possible tip radius is limited to the radius of the tool used. Even an ideally machined tip using a tool with a radius as small as 0.0254 mm exceeds the tip radius of a steel needle (which is estimated to be around 4.7 microns) and it is significantly more difficult to produce than a forged tip insert.

2.4 Materials tested for needle development

A wide range of resins were tested to make plastic hypodermic needles. Resin selection was based primarily upon the strength of the material. Stronger materials are more desirable for this application because a stronger needle will be less likely to buckle as a result of excessive loading. The elastic modulus of a conventional steel needle is around 200 GPa [19], where as the elastic modulus of one of the strongest available plastics, Ixef 1022, is 20 GPa [20]. The importance of the strength of the needle is discussed later in Chapter 5, but for this stage of material selection it is assumed that a strong plastic is necessary to manufacture a successful needle. A table of mechanical properties of resins considered in this study compared to steel can be seen in Table 1.

Table 1 - Mechanical properties of various resins

Material	Elastic Modulus (GPa)	Tensile Strength (MPa)
Steel [19]	190-210	460
Ixef 1022, 50% Glass Filled (PARA) [20]	20	280
KT-880-CF30, 30% Carbon Filled (PEEK) [21]	20.9	223
Vectra A130, 30% Glass Filled (LCP) [22]	15	190
Vectra MT1300, Unfilled (LCP) [22]	10.6	182
Lexan 3413R, 30% Glass Filled (PC) [23]	6.61	99
Durolon V-2500, Unfilled (PC) [24]	2.3	78
TOPAS 8007X10, Unfilled (COC) [25]	2.6	63
Polystyrene [26]	2.8 – 3.5	18.7 – 55.9

Of the resins listed in Table 1, all were used to fabricate plastic hypodermic needles except for the PEEK resin. PEEK was considered as a viable option, but the processing requirements exceeded the capabilities of the Sumitomo injection molding machine at Georgia Tech. The Vectra MT1300 was not used to fabricate the needles at Georgia Tech, however it was used to make one version of the SS&B needles. This material should be considered for further testing in the needles made in house. Of the remaining materials only the polystyrene and Vectra A130 successfully filled the mold cavities. The other resins did not fill the narrow channel of the mold completely so the needles were of no use. The molds used are not heated because the mold housing used is not designed to do so. It is possible that heating the molds would produce a broader range of results, as it would allow for better flow into the mold cavity. This is a possible area of further exploration. The polystyrene needles produced were incapable of withstanding any type of axial loading. The low strength of polystyrene eliminates it as a

possibility for use. Figure 14 displays the low strength of polystyrene needles. The needle in the image is being easily bent between two fingers. Doing the same to a steel needle would result in injury to the person attempting to bend the needle.

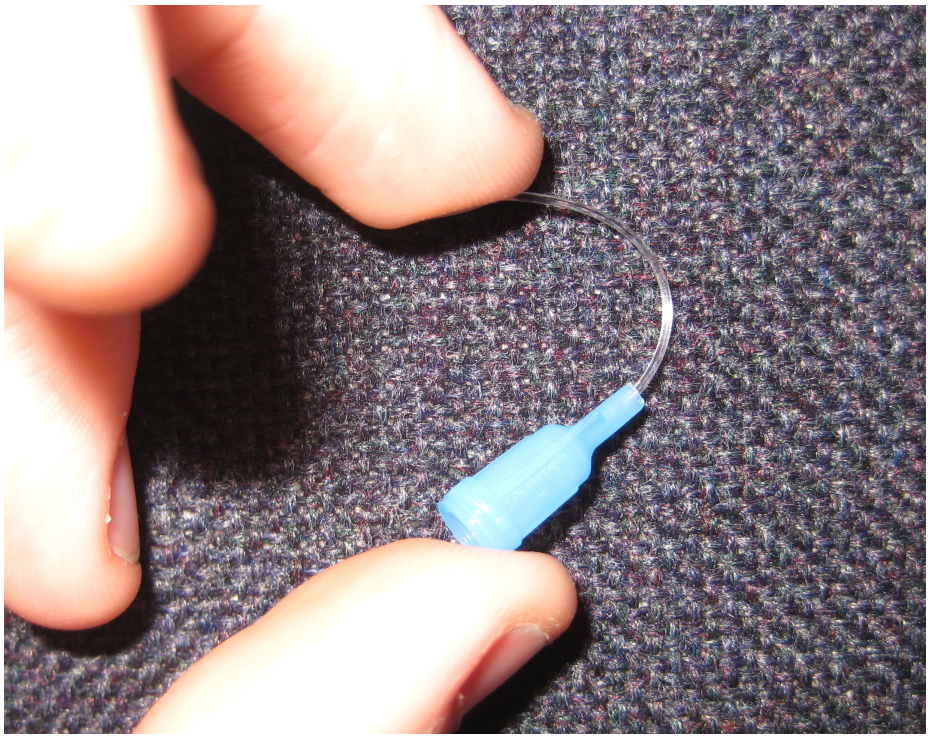

Figure 14 - Polystyrene needle being bent

Vectra A130 was the resin that produced the best plastic needles. They are sufficiently strong, and require the lowest penetration force seen in plastic needles thus far, which is comparable to that seen from steel needles. In addition, the likeness of the plastic needle to a steel needle is very close. The tip radius of the plastic needles is estimated to be between 4.8 and 5.5 microns, where the tip radius of a steel needle is estimated to be around 4.7 microns. All other dimensions of the plastic needles are the same as their steel counterpart. A magnified image comparing the tips of steel and plastic needles can be seen below in Figure 15. An analysis of the penetration abilities of needles is discussed in Chapter 5.

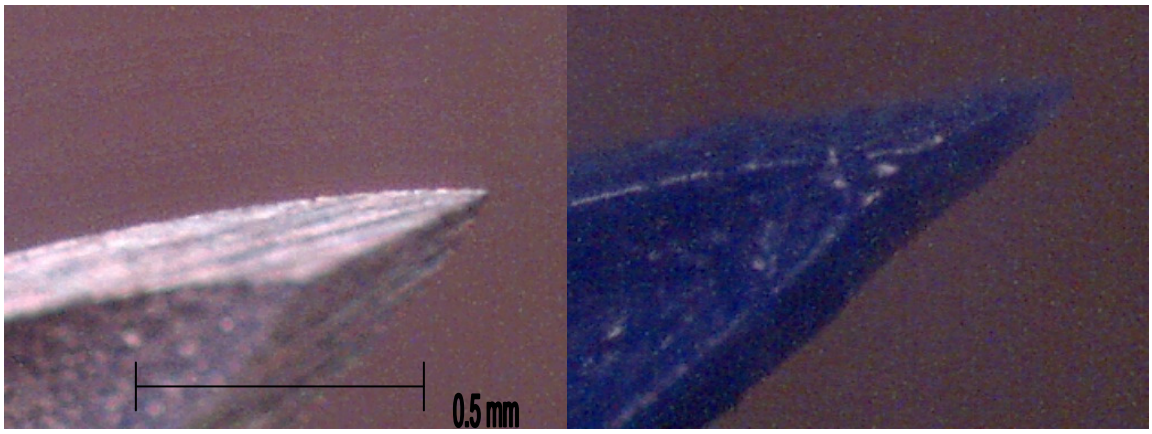

Figure 15 – Steel (left) and plastic (right) needle comparison, 200x magnification

2.5 Fabrication method used by SS&B

SS&B Technology Ltd., Australia, manufactures another version of plastic needle that is tested [17]. Their version is 22 gage and is a one piece integral needle. It is tested in both 25.4 mm and 16 mm lengths. An integral needle refers to having two parts, the hub and cannula, made into a single piece. In a conventional steel needle, the hub and cannula are two pieces that must be glued together. Integrating these pieces reduces the steps necessary during manufacturing and reduces the overall manufacturing cost. The needle is manufactured using a gas assisted injection molding (GAIM) [27] technique which produces the hollow core in the cannula. A cut-away schematic of the mold used for this process is shown in Figure 16.

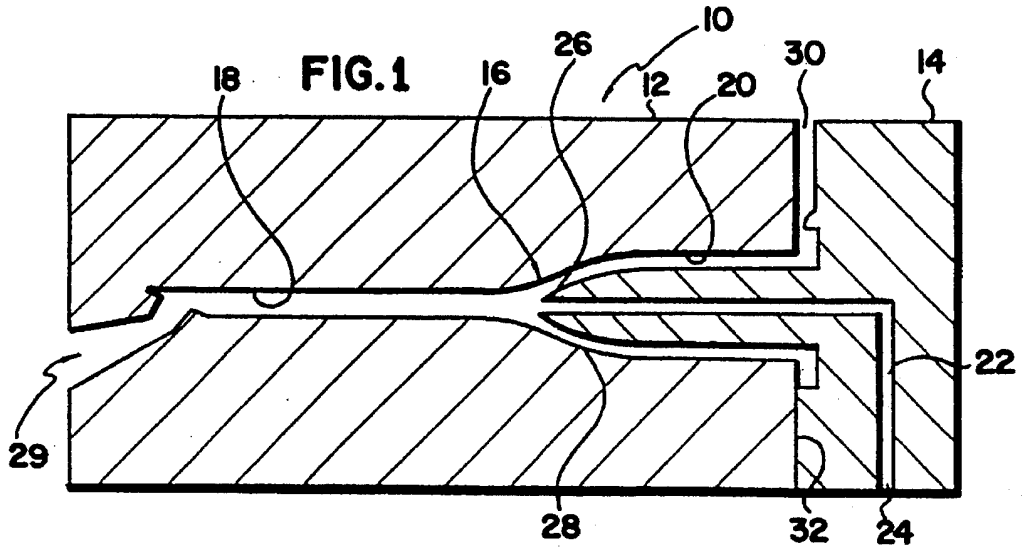

Figure 16 - Schematic of SS&B mold for plastic hypodermic needle [17]

From Figure 16 the different portions of the mold can be described. The portion labeled 10 refers to a two part mold that houses the cavity of the needle, 16. The cavity has two portions, the cannula (18) and the hub (20). The mold also has a gas inlet, 24, and an outlet, 26, which channels the gas through the cannula during molding and out the channel at the end of the cannula, 29. The gas that is forced through the cannula during the molding process pushes the molten polymer against the walls of the mold and a hollow core.

The molding process begins with the two halves of the mold being clamped together with all of the cavities and channels empty. A flow of polymeric resin is injected into the mold via the runner, 30, using the pressure generated by the injection molding machine. The resin flow is stopped before the entire cavity is filled. This step is shown in Figure 17.

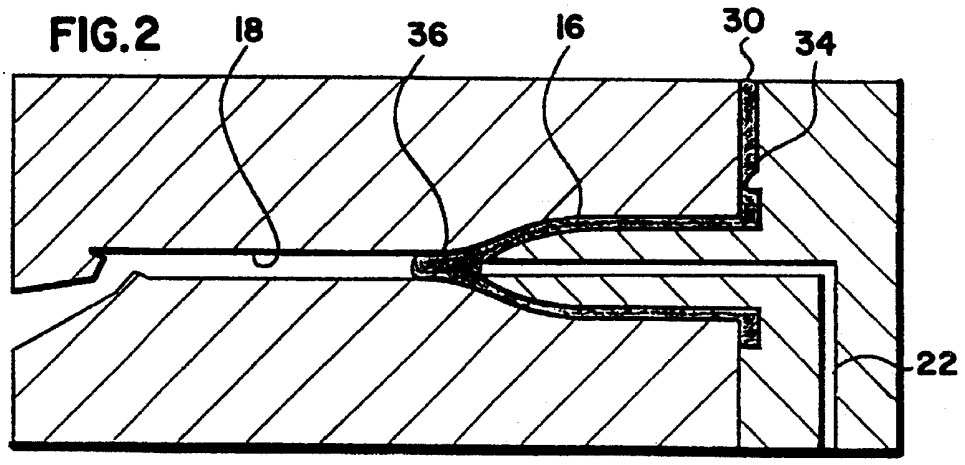

Figure 17 - Molten resin partially filling mold cavity [17]

The gas then is injected into the mold through the channel until the resin reaches the end of the mold, completely forming the needle. Any excess resin is expelled through the exit channel at the end of the cannula. This is illustrated in Figures 18 and 19.

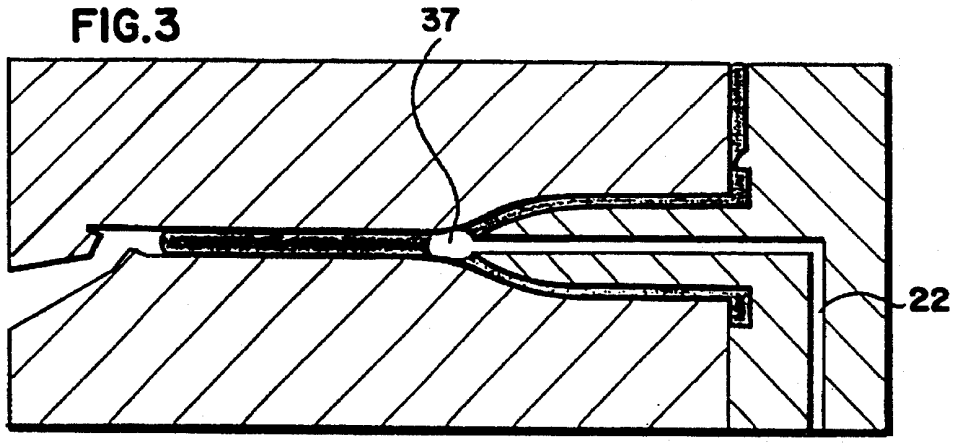

Figure 18 - Gas being injected into mold [17]

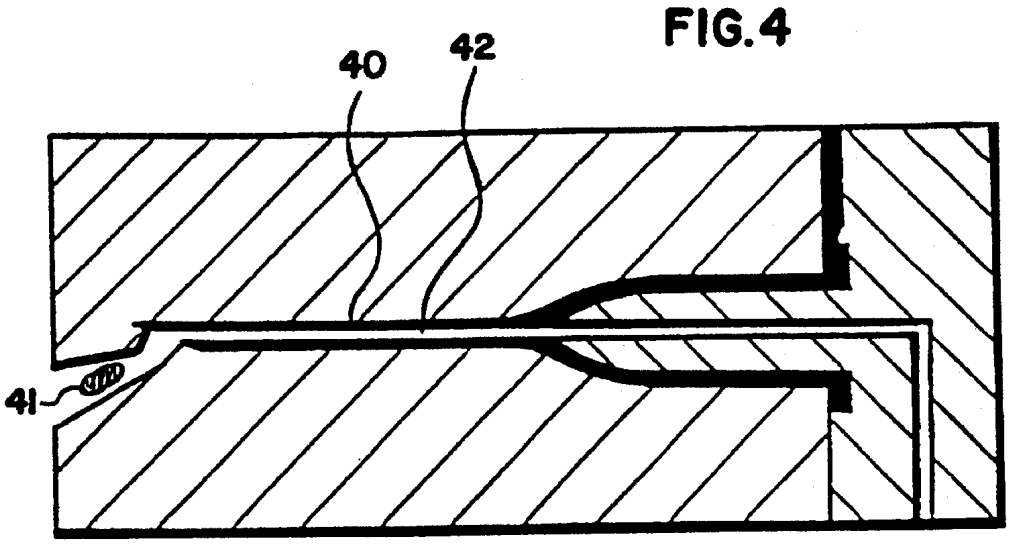

Figure 19 - Mold completely filled after gas injection [17]

The mold is separated and the needle is removed and separated from the runner. This process has proven to provide usable plastic needles. An analysis of these needles is outlined in Chapter 5.

2.6 Summary

This chapter focuses on the manufacturing techniques for plastic hypodermic needles. It covers mold design, mold manufacturing, mold development process, plastic selection, and description of the needles produced. These needles are tested for their penetrative abilities and buckling strengths using a protocol outlined in Chapter 3.

CHAPTER 3

DESCRIPTION OF EXPERIMENT

3.1 Penetration study

The primary focus of this thesis is to study and characterize the penetration of a hypodermic needle. To do this, an experimental setup was developed to mimic the penetration of a needle through skin. While this setup is not exactly penetration through skin, it serves as an acceptable alternative. The film used offers a consistent medium for penetration that allows accurate comparisons between different needle types.

3.1.1 Description of penetration experiment

The penetration experiments are conducted using a 0.381 mm thick polyurethane film as the penetration medium (McMaster-Carr #1446T31). The elastic modulus of the film is 5.0 MPa [11] and has been used as a skin mimic in previous studies and standards [28]. As can be seen from Table 2 the properties of polyurethane are lower than that of skin, however consistency between samples is more important for this study.

Table 2 - Properties of skin [11]

Layer	Thickness (mm)	Elastic Modulus (MPa)
Stratum Corneum	0.01-0.02	12000
Living Epidermis	0.03-0.13	16
Dermis	1.1	12
Subcutaneous Fat	1.2	20

It is known that the handling and preservation of biological material can have a significant impact on the mechanical properties of the material [29] and that the properties of skin can vary from person to person [30], therefore a manufactured material

is selected for testing. While it may not produce an exact replication of skin, it will provide for a consistent comparison between plastic and steel needles.

The polyurethane is tested using an Instron 33R4466 (Norwood, MA) single axis load versus displacement testing machine. The polyurethane is constrained in an aluminum clamping device that keeps the film immobile and maintains a neutral tension on the film up until the penetration begins. The clamping device consists of two elevated 76.2 mm square aluminum plates that are 9.5 mm thick. They are stacked and bolted together at the corners allowing a 50.8 mm strip of the film to pass between the plates and be held in place as the bolts are tightened. The clamp keeps the film perpendicular to the axis of motion of the Instron's crosshead. There is a 28 mm hole in the center of the plates to allow for the needle being tested to be forced through the film without obstruction. The bottom plate has an elevated ridge surrounding the hole and the upper plate contains the complementary raised ridge. This ridge increases clamping pressure on the film and eliminates slippage during testing. The hole in the clamp and the needle are aligned coaxially. The hub of the needle being tested attaches to a protrusion similar to a syringe that is on a 25 N load cell (Interface SMT1-25N, Scottsdale, AZ). The load cell is mounted to the cross-head of the Instron which moves at a rate of 100 mm/min [31] for these tests. The needle testing protocol is outlined in Appendix B. The experimental setup can be seen in Figure 20.

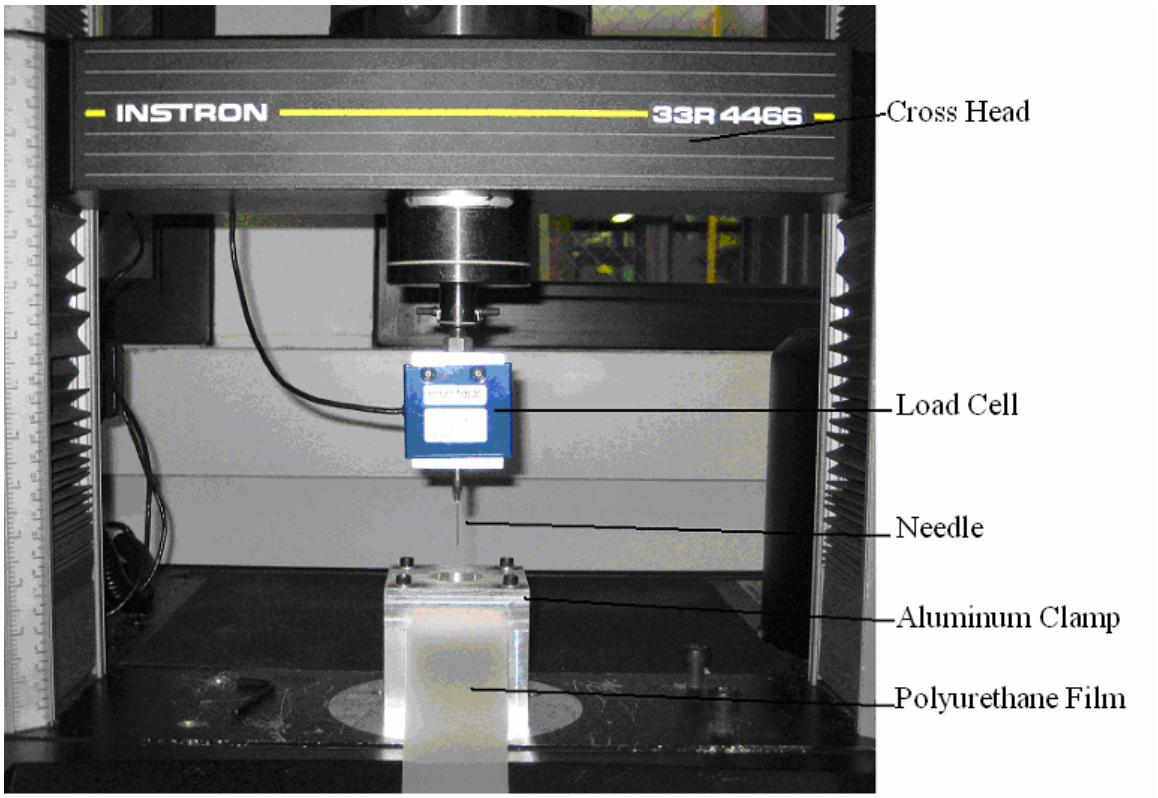

Figure 20 - Experimental setup used in penetration testing

3.1.2 Outline of needles and lubricants tested

Data covering a wide range of needle types are necessary to characterize needle penetration into film. For the penetration experiments eight different varieties of needles are tested, each with five groups studying the differences between four types of lubricants and bare needles. The eight types of needles are 18 gage Inviro Medical (Lawrenceville, GA), 22 gage Inviro Medical (Lawrenceville, GA), 22 gage Myco Medical (Cary, NC), 22 gage in-house Vectra A130, 22 gage SS&B (Australia) Vectra MT1300 in 25.4 mm and 16 mm cannula lengths, 26 gage Myco Medical (Cary, NC), and 30 gage Inviro Medical (Lawrenceville, GA). The four types of lubricant are "as-received" which is Dow Corning MDX4-4159 applied to the needles by the manufactures, MDX4-4159

applied to the needles at Georgia Tech, Dow Corning 360 Medical Fluid 1000 CST, and TriboGlide. Table 3 outlines the number of needles tested for each test group.

Table 3 - Penetration test groups

Needle Type	As-received	MDX	Silicone	TriboGlide	Bare
18 ga. Inviro Medical (38.1 mm)	30	20	20	10	30
Multiple Penetrations	No	No	No	No	No
22 ga. Inviro Medical (25.4 mm)	30	20	30	10	30
Multiple Penetrations	No	Yes	Yes	No	No
22 ga. Myco Medical (25.4 mm)	11	20	20	15	11
Multiple Penetrations	Yes	Yes	Yes	Yes	Yes
22 ga. In-house (25.4 mm)	NA	10	8	10	
Multiple Penetrations	No	No	No	No	No
22 ga. SS&B (25.4 mm)	NA	10	10		10
Multiple Penetrations	No	No	No	No	No
22 ga. SS&B (16 mm)	NA	9	10		10
Multiple Penetrations	No	No	No	No	No
26 ga. Myco Medical (12.7 mm)	11	20	20	15	11
Multiple Penetrations	Yes	No	Yes	Yes	Yes
30 ga. Inviro Medical (12.7 mm)	30	20	20	10	30
Multiple Penetrations	No	No	No	No	No

In addition to the single penetration tests, a select group of needles are penetrated through the polyurethane film three times in order to observe the affect that multiple

penetrations has on both the physical needle and the lubricant. Needles are typically inserted into a vial through a butyl rubber stopper to withdraw the medicine into the syringe. The multiple penetration tests are designed to determine a needle's ability to withstand the multiple penetrations that may be required for an injection.

3.2 Buckling study

In addition to penetration tests, the buckling load among the needles in the 22 gage group are studied and compared. The buckling of a needle can be divided into two categories, the buckling of the tip and the buckling of the cannula. If the tip buckles then the outcome is not necessarily catastrophic needle failure, so a better understanding of how various degrees of tip deformation affect the penetration force is useful for both characterizing penetrations and the design of the plastic needles. However the penetration force cannot exceed the critical buckling load of the cannula or the penetration will fail. Therefore it is useful to have an estimated set of load limits for a needle cannula based upon the materials used in this study, as well as a lower limit on the strength of potential plastic needle materials.

It is necessary to perform three types of analyses to get a complete sense of the different buckling modes (tip, cannula, and complete needle). The three types of analyses used are physical tests, finite element models, and buckling equations. Physical tests are the best way to evaluate the buckling strengths of needles. However, they are not as useful for determining tip and cannula strengths separately, which is necessary to understand the separate strength requirements. Finite element models are used for this purpose, as the model can be broken down into different portions and tested accordingly. Buckling equations are used to support the finite element analysis. The scope of the

buckling equations is limited, and it would be impractical to use them for a complex geometry such as a needle tip. They are useful for simple shapes such as the needle cannula, which can be compared directly to the finite element model. The similarity between the FEA and analytical models gives credibility to the finite element analysis of the tip.

3.2.1 Physical buckling tests

Physical testing is performed on ten samples from each of the five types of 22 gage needles: solid 25.4 mm MT 1300, solid 16 mm MT 1300, hollow 16 mm MT 1300, solid 25.4 mm A130, and steel Inviro Medical. The tests are conducted using the same Instron machine used for the penetration testing. A 500 N load cell, Instron (Norwood, MA), is used instead of the 25 N load cell, as the buckling load of the steel needles exceeds 25 N. The needle is held in place by an attachment that replicates the hub on a syringe. To determine the buckling load, needles are forced into a steel plate at a rate of 100 mm/min. The steel plate has a dimple at the point of needle contact to prevent deflection in a direction other than the axis of loading. The experimental setup is shown in Figure 21.

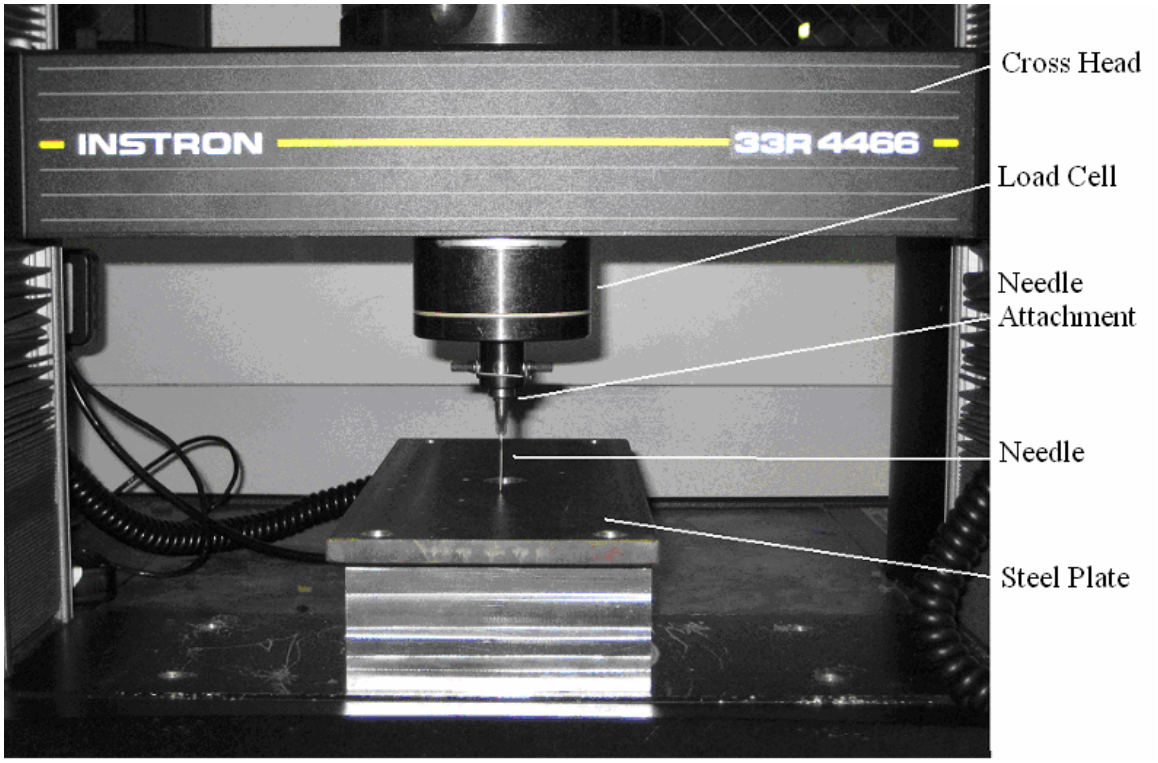

Figure 21 - Needle buckling experimental setup

The Instron machine outputs loading data as it does for the penetration testing. The maximum load reached before needle failure is recorded and taken to be the critical buckling load of that particular needle.

3.2.2 Finite element buckling analysis

In addition to physical testing, a simplified needle design representing the shaft of a needle and a complete model of a steel needle are tested using ANSYS finite element software. The two models are tested to provide information on cannula strength as well as tip strength. The different properties of each material type are studied and compared to the physical tests.

In order to estimate the strength of the cannula, the needle model is simplified to a cylinder with length and diameter corresponding to a 22 gage needle. Two models are

tested in 16 mm and 25.4 mm lengths, and both have an outer diameter of 0.7112 mm. Models of both lengths are tested with and without a hollow core in order to quantify the significance the core has on the critical buckling load. The diameter of the hollow core, if included, is 0.4572 mm. The meshed models of the hollow 25.4 mm and 16 mm needles can be seen in Figure 22 and the meshed models of the solid 25.4 mm and 16 mm needles can be seen in Figure 23.

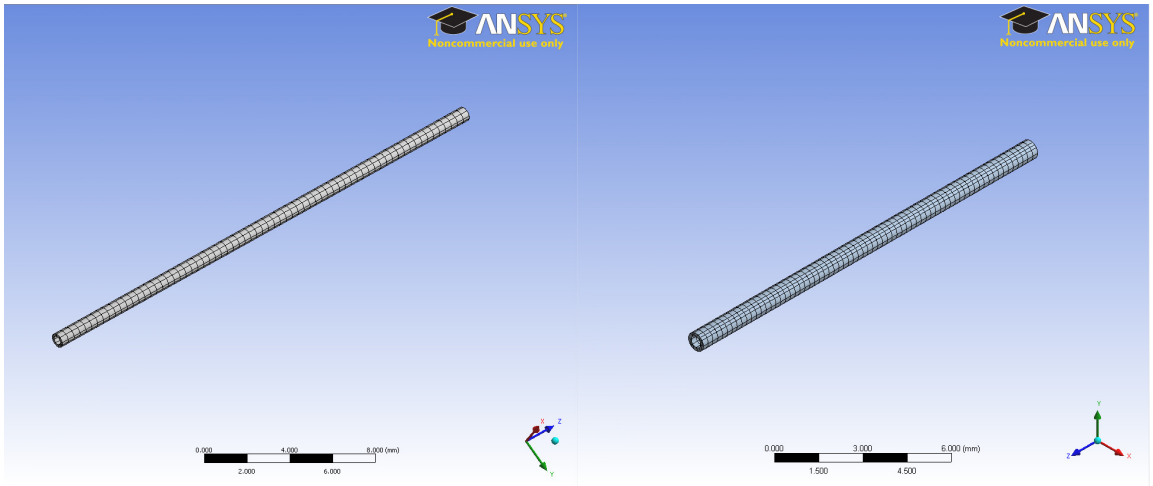

Figure 22 - Meshed FEA 25.4 mm and 16 mm, respectively, hollow needle models

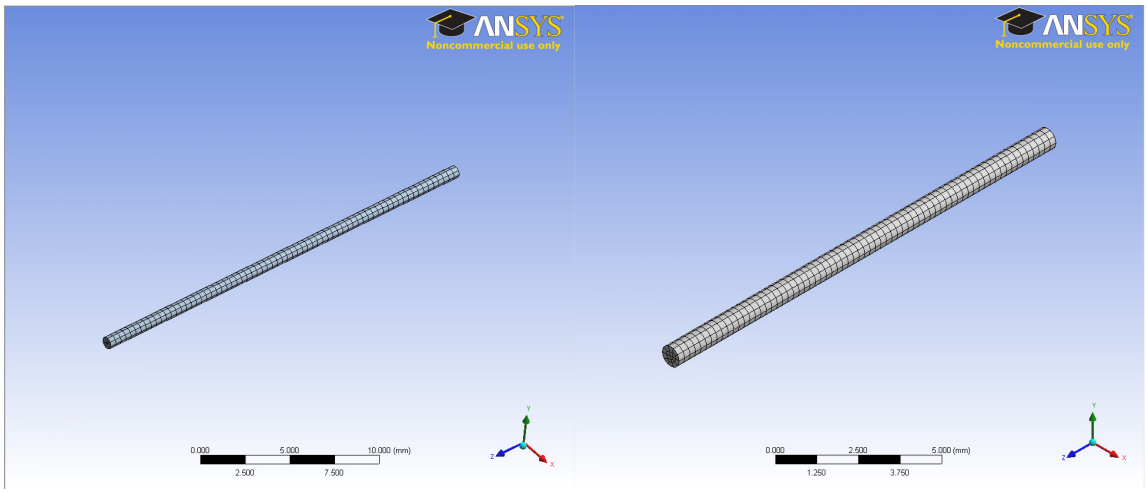

Figure 23 - Meshed FEA 25.4 mm and 16 mm, respectively, solid needle models

A complete model of a 25.4 mm steel needle also is analyzed. This model includes the tip of the needle. The buckling load of the model is returned for the weakest

point of the model. When the tip is included it becomes the weakest point, so its strength is the critical load returned. This information gives an idea of minimum useful material strength for the plastic needles. The complete meshed hypodermic needle and a close up image of the tip are shown in Figure 24.

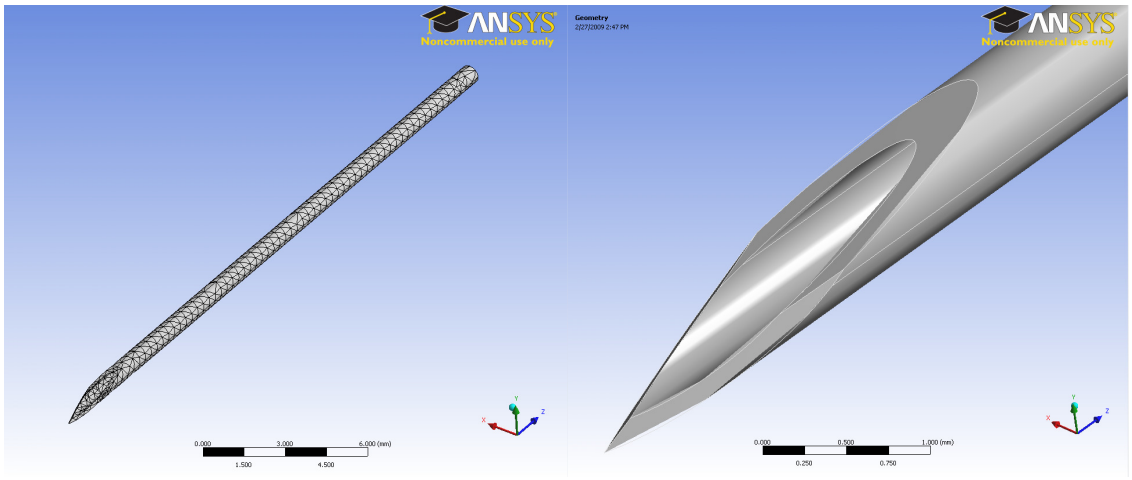

Figure 24 - Complete FEA needle model

All models are constrained in a fixed-pinned configuration. The hub end is completely restrained in all six degrees of motion and the tip end is restrained in the X and Y directions (directions perpendicular to the axis of loading), free in the Z direction (direction of the shaft), and free to rotate about all three axis. This simulates a pinned end. A compressive force is applied at the pinned end, and the value of this force is recorded once instability in the needle is reached.

3.2.3 Buckling equations

To support the finite element output, buckling analysis is performed on the cylindrical cannula model using buckling equations [19]. In order to determine which type of buckling equation to use, Johnson or Euler, the critical slenderness ratio for each needle type must be determined. This equation can be seen as Equation 1 [19],

$$\left(\frac{L}{r}\right)_c = \sqrt{\frac{\pi^2 E}{\sigma_y}} \tag{1}$$

where L is the length of the needle, r is the radius of gyration, E is the elastic modulus of the material, and σ_y is the compressive yield strength of the material. The radius of gyration, r, is defined as the square root of the moment of inertia, I, over the cross sectional area of the needle, A, or as seen in Equation 2 [19].

$$r = \sqrt{\frac{I}{A}} \tag{2}$$

The moment of inertia for a hollow cylinder is defined by Equation 3 [19].

$$I = \frac{\pi}{4}\left(r_o^{\,4} - r_i^{\,4}\right) \tag{3}$$

In Equation 3, r_o is the outer radius of the needle cannula and r_i is the inner radius of the needle cannula. In order to solve for a solid needle, r_i is set equal to zero. If the slenderness ratio of the needle being tested is greater than the critical slenderness ratio then Euler buckling equations may be applied. The Euler buckling equation for critical load of a column is shown in Equation 4.

$$P_{cr} = \frac{\pi^2 EI}{(KL)^2} \tag{4}$$

From the equation, K is the effective length factor and depends upon the end conditions of the column. In the case of the experimental setup the needle has one pinned end, the tip, and one fixed end, the hub. This corresponds to a value of 0.699 for K. It is important that this value is selected for an idealized situation. An alternate end condition would be a free-fixed configuration, which would correspond to a K value of 2. In practice, the actual value would likely be between these two estimates. If the slenderness

ratio of the needle is less than that of the critical slenderness ratio then the Johnson buckling equations must be used to determine the critical load. The Johnson buckling equation is shown in Equation 5 and 6 [11].

$$P_{cr} = A(\sigma_y - b\left(\frac{KL}{r}\right)^2) \tag{5}$$

$$b = \frac{1}{4E}\left(\frac{\sigma_y}{2\pi}\right)^2 \tag{6}$$

These buckling equations are used as a quality assessment for the results from the finite element models. They are used to calculate the critical buckling loads of 22 gage 25.4 and 16 mm needles, and then compared to the results of both the finite element models and the physical tests. The results are presented in Chapter 4.

3.3 Tip characteristic measurements

One of the aspects of this thesis is to determine the effect that the needle characteristics-tip radius, tip angle, and diameter-have on the penetration forces. The diameter of the needles is measured using a set of Mitutoyo, Aurora, IL, digital calipers, model number CD-6”CSX, with an accuracy of ±0.005 mm. The tip radius and angel are measured using a Leica, Solms, Germany, DMRM digital microscope with an accuracy of ±1 μm and ±1°. The microscope images are captured at 200x magnification and the tip characteristics are measured using built in analysis software. Chapter 4 presents tables showing diameter, tip angle, and tip radius along with the corresponding penetration forces.

3.4 Coefficient of friction testing

Another characteristic of needles that affects penetration force is the lubricant on the needle [11]. The coefficients of friction between the various needle types and the polyurethane film are a useful tool for quantifying the affect that the lubricant has on penetration. As no data could be found on the coefficients of friction between the materials and lubricants being tested, the data are obtained experimentally. The tests are based upon the free body diagram shown in Figure 25.

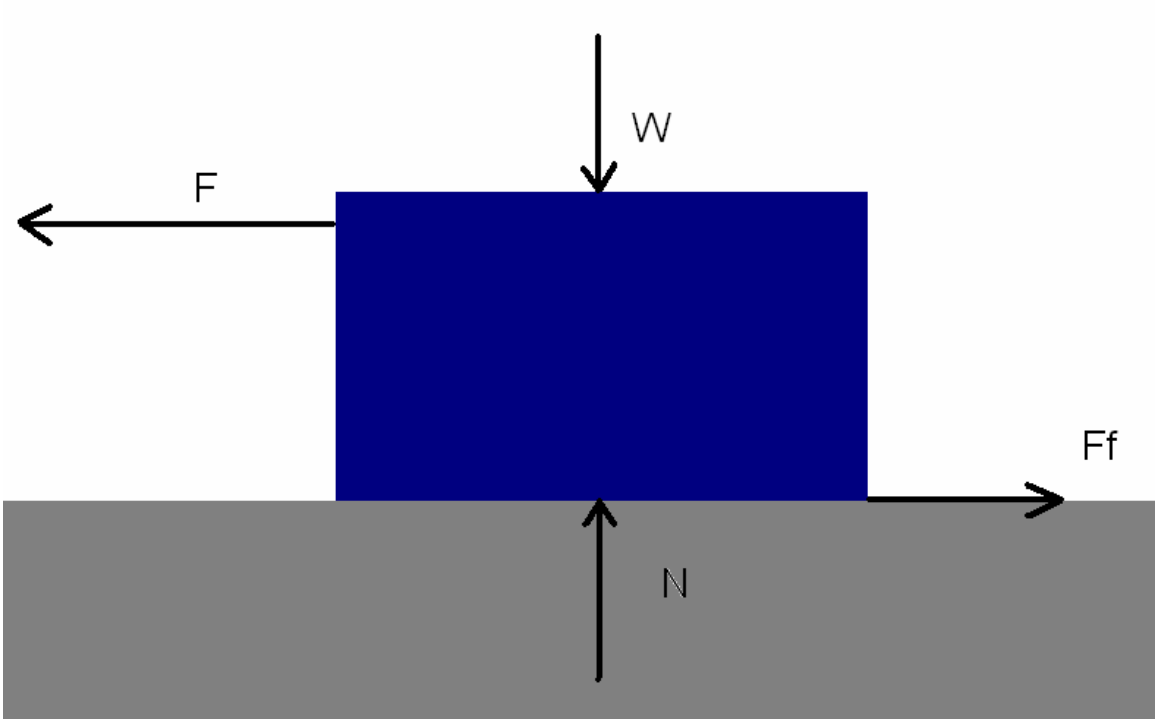

Figure 25 - Friction free body diagram

Using Equation 7,

$$F_f = \mu N \tag{7}$$

where F_f is the frictional force, μ is the coefficient of friction, and N is the normal force which is equal to the weight of the block, the coefficient of friction can be determined.

This is replicated experimentally using the Instron machine. Blocks of steel that are either lubricated or bare are pulled across a sheet of polyurethane film by means of the Instron machine. As the Instron machine's direction of travel is perpendicular to the direction necessary for this experiment, the direction must be altered by means of a pulley. A string is attached to the load cell and routed through a pulley at the base of the machine. The string is then attached to the block which is sitting on a piece of polyurethane film. Special care is taken to keep the pulling force parallel to the surface the block is sitting on. When the test begins the raising cross head pulls the block across the film and the force is continually recorded. By static equilibrium the average pulling force recorded is equal to the frictional force seen in Equation 7. Thus, the coefficients of friction of the various lubricants can be determined. All friction tests are conducted at the same rate (100 mm/min) as the penetration tests [28, 31]. Trials were conducted at varying pulling speeds; however no variation of results was detected. The results of these tests are presented in Chapter 4.

3.5 Summary

This chapter summarizes the tests conducted to characterize hypodermic needle penetration through film. This includes a description of the experimental setup used for the penetration and buckling tests. It also outlines the grouping of needle and lubricant combinations that are tested. In addition, it presents the three types of buckling tests conducted and outlines the methods for each. Needle tip characteristics, coefficient of friction, and material stiffness also are believed to have an impact on the penetration force. These different properties are tested for by methods outlined in this chapter. Chapter 4 presents the results of these tests.

CHAPTER 4

EXPERIMENTAL RESULTS

Chapter 4 presents the results of the tests described in previous chapters. The results of penetration, buckling, coefficient of friction, and tip measurements tests are discussed and the meanings of those results are interpreted.

4.1 Penetration results

4.1.1 Needle failure percentage

Before the penetration forces are presented, it is important to discuss the penetration percentage (percentage of penetrations without failure) of the various types of needles. All of the steel needles penetrated the film without failure; however the same is not true for the plastic needles. Table 4 lists each needle type along with its penetration percentage.

Table 4 - Successful penetration percentage

Lubricant / Needle Type	TriboGlide	MDX	As-received	Silicone	Bare
18 Gage					
Inviro Medical	100	100	100	100	100
22 Gage					
Inviro Medical	100	100	100	100	100
Myco Medical	100	100	100	100	100
Plastic MT1300 16 mm		100	NA	40	0
Plastic MT1300 25.4 mm		80	NA	10	0
Plastic A130 25.4 mm	90	89	NA	88	
26 Gage					
Myco Medical	100	100	100	100	100
30 Gage					
Inviro Medical	100	100	100	100	100

Most of the plastic needles tested proved to be relatively reliable. However, the bare and silicone coated needles were not as successful as the others. This highlights the importance that lubricant has on the penetration forces of the needle and will be further discussed in Chapter 5.

4.1.2 Average maximum penetration force

The output of the penetration testing is a series of displacement data points with the corresponding load at each point. The entire load versus displacement graph is useful for studying the characteristics of the penetration and determining what type of penetration occurred. The different stages of loading and penetration can be examined and compared and this can be used to determine what portion of the needle is having the most significant affect on the penetration force. This will be elaborated upon in Chapter 5. One observation made by examining the load versus displacement plots of the needles is that the plot for a steel needle differs from the plot of a SSB MT1300 plastic needle. An example of a needle penetration load versus displacement graph for a 22 gage Inviro Medical needle tested as-received is shown in Figure 26.

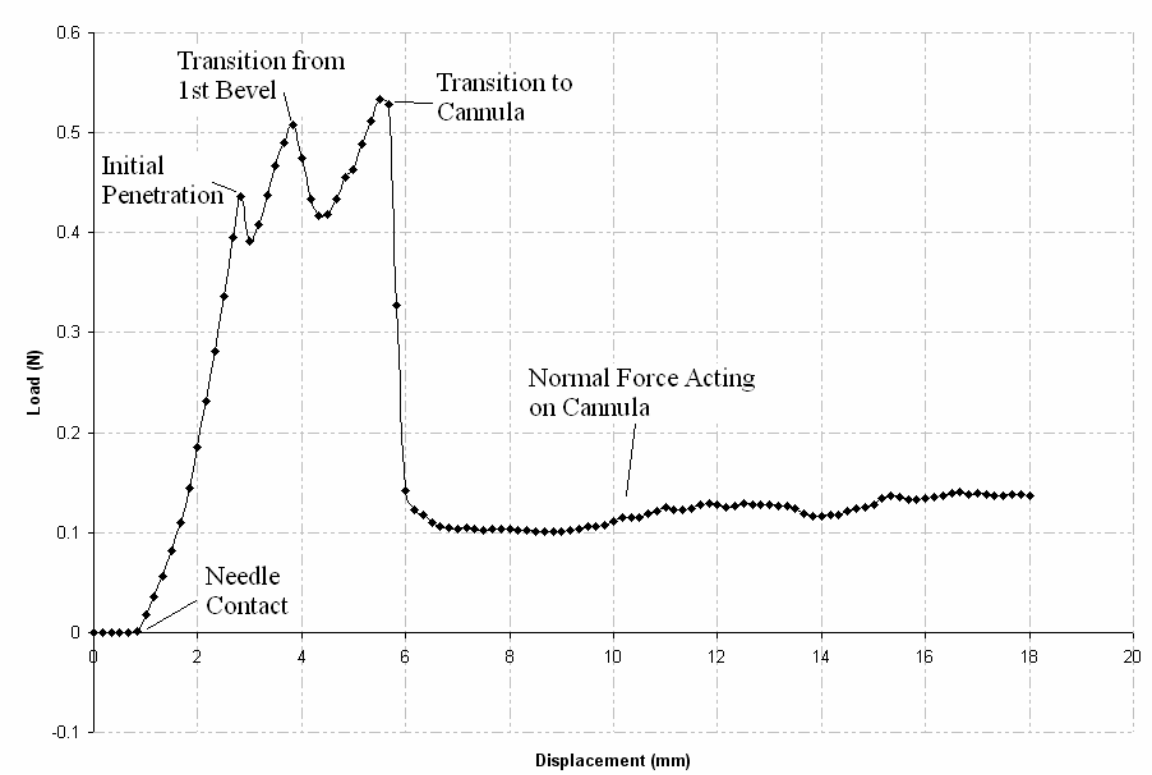

Figure 26 – Load vs. displacement plot, 22 ga. Inviro Medical as-received

As seen in Figure 26, a steel hypodermic needle has clear slope changes that correlate to the different regions of the needle. The initial penetration of the needle into the polyurethane, the transition from the first bevel of the needle to the second, and the transition from the second bevel to the cannula can all be clearly seen on the plot. These distinctive characteristics become less clear as the tip radius of the needle increases. This is likely attributed to the mechanism of penetration transitioning from cutting to tearing of the polyurethane. This is particularly evident on the plots of the SSB MT1300 plastic needles, as the total penetration occurs at one point in the plot, which is the maximum penetration force. A plot of a MDX coated SSB MT1300 plastic needle is shown in Figure 27.

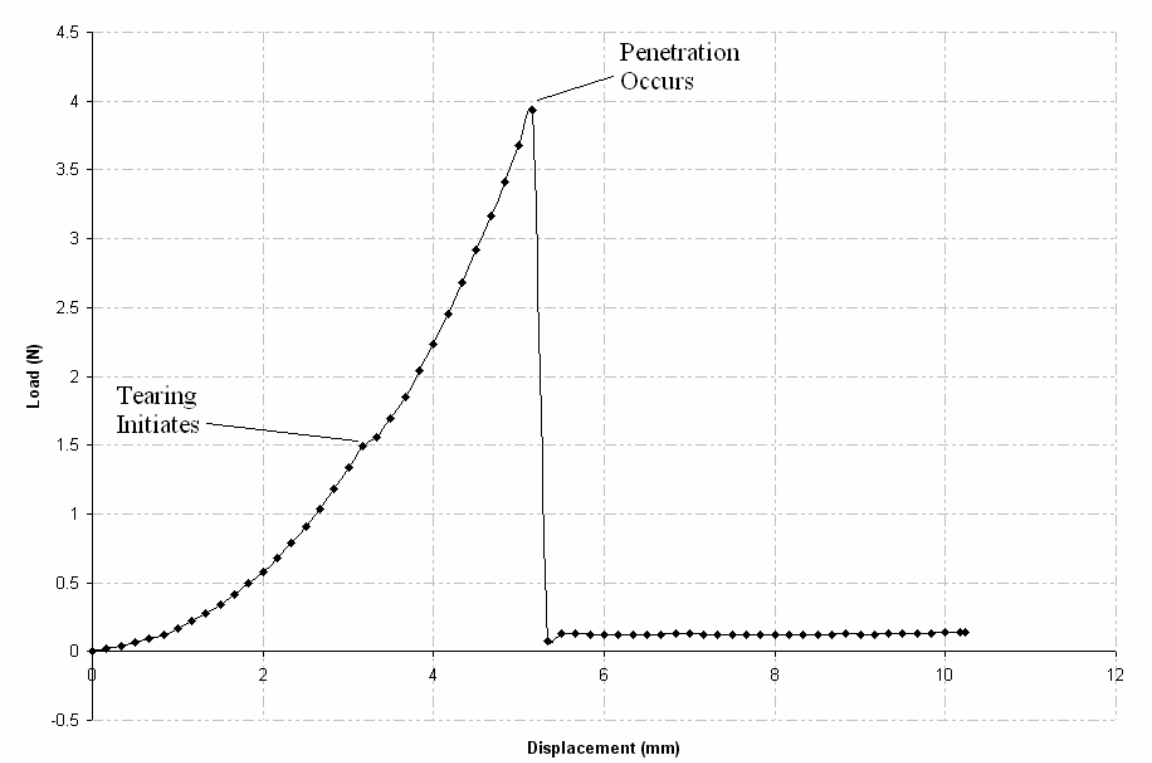

Figure 27 - Load vs. displacement plot, 22 ga. SSB MT1300 MDX

The differences between the figures show that the type of penetration that occurs is dependent upon the tip radius of the needle. The duller plastic needles tend to tear through the polymer as it is stretched over the tip of the needle; where as the sharper steel needles tend to cut through the polymer by means of shear failure. The A130 plastic needles exhibit data that resemble both the steel needle and SSB MT1300 plots. Therefore it can be concluded that the tip radius transition point from cutting to tearing of polyurethane film occurs within the range of tip radii that the A130 needles posses. This transition further is discussed and determined in Chapter 5.

The most important piece of data from the penetration experiments is the maximum penetration force of each needle. In Figure 26, the maximum penetration force for the particular needle is around 0.56 N. This number is important because it is associated with the amount of pain caused by the needle, i.e., the lower the penetration

force, the better. In order to rank the penetration ability of the different types of needles, the maximum penetration forces from a group are averaged and compared to other groups of needles. The collection of these data points for the needles in each experimental group is averaged and presented in Table 5.

In addition the standard deviation of the average maximum penetration force is presented. At some point during processing or experimentation a few needles were damaged and thus their data were determined to be invalid. Damaged needles are determined by examining magnified images (200 times) taken before and after penetration. If sufficient damage is observed, then the data point is eliminated from the average. Both the overall average and the un-damaged average are presented in the table; however the un-damaged average is taken to be the more accurate of the two and is used when comparing the needle groups. The damaged needle data are still useful in determining the effect that the tip radius has on penetration force, so these data points are saved for further analysis. The complete list of maximum penetration forces for each needle tested is presented in Appendix C.

Table 5 - Average maximum penetration force

	Number of Needles	Average Force (N)	Standard Deviation	Number Damaged	Average Force Un-Damaged (N)	Standard Deviation
18 Gage						
Inviro Medical						
TriboGlide	10	1.178	0.286	5	0.964	0.046
MDX	20	0.934	0.043	0	0.934	0.043
As-received	30	0.920	0.070	0	0.920	0.070
Silicone	20	1.156	0.063	0	1.156	0.063
Bare	30	2.927	0.097	0	2.927	0.097
22 Gage						
Inviro Medical						
TriboGlide	10	0.698	0.079	3	0.668	0.025
MDX	20	0.620	0.048	7	0.599	0.036
As-received	30	0.683	0.107	1	0.672	0.091
Silicone	30	0.876	0.057	3	0.871	0.055
Bare	30	1.764	0.081	0	1.764	0.081
Myco Medical						
TriboGlide	15	0.763	0.041	2	0.758	0.041
MDX	20	0.622	0.042	3	0.612	0.036
As-received	11	0.655	0.113	3	0.602	0.043
Silicone	20	0.885	0.063	1	0.877	0.051
Bare	11	1.803	0.087	0	1.803	0.087
SSB MT1300 16 mm						
TriboGlide	--	--	--	--	--	--
MDX	10	3.486	0.515	0	3.486	0.515
Silicone	4	10.687	0.840	0	10.687	0.840
Bare	0	NA	NA	NA	NA	NA
MT 1300 25.4 mm						
TriboGlide	--	--	--	--	--	--
MDX	8	5.393	1.309	0	5.393	1.309
Silicone	1	7.951	0.000	0	7.951	0.000
Bare	0	NA	NA	NA	NA	NA
A130 25.4 mm						
TriboGlide	9	1.739	0.391	1	1.626	0.212
MDX	16	1.760	0.582	1	1.693	0.541
Silicone	7	2.430	1.244	1	1.974	0.324
26 Gage						
Myco Medical						
TriboGlide	15	0.641	0.211	1	0.587	0.030
MDX	20	0.547	0.105	10	0.491	0.032
As-received	11	0.531	0.045	4	0.505	0.028
Silicone	20	0.764	0.049	0	0.764	0.049
Bare	11	1.281	0.073	0	1.281	0.073
30 Gage						
Inviro Medical						
TriboGlide	10	0.501	0.137	9	0.394	0.000
MDX	20	0.383	0.029	0	0.383	0.029
As-received	30	0.511	0.028	1	0.509	0.023
Silicone	20	0.615	0.081	2	0.597	0.037
Bare	30	0.955	0.064	0	0.955	0.064

From Table 5, the lubricants that performed the best (lowest average penetration force) on the various needle types are as follows: 18 ga. Inviro Medical, as-received, 0.920 N; 22 ga. Inviro Medical, MDX, 0.599 N; 22 ga. Myco Medical, as-received, 0.602 N; SSB MT1300 16 mm, MDX, 3.486 N; SSB MT1300 25.4 mm, MDX, 5.393 N; Vectra A130, TriboGlide, 1.626 N; 26 ga. Myco Medical, MDX, 0.491 N; 30 ga. Inviro Medical, MDX, 0.383 N.

In addition to low penetration force, the standard deviation of a particular group serves to determine the consistency within a group. As seen in Table 5, most steel groups have a low standard deviation. The MDX and TriboGlide groups consistently produced the lowest standard deviation, and the bare and silicone groups were typically higher. The plastic needles displayed higher variation within the groups, which is typically an order of magnitude higher than the steel groups. The higher variation can likely be attributed to inconsistencies between the needles being tested, as it is more likely for a group of prototypes to display high variation than a group that is commercially produced.

These data are represented graphically in Figures 28, 29, 30, and 31. These graphs show the average penetration forces of each group. The box represents the average penetration force +/- the standard deviation of that particular group, i.e., a thicker bar represents more variation among a group. The whisker extending beyond the box represents two standard deviations.

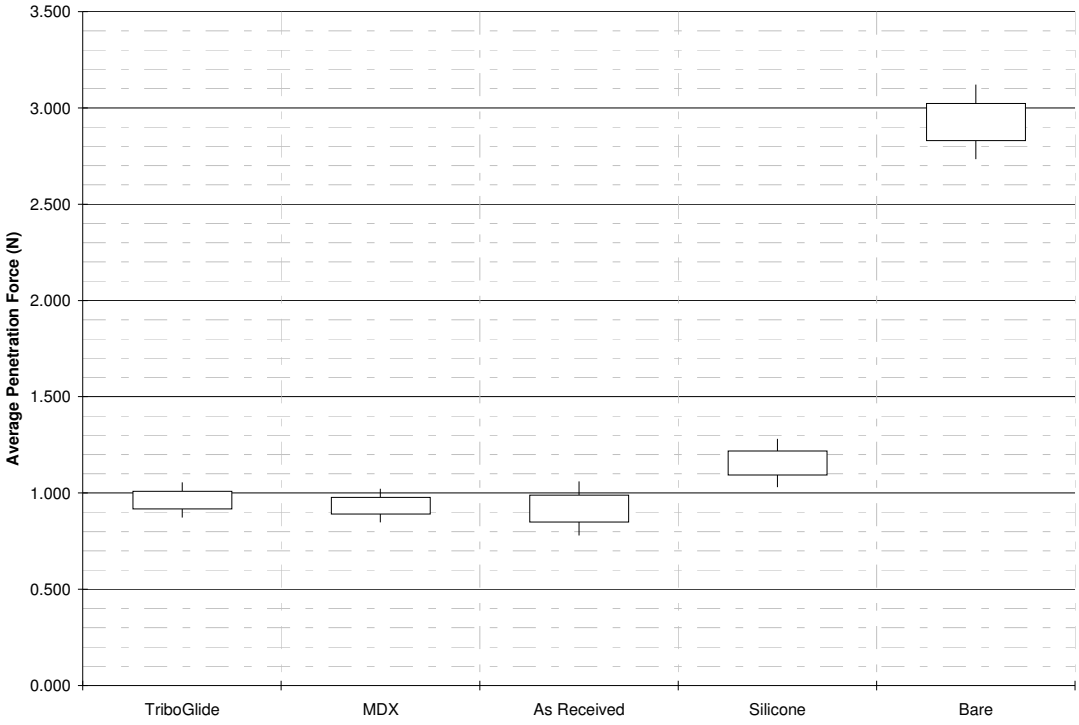

Figure 28 - Average penetration forces, 18 Gage Inviro Medical

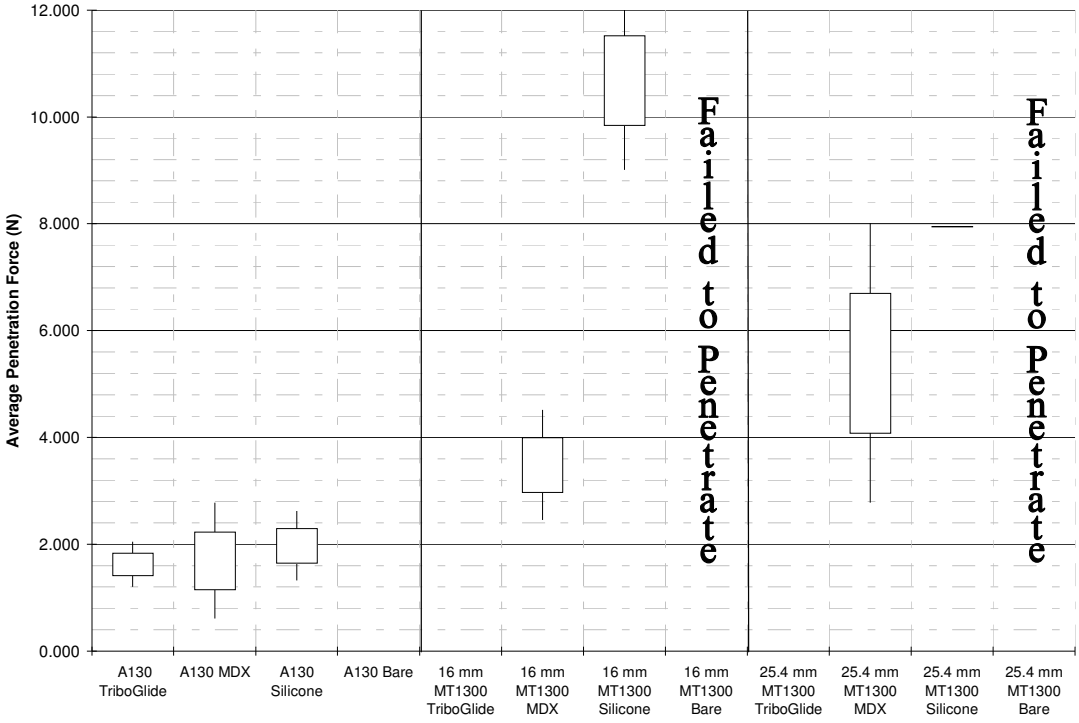

Figure 29 - Average penetration forces, 22 gage plastic

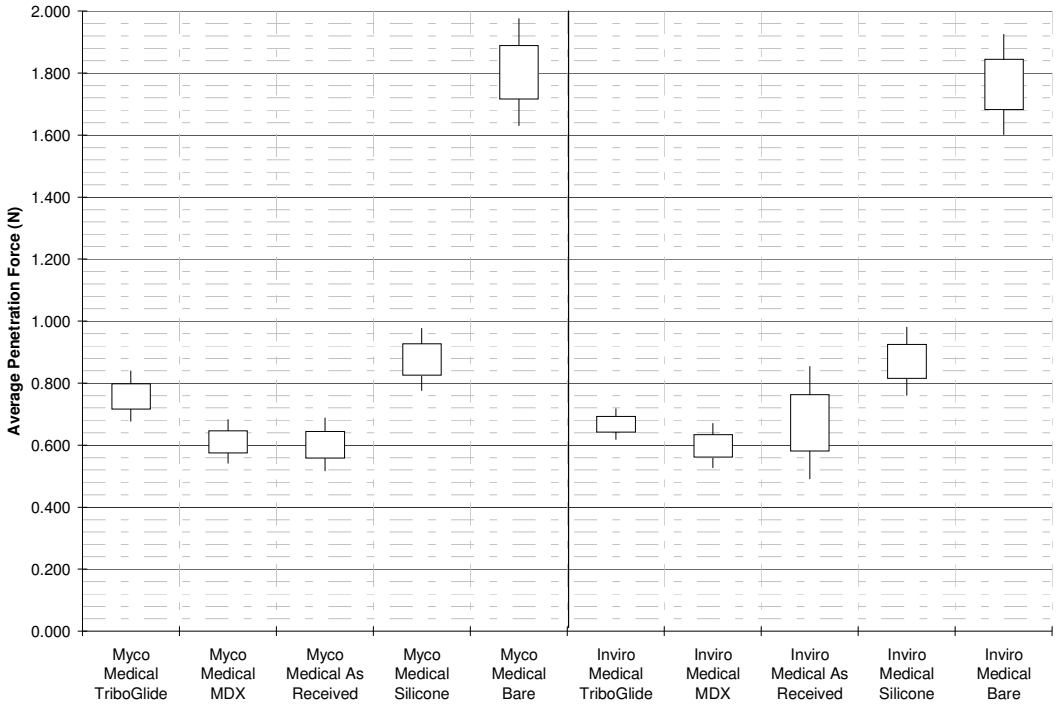

Figure 30 - Average penetration forces, 22 gage steel

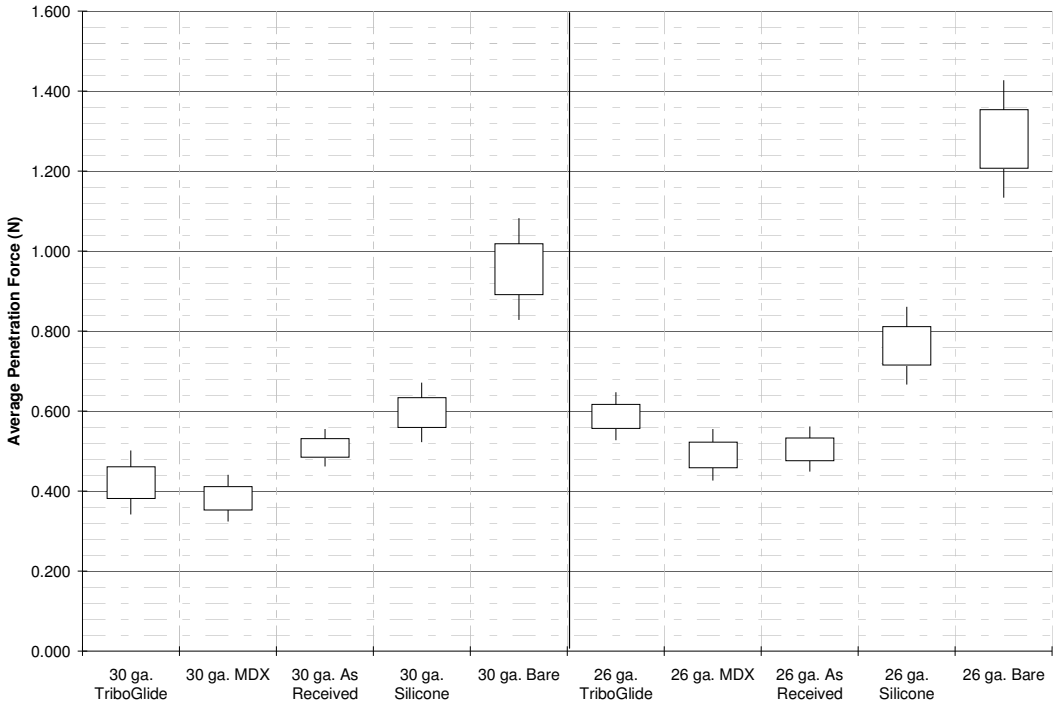

Figure 31 - Average penetration forces, 26 gage and 30 gage

The data from the different needle groups are analyzed statistically to determine if the different average values are statistically dissimilar. A single factor analysis of variance (ANOVA) test was conducted on each group to determine if there were dissimilarities within the groups [32]. All groups showed statistical dissimilarity. The groups then were analyzed using the Tukey method of multiple comparisons to determine which groups could be determined statistically dissimilar. All tests are conducted at a 95% confidence level. The results are shown in Table 6. A "Yes" means the groups are statistically dissimilar, a "No" means the groups could not be proven dissimilar.

Table 6 - Results of Tukey multiple comparison for steel average penetration force

Groups Compared	18 ga. Inviro Medical	22 ga. Myco Medical	22 ga. Inviro Medical	26 ga. Myco Medical	30 ga. Inviro Medical
As-received vs. TriboGlide	Yes	Yes	No	No	No
As-received vs. Silicone	Yes	Yes	Yes	Yes	Yes
As-received vs. MDX	No	No	Yes	No	Yes
As-received vs. Bare	Yes	Yes	Yes	Yes	Yes
TriboGlide vs. Silicone	Yes	Yes	Yes	Yes	Yes
TriboGlide vs. MDX	No	Yes	No	No	No
TriboGlide vs. Bare	Yes	Yes	Yes	Yes	Yes
Silicone vs. MDX	Yes	Yes	Yes	Yes	Yes
Silicone vs. Bare	Yes	Yes	Yes	Yes	Yes
MDX vs. Bare	Yes	Yes	Yes	Yes	Yes

From Table 6 it is seen that most of the different types of lubricant proved to be dissimilar. The MDX and 'as-received' groups are assumed to be the same which corresponds to the fact that they are the same lubricant type. The only time that they are dissimilar is when the MDX group showed significantly lower penetration results. In

addition the TriboGlide and 'as-received' groups are assumed equal for the 26 gage Myco Medical and 22 gage Inviro Medical groups. The TriboGlide group also cannot be proven dissimilar from the MDX group for every needle type except the 22 gage Myco Medical group. In addition to comparing lubricants within groups, the two 22 gage groups are statistically compared to determine if the two needle types can be proven to be dissimilar. The results show that the groups that are lubricated in-house, MDX, silicone, and bare, cannot be proven dissimilar. The other groups that were lubricated by different sources can be proven dissimilar.

This data supports the assumption that penetration force is dependent upon both lubrication and needle diameter. The effect of lubrication is represented numerically by the coefficients of friction of the different lubricant types. These coefficients are presented in Section 4.4.

4.1.3 Triple penetration test results

Tests were conducted in which a single needle is used to penetrate different pieces of polyurethane film three times. These tests are conducted to study the effect that multiple penetrations have on the needle and the lubricant. The results of these tests are shown in Table 7. Included in the table are the average penetration forces for each of the three penetrations of the 10 different needle and lubricant groups tested. Also, the number of needles included in each average as well as the standard deviation of penetration forces within the groups is included.

Table 7 - Multiple penetration test results

Needle Type	Un-Damaged	1st Pene-tration	Standard Deviation	Un-Damaged	2nd Pene-tration	Standard Deviation	Un-Damaged	3rd Pene-tration	Standard Deviation
22 Ga. Myco Medical									
As-received	8	0.602	0.043	8	0.598	0.038	8	0.591	0.043
TriboGlide	13	0.758	0.041	12	0.728	0.043	12	0.718	0.036
Silicone	19	0.877	0.051	19	0.831	0.051	19	0.808	0.067
MDX	17	0.610	0.036	16	0.612	0.043	16	0.636	0.043
Bare	11	1.803	0.087	11	1.758	0.100	10	1.762	0.076
22 Ga. Inviro Medical									
Silicone	28	0.875	0.054	28	0.806	0.036	28	0.842	0.037
MDX	17	0.610	0.042	17	0.613	0.041	17	0.598	0.034
26 Ga. Myco Medical									
As-received	7	0.505	0.028	7	0.521	0.022	4	0.578	0.027
Silicone	9	0.762	0.033	9	0.767	0.038	9	0.810	0.039
TriboGlide	14	0.587	0.030	14	0.593	0.035	13	0.627	0.024
Bare	11	1.281	0.073	11	1.227	0.093	11	1.266	0.090

For the 22 gage needles, most of the subsequent penetrations required lower penetration forces than the previous penetrations, and all showed lower penetration forces for the third penetration versus the first penetration. The opposite is true for the 26 gage needles, as the average penetration force increased with each penetration. The 22 gage Myco Medical silicone coated needles had the greatest decrease in penetration force from 0.877 N for the first penetration to 0.808 N for the third penetration. The data from Table 5 are presented graphically in Figures 32, 33, and 34. The boxes on the plots represent the average needle penetration force +/- the standard deviation of that particular group, the whiskers represent two standard deviations. The first, second, and third penetrations are grouped together on the plots.

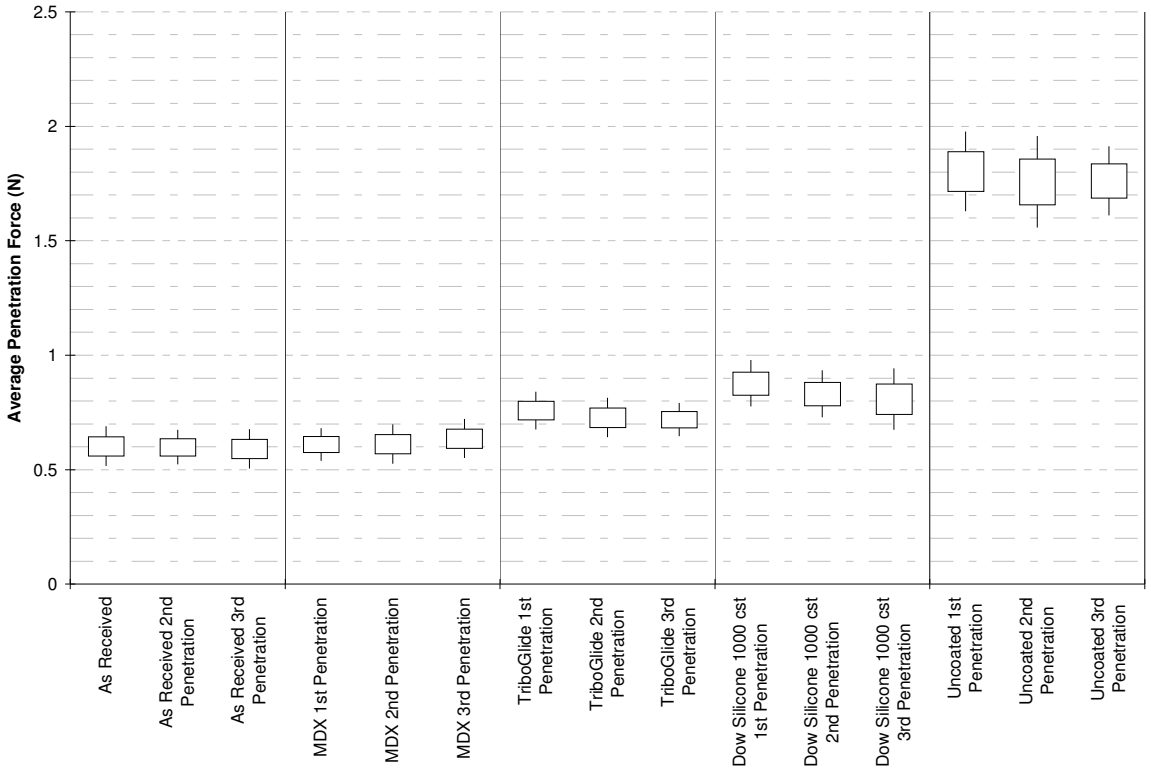

Figure 32 - Average penetration force, 22 ga. Myco Medical multiple penetrations

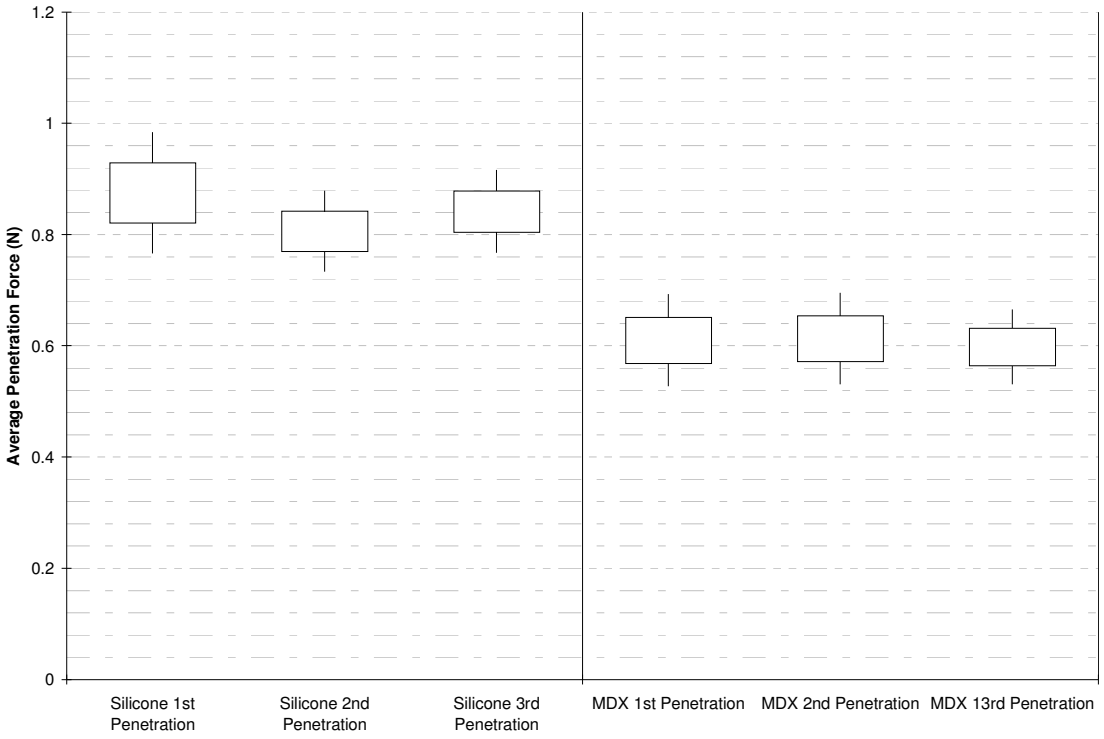

Figure 33 - Average penetration force, 22 ga. Inviro Medical multiple penetrations

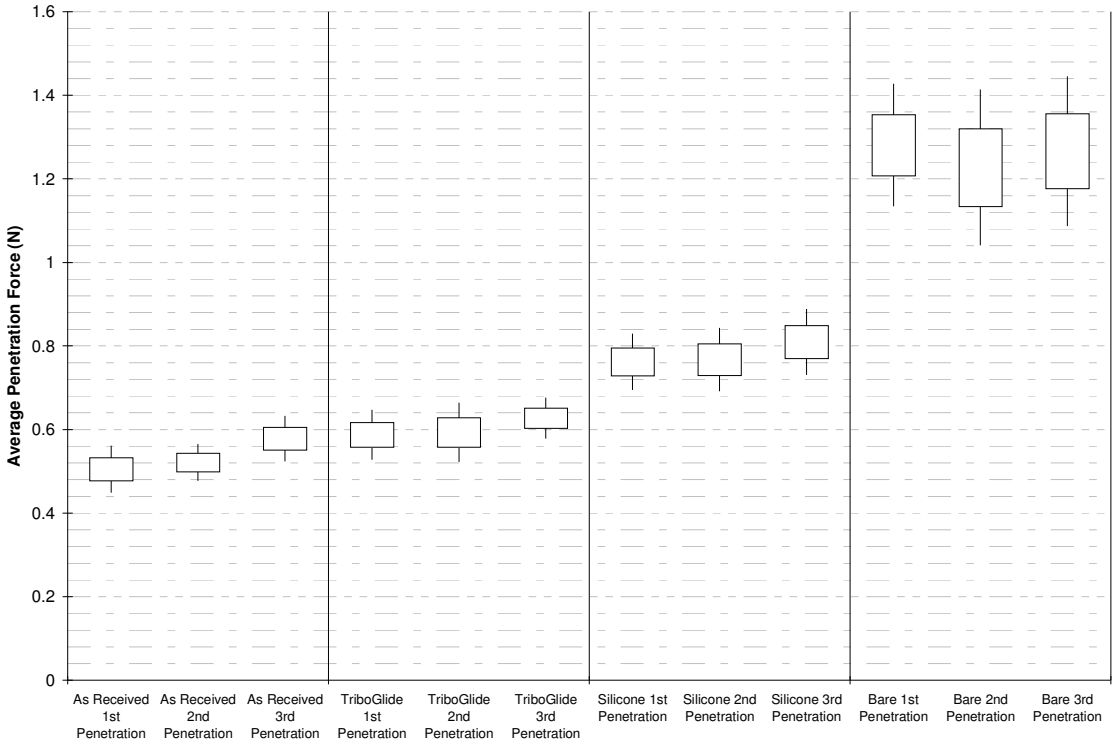

Figure 34 - Average penetration force, 26 ga. Myco Medical multiple penetrations

Although many of the groups showed a slight decrease in average penetration force, many of them could not be proven statistically dissimilar. Using a single factor analysis of variance (ANOVA) method the multiple penetrations within the groups are compared statistically. An ANOVA test was run for each test group comparing the differences between penetrations. Three of the 22 gage Myco Medical needle groups could not be proven statistically dissimilar. These groups are as-received, MDX, and bare. The other two groups TriboGlide and silicone showed statistical differences between penetrations. Of the 22 gage Inviro Medical needles tested with multiple penetrations the MDX group could not be proven statistically dissimilar between penetrations, but the silicone group could. The 26 gage Myco Medical bare group could not be proven dissimilar; the as-received, TriboGlide, and silicone groups could be

proven statistically dissimilar. All ANOVA tests are conducted at a 95% confidence interval.

4.1.4 Minimum penetration force for each group

In addition to the average penetration force, the lowest penetration force represents the ideal penetration force that the various needle types are capable of. It is more useful for comparing the penetration abilities of the plastic needles because they show significantly more intra-group variance than the steel needles. One of the goals of this study is to reduce this variance and determine the primary contributors, so that the variance can be minimized. Table 8 shows the lowest penetration force seen among the different needle types.

Table 8 - Minimum penetration force (N)

	TriboGlide	MDX	As-received	Silicone	Bare
18 Gage					
Inviro Medical	0.905	0.836	0.802	1.038	2.748
22 Gage					
Inviro Medical	0.629	0.544	0.540	0.743	1.537
Myco Medical	0.688	0.553	0.533	0.813	1.653
SSB MT1300 16 mm		2.726	NA	9.724	NA
MT 1300 25.4 mm		3.647	NA	7.951	NA
A130 25.4 mm	1.322	1.064	NA	1.666	
26 Gage					
Myco Medical	0.539	0.421	0.461	0.680	1.157
30 Gage					
Inviro Medical	0.393	0.339	0.460	0.532	0.806

As seen in Table 8, the as-received needles had the lowest penetration force for the 18 and 22 gage steel needles. The MDX coating had the lowest force for all other needles. For the 22 gage needles the lowest penetration force is 0.533 N, which was

achieved by a Myco Medical needle. The lowest plastic needle penetration force is around twice the steel needle force at 1.064 N. There is still room for improvement; however this value is more than half the value of the lowest penetration force seen in previous studies [11].

4.2 Buckling results

Three types of buckling analysis are presented in this section. First, they are presented separately, and then compared to one another in Section 4.2.4.

4.2.1 Physical buckling results

The results from the 22 gage buckling tests are as follows: 22 gage steel 25.4 mm, 42.18 N; 22 gage Vectra A130 25.4 mm solid, 5.79 mm; 22 gage SSB MT1300 25.4 mm solid, 6.98 N; Vectra SSB MT1300 16 mm solid, 8.98 N; SSB MT1300 16 mm hollow, 9.70 N. These data are also presented in Table 9. The table includes the average critical buckling load for the five needle types tested, along with the standard deviation among the groups.

Table 9 - Physical buckling test results

	Average Critical Buckling Load (N)	Standard Deviation
22 Ga. Steel 25.4 mm		
Hollow	42.18	2.81
A130 25.4 mm		
Solid	5.79	0.24
MT 1300 25.4 mm		
Solid	6.98	1.63
MT 1300 16 mm		
Solid	8.98	1.70
Hollow	9.70	1.84

4.2.2 Finite element buckling results

The results from the ANSYS finite element analysis of the simplified needle design are shown in Table 10. The table includes the critical buckling load of the different types of needle along with the percent difference between the hollow and solid needle analysis results.

Table 10 - ANSYS simplified needle critical buckling loads, cannula only

Needle Type	Critical Buckling Load (N)		Elastic Modulus (GPa)
	25.4 mm	**16 mm**	
Steel			
Hollow	64.712	161.83	200
Solid	78.179	196.49	200
Ixef 1022			
Hollow	6.471	16.183	20
Solid	7.818	19.649	20
Vectra A130			
Hollow	4.853	12.137	15
Solid	5.863	14.736	15
SSB MT1300			
Hollow	3.43	8.577	10.6
Solid	4.143	10.414	10.6
Polystyrene			
Hollow	0.971	2.427	3
Solid	1.173	2.947	3

From Table 10, the critical buckling load of the steel needle is significantly higher than that of the other materials; however the buckling load of all of the materials except polystyrene is higher than the average penetration force seen in all of the plastic needles for both hollow and solid needles. In addition the buckling strength of the solid needles is around 21% higher than that of the hollow needles. This value is worth noting; however the estimated critical loads for the hollow needles are below the penetration forces of the plastic needles. Therefore the use of solid needle prototypes is a viable method for testing needle designs. One clear interpretation of the data is that a directly

linear relationship exists between a material's elastic modulus and the critical buckling load of the needle. The critical buckling load versus elastic modulus data points are plotted and trend lines are fitted to obtain the linear equations that correlate to the different needle types. This is shown in Figure 35.

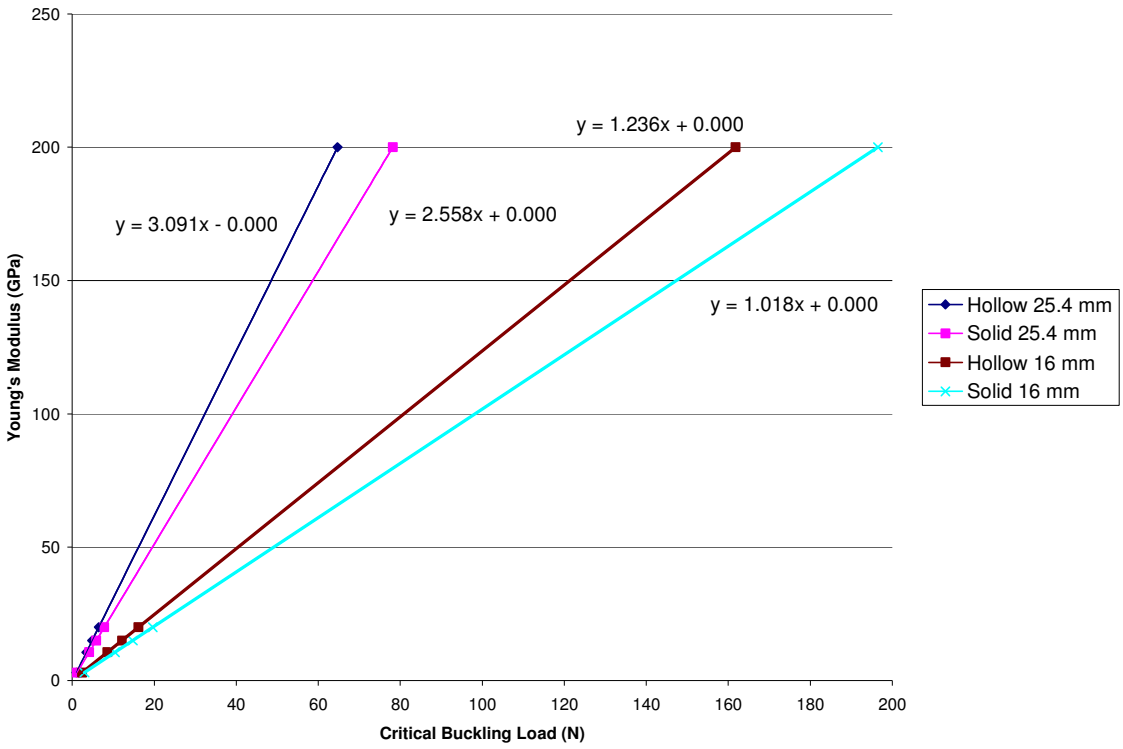

Figure 35 - Plot of ANSYS buckling data

The equations developed by linear regression for linear buckling of the simplified 25.4 mm solid and hollow needle are Equations 8 and 9, respectively.

$$E = 2.558P_{cr} + 3.265*10^{-4} \quad (8)$$

$$E = 3.091P_{cr} - 1.959*10^{-5} \quad (9)$$

In Equations 7 and 8, E represents the elastic modulus of the material (GPa) and P_{cr} represents the critical buckling load (N). They are setup to determine the elastic

modulus that corresponds to a particular buckling load. If the average penetration force of the plastic needles is input into these equations, then the lower limit of a useful elastic modulus can be determined. Using the average penetration force from the MDX coated Vectra A130 needles (1.626 N), the corresponding minimum elastic modulus for a 25.4 mm hollow needle is 5.03 GPa. This does not include any safety factor. This eliminates polystyrene from being a viable option, as its elastic modulus is only 3 GPa. This supports the assumption presented earlier in Chapter 2.

The equations developed for linear buckling of the simplified 16 mm solid and hollow needle are Equations 10 and 11, respectively.

$$E = 1.018P_{cr} + 2.913*10^{-4} \quad (10)$$

$$E = 1.236P_{cr} - 2.340*10^{-4} \quad (11)$$

Using Equation 11 and the penetration data from the Vectra A130 needles, the minimum elastic modulus for a 16 mm plastic needle is 2.00 GPa. This does not include the strength of the tip, only that of the cannula.

To determine the strength of the tip, finite element models were run of the entire 22 gage needle model. Figure 36 shows the deformation output from ANSYS of the complete model with steel material properties.

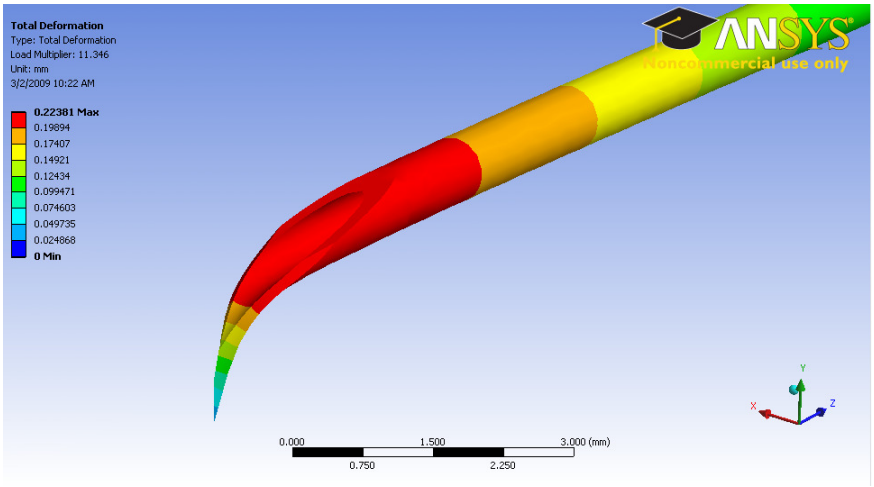

Figure 36 - Deformed tip model from ANSYS analysis

This model does not include deformation of the needle shaft because the finite element analysis is stopped once a critical deformation is reached. This critical deformation will occur in the tip because it is clearly the weakest point of the model. Deformation of the tip does not necessarily correlate with complete needle failure because the shaft is still capable of supporting a load even with the tip deformed. This is supported by the difference between the physical buckling data and the FEA buckling data of the complete model. The data from the FEA of the complete model are shown in Table 11. The data include the analysis of five different materials considered for plastic needles.

Table 11 - ANSYS critical tip loads

	Critical Tip Load (N)	Elastic Modulus (GPa)
Steel	11.35	200
Ixef 1022	1.13	20
Vectra A130	0.85	15
Vectra MT1300	0.60	10.6
Polystyrene	0.17	3

The data from Table 11 is plotted and a linear model is fit relating critical tip load and elastic modulus. This plot can be seen in Figure 37.

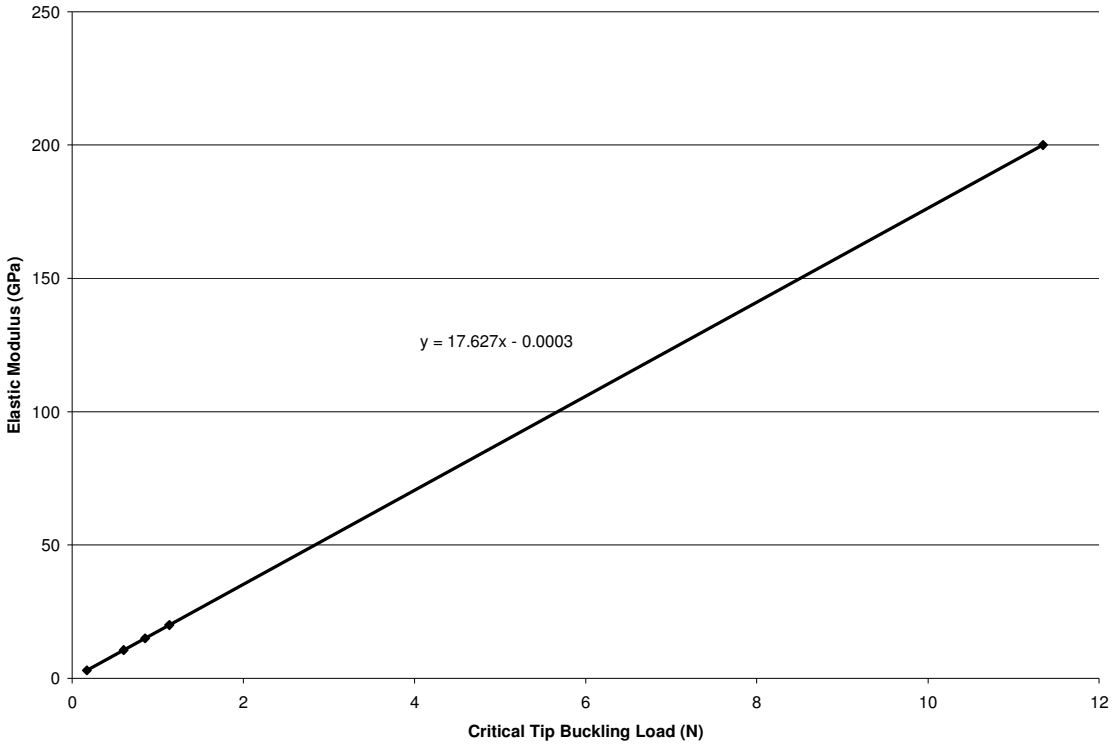

Figure 37 - Critical tip load plot

Equation 12 is derived from Figure 36. It relates critical tip load to material strength. This equation is only valid for tips with the geometry of a 22 gage steel hypodermic needle. This equation is used for further discussion in Chapter 5.

$$E = 17.627 P_{cr} - 0.0003 \tag{12}$$

Equation 12, like the others, returns the estimated elastic modulus for an input critical tip load. These estimates are made in Chapter 5.

4.2.3 Buckling equation results

The critical buckling loads of the simplified needle model also are determined using the equations presented in Chapter 3. The analysis was conducted using an Excel spreadsheet. The physical characteristics of the different needle types are shown in Table 12.

Table 12 - Physical properties of needle types

	Moment of Inertia (m^4)	Cross Sectional Area (m^2)	Radius of Gyration (m)	Actual Slenderness Ratio
25.4 mm				
Hollow	1.041E-14	2.331E-07	0.000211	120.16
Solid	1.256E-14	3.973E-07	0.000178	142.85
16 mm				
Hollow	1.041E-14	2.331E-07	0.000211	75.69
Solid	1.256E-14	3.973E-07	0.000178	89.98
Critical Slenderness Ratio				
Vectra A130	27.91			
Vectra MT1300	23.97			
Ixef 1022	26.55			
Polystyrene	31.41			
Steel	65.50			

As can be seen from Table 12, the slenderness ratio of every needle type is greater than the critical slenderness ratio corresponding to the different material properties. Therefore the Euler buckling equations are used to determine the critical buckling load relating to each needle type. The critical buckling loads determined by solving the Euler buckling equations are shown in Table 13.

Table 13 - Buckling equation results

	Type	P_{cr} (N)
Hollow 25.4 mm		
Steel	Euler	65.21
Ixef 1022	Euler	6.52
Vectra A130	Euler	4.89
Vectra MT1300	Euler	3.46
Polystyrene	Euler	0.98
Solid 25.4 mm		
Steel	Euler	78.64
Ixef 1022	Euler	7.86
Vectra A130	Euler	5.90
Vectra MT1300	Euler	4.17
Polystyrene	Euler	1.18
Hollow 16 mm		
Steel	Euler	164.34
Ixef 1022	Euler	16.43
Vectra A130	Euler	12.33
Vectra MT1300	Euler	8.71
Polystyrene	Euler	2.47
Solid 16 mm		
Steel	Euler	198.19
Ixef 1022	Euler	19.82
Vectra A130	Euler	14.86
Vectra MT1300	Euler	10.50
Polystyrene	Euler	2.97

4.2.4 Comparison of buckling data

Both forms of simplified needle analyses yielded similar results, however the complete needle analyses varied significantly. During physical testing, the needle tip buckled before catastrophic cannula failure. Tip deformation results in the cannula no longer being coaxial with the direction of loading. This causes the loading to be transferred from a purely axial loading to an axial load as well as a moment about the hub (eccentric loading). This combination of loading reduces the critical buckling load of a column [19], and can explain the variation in the data. Table 14 shows a comparison of all the buckling data.

Table 14 - Combined buckling data

	Equations (N)	FEA Simplified (N)	Physical (N)	FEA Tip (N)
Hollow 25.4 mm				
Steel	65.21	64.71	42.18	11.35
Ixef 1022	6.52	6.47		1.13
Vectra A130	4.89	4.85		0.85
Vectra MT1300	3.46	3.43		0.60
Polystyrene	0.98	0.97		0.17
Solid 25.4 mm				
Steel	78.64	78.18		
Ixef 1022	7.86	7.82		
Vectra A130	5.90	5.86	5.79	
Vectra MT1300	4.17	4.14	6.98	
Polystyrene	1.18	1.17		
Hollow 16 mm				
Steel	164.34	161.83		
Ixef 1022	16.43	16.18		
Vectra A130	12.33	12.14		
Vectra MT1300	8.71	8.58	9.70	
Polystyrene	2.47	2.43		
Solid 16 mm				
Steel	198.19	196.49		
Ixef 1022	19.82	19.65		
Vectra A130	14.86	14.74		
Vectra MT1300	10.50	10.41	8.98	
Polystyrene	2.97	2.95		

The plastic needle results are consistent across the three types of analysis. The physical tests for the MT1300 group were slightly lower than the analytical results. This difference is likely attributable to the tip of the needles. The deformation of the tip is unaccounted for in the analytical results. This deformation results in eccentric loading of the needle, and thus lowers critical buckling loads. The same type of deformation can be attributed to the difference in the physical and analytical analyses of the steel needles.

In addition, the steel and MT1300 needles tended to buckle via ductile failure, where as the A130 needles tended to buckle via brittle failure. Therefore, the steel and MT1300 needles tend to deform more than the A130 needles prior to failure. This

increased deformation would account for increased eccentric loading that is not accounted for in the analytical models.

The consistency of the testing allows for assumptions on material strength to be made based upon the FEM analysis. These conclusions are presented in Chapter 5.

4.3 Tip characteristic measurements

Three physical characteristics of the needles that are measured are cannula diameter, tip radius, and tip angle. The diameters of ten needles from each group were measured using digital calipers. There was no discernable variation between measurements, so the data are not presented as an average. The diameters of the needles are reported in Table 15.

Table 15 - Needle cannula diameter measurements

Needle Type	Measured Cannula Diameter (mm)	Required ISO 9620 Diameter (mm)
30 ga. Inviro Medical	0.30	0.30
26 ga. Myco Medical	0.44	0.45
22 ga Myco Medical	0.69	0.71
22 ga. Inviro Medical	0.69	0.71
22 ga. Vectra A130	0.71	0.71
22 ga. Vectra MT1300	0.75	0.71
18 ga. Inviro Medical	1.26	1.27

In addition, the tip radii of the needles used for testing are measured. The results are grouped by tip radius within a range of three micrometers, i.e., 0-3 μm, 3-6 μm, 6-9 μm. The grouped data are averaged to provide a value associated with each range of tip radii. The average penetration forces among each group of tip radii are presented in Tables 16, 17, 18, and 19. The data are separated by needle diameter, tip radii, and lubricant used.

Table 16 - Average load (N) with corresponding tip radius, 18 gage

Tip Radius (μm) / Needle Type	0-3	3-6	6-9	9-12	12-15	21-24	27-30	45-48
As-Received	0.855	0.960	0.963	1.148				
TriboGlide	0.929	1.011		0.905	1.246	1.105	1.424	1.799
Silicone	1.038	1.145	1.213	1.266				
MDX	0.851	0.932	0.974					
Bare	2.880	2.951	2.946					

Table 17 - Average load (N) with corresponding tip radius, 22 gage Myco Medical

Tip Radius (μm) / Needle Type	0-3	3-6	6-9	9-12	12-15	15-18	21-24	24-27	27-30	57-60	69-70
As-Received	0.599	0.591	0.587					0.874			
TriboGlide	0.718	0.701	0.784	0.755			0.873				
Silicone	0.749	0.804	0.815		0.806	0.812	0.823			2.198	
MDX	0.573	0.624	0.682								
Bare	1.757	1.777	1.777	1.758				1.733	1.732		3.531

Table 18 - Average load (N) with corresponding tip radius, 26 gage

Tip Radius (μm) / Needle Type	0-3	3-6	6-9	9-12	12-15	15-18	18-21	24-27	27-30	42-45	48-51
As-Received		0.599	0.577			0.590	0.583	0.676			
TriboGlide	0.646	0.617	0.614		0.633		0.696	0.647			
Silicone	0.763	0.766	0.831	0.828							
MDX	0.456	0.495	0.500						0.543	0.693	0.725
Bare		1.305	1.248		1.354			1.225			

Table 19 - Average load (N) with corresponding tip radius, 30 gage

Tip Radius (μm) / Needle Type	0-3	3-6	6-9	9-12	18-21	27-30
As-Received	0.503	0.512	0.477	0.595		
TriboGlide	0.394		0.477	0.469	0.497	0.884
Silicone	0.550	0.598	0.599	0.641		
MDX	0.376	0.370	0.394			
Bare	0.927	0.990	1.010			

If no value is present in the table, then a needle correlated to the tip radius range and needle type of the vacancy was not tested. From Tables 16, 17, 18, and 19, it is evident that the load increases as the tip radius increases. Therefore it can be concluded that penetration force is dependent upon tip radius. This data is used in Chapter 5 to develop a model relating penetration force to tip radius.

The tip radii of the SSB MT1300 needles are consistent for all of the needles tested. Because their geometry varies significantly from the 22 gage steel needles, the tip contact area is estimated to form a comparison instead of tip radius. The tip contact area of the SSB MT1300 needles is estimated to be $2.69*10^{-8}$ m^2. The tip radii for the Vectra A130 needles are also measured. The results of these measurements are presented with the corresponding penetration force for each needle in Table 20.

Table 20 – 22 gage Vectra A130 tip radii measurements

	Tip Radius (µm)	Penetration Force (N)
TriboGlide	21	1.38
	75	2.54
	33.5	1.34
	46	1.73
	32.5	1.63
	20	1.61
	75	3.40
	27	1.66
	20	1.71
Silicone	55	2.46
	32.5	1.84
	35	2.25
	103	5.17
	30	1.93
	15	1.67
	35	1.66
MDX	31	2.29
	45	1.31
	19	1.47
	17	1.23
	34	1.14
	21	1.06
	19	1.44
	67	2.62
	30	1.76
	73	2.15
	84	2.36
	54	2.69
	49	2.30
	20	1.30
	26	1.21

The tip angles of the various needles also are measured using the same method that was used for the tip radius measurements. The average measured tip angles for the different needle types are as follows: 30 gage, 45.8°; 26 gage, 47.3°; 22 gage, 55°; 18 gage, 63°. No needles tested had variations in tip angle within groups, i.e., all 18 gage needles had the same tip angle, all 22 gage needles had the same tip angle, etc. Despite

the lack of tip angle variation among groups, an effect of tip angle was detectable between gages, as the greater tip angle required more penetration force. The effect that tip angle has on penetration force, as well as the method for determining this effect, is discussed thoroughly in Chapter 5.

4.4 Coefficient of friction test results

The coefficients of friction for steel coated with MDX against polyurethane, steel coated with silicone against polyurethane and bare steel against polyurethane were measured by the method outlined in Chapter 3. The resulting coefficients are presented in Table 21.

Table 21 - Measured coefficients of friction for steel against polyurethane

Lubricant	Coefficient of Friction
MDX	0.11
Silicone	0.17
None	0.87

From Table 21, it can be seen that MDX has the lowest measured coefficient, and the coefficient of bare steel is significantly higher than that of the lubricants. Coefficients for the other lubricants could not be measured directly. The steel blocks used for estimating the coefficients were too large to fit within the device used to apply the TriboGlide coating, and the two manufactures of needles that were tested do not provide information on their coating processes. Therefore, coefficients of friction for the TriboGlide and as-received lubricants must be estimated using the known coefficients of the MDX and Silicone treatments and the data from the penetration tests. In addition, plastic blocks made out of the resins used to manufacture plastic needles were not available. Therefore the plastic coefficients could not be directly measured.

It is known that a portion of the penetration force is a result of the friction between the polyurethane and the needle [11]. After penetration, the normal force of the polyurethane acting on the cannula of the needle tends to level out to a particular value depending upon the lubricant on the needle. This is shown in Figure 26 in Section 4.1.2. This portion of the data provides information that can be used to extract the coefficient of friction based on Equation 7 from Chapter 3. The post-penetration data are collected and averaged over multiple penetrations for the different needle and lubricant types to provide the frictional force. The data are plotted against the corresponding known coefficient of friction, providing two data points for each of the five needle types. A linear regression is fit to each of the five data sets providing five equations relating average frictional force to coefficient of friction. Using these five equations and the corresponding frictional forces of the TriboGlide and as-received needle groups, the unknown coefficients of friction can be solved for. The equations provide five estimates for the coefficients of friction which are averaged to provide a single value for the coefficient of friction between TriboGlide coated steel and polyurethane. The process for TriboGlide application is known to be similar for all needle types, so it is assumed that averaging the results across all five needle types will provide a more accurate estimation. The values for the as-received needles are not averaged because the application process for each needle type is not known. In addition, these estimations are based on the assumption of a linear relationship between the coefficients of friction, particularly between the range of the MDX and silicone coefficients (0.11 – 0.17). The coefficient of friction between bare steel and polyurethane is not included in the analysis because its value is much greater

than the other coefficients. These five plots relating frictional force and coefficient of friction are shown in Figure 38.

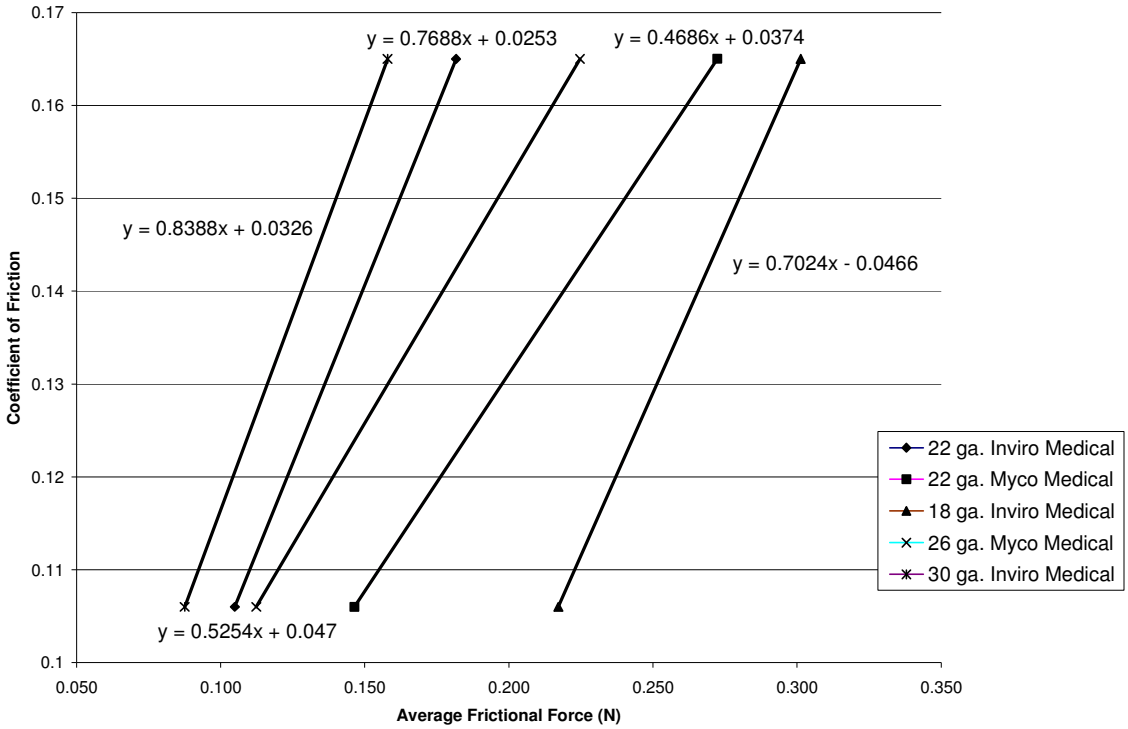

Figure 38 - Average post-penetration frictional force vs. coefficient of friction

The developed regression equations for the five needle types are as follows:

22 gage Inviro Medical

$$\mu = 0.7688F_f + 0.0253 \tag{13}$$

22 gage Myco Medical

$$\mu = 0.4686F_f + 0.0374 \tag{14}$$

18 gage Inviro Medical

$$\mu = 0.7024F_f - 0.0466 \tag{15}$$

26 gage Myco Medical

$$\mu = 0.5254F_f + 0.047 \tag{16}$$

30 gage Inviro Medical

$$\mu = 0.8388F_f + 0.0326 \quad (17)$$

In Equations 13-17, F_f is the average post-penetration frictional force (N). The unknown coefficients of frictions are determined using these equations and the average frictional force of the TriboGlide and the as-received needles. The results are shown in Table 22.

Table 22 - Estimation of coefficients of friction

	Average Frictional Force (N)				**Coefficient of Friction**	
	TriboGlide	**MDX**	**Silicone**	**As-Received**	**TriboGlide**	**As-Received**
22 ga. Inviro Medical	0.142	0.105	0.182	0.098	0.135	0.101
22 ga. Myco Medical	0.195	0.146	0.272	0.130	0.129	0.098
18 ga. Inviro Medical	0.244	0.217	0.301	0.206	0.125	0.098
26 ga. Myco Medical	0.177	0.112	0.225	0.126	0.140	0.113
30 ga. Inviro Medical	0.124	0.088	0.158	0.130	0.137	0.142
				Average Coefficient	0.133	

From Table 22, it is seen that the coefficient of friction for TriboGlide falls between the MDX and Silicone treatments at 0.133. The as-received lubrication is slightly lower than the others at 0.1. These coefficients are estimated under the assumption that the normal force acting on the needle after penetration occurs is the same for all steel needles, based upon the fact that they all have the same tip geometry and same penetration mechanism. As pointed out earlier in Section 4.1.2, the penetration mechanism for the plastic needles is not consistent with that of the steel needles, so the same assumption cannot be made. Therefore, the coefficient of friction between the plastic needles and polyurethane film is left undetermined at this point.

4.5 Summary

The data recorded that are used to characterize a hypodermic needle penetration through polyurethane film are presented in Chapter 4. The data are the results of testing outlined in Chapter 3. Results for maximum penetration force, multiple penetration force, buckling tests, needle characteristic measurements, coefficients of friction, and polyurethane stiffness are presented both graphically and by tables showing the raw data. This information is used in Chapter 5 to characterize a hypodermic needle penetration through film.

CHAPTER 5

ANALYSIS AND DISCUSSION

Chapter 5 discusses the data presented in Chapter 4, which are used to develop a penetration equation through polyurethane film. In addition, conclusions are drawn on plastic needles and comparisons are made between steel and plastic needle penetration.

5.1 Analysis of penetration

Many studies have been conducted on the behavior of a needle penetration [33-37]. One model [33] suggests the penetration force is composed of three parts: stiffness force, which is attributed to the stiffness of the penetration material that is dependent upon the elastic modulus of that material and is related to the force necessary to open the material; frictional force, which is attributed to the friction seen between the needle and the material being penetrated; and cutting force, which is the force required to tear the material. This model is represented by Equation 19.

$$F_{total} = F_s + F_f + F_c \tag{19}$$

Where F_{total} represents the total penetration force, F_s represents the force associated with the stiffness of the material being penetrated, F_f represents the frictional force, and F_c represents the cutting force. This model is used to estimate the penetration force into a solid object, such as a bovine liver, and postulates that the force existing at the tip of the needle is a combination of stiffness and cutting forces. The definition of penetration in these studies is breaking through the outer membrane of the material being penetrated, and the cutting force is considered to be the force required to tear the object

after penetration [34]. The stiffness forces are a result of compressed tissue in front of the needle tip [33].

Most of the information used to create the penetration force model is obtained from the penetration plot of the needle into polyurethane. An example plot of a 22 gage steel needle with silicone lubrication is shown in Figure 39.

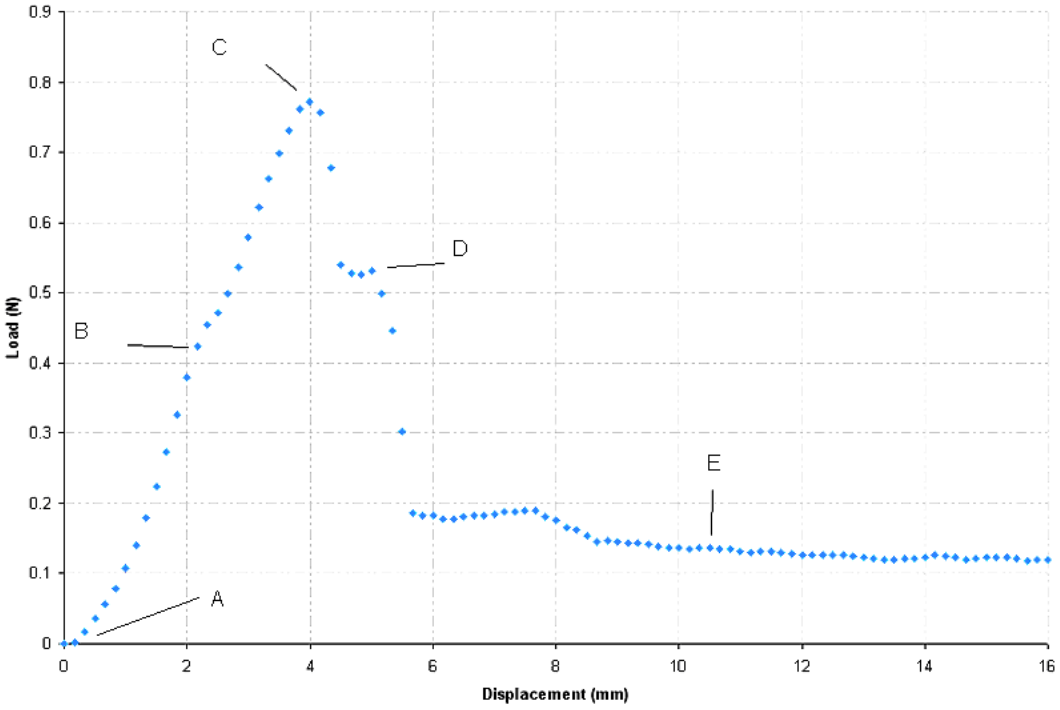

Figure 39 - Example steel hypodermic needle penetration into polyurethane film plot

The different regions of the plot can be described as follows. The region denoted as "A" on the plot is the point of initial contact between the needle and polyurethane material. Once the needle contacts the film, the load increase up until point "B" is directly related to the stiffness of the material. Point "B" is the puncture point which is the point of initial penetration, when the needle tip initially breaks through the polyurethane. Point "C" is the point at which the cutting of the film is complete and the

needle has been inserted up to its widest point, i.e., the outer diameter of the needle. Point "D" is the point of insertion where the film is transferred from the beveled face of the needle tip to the cannula. Relaxation and equilibrium of penetration force occur at "E", as this is the point of the penetration where the film slides along the cannula of the needle. All of these points are useful in determining how the different variables affect the penetration force, particularly points "C" and "E". "C" is the maximum penetration force and is the primary source of the penetration equations. "E" is used to determine unknown coefficients of friction. The method for determining equations relating friction, tip radius, and diameter are outlined in the next two sections.

5.1.1 Effect of frictional force

Many methods have been tested to determine the effect of frictional force on the penetration of a needle. One test utilizes a 7-axis load cell to determine the frictional affect [36]. Another method used repeated penetrations into an existing hole which was made by the needle [33]. While these methods proved to be effective at estimating frictional force, a simpler method was developed for this study that produced an accurate model of the frictional force. This method uses the coefficients of friction between the various lubricants and polyurethane along with maximum penetration force for each needle. Using an altered form of Equation 19 for the summation of forces which combines the cutting and stiffness forces and the assumption that the ideal cutting force will be constant [33] for all penetrations of the same gage needle regardless of coefficient of friction, Equations 20 can be developed.

$$
\begin{aligned}
F_t &= F_f + F_c \\
F_{t\_1} &= F_{f\_1} + F_{c\_1} \\
F_{t\_2} &= F_{f\_2} + F_{c\_2} \\
F_{c\_1} &= F_{c\_2} \\
F_{t\_1} - F_{t\_2} &= \Delta F_{1\_2} = F_{f\_1} - F_{f\_2}
\end{aligned}
\qquad (20)
$$

For Equations 20, the subscript *t* represents total force, *f* represents frictional force, and c represents cutting force. The numerical subscripts *1* and *2* represent two different lubricant types. Based on these equations the difference in total penetration force between needles with different lubricants is solely dependent upon the difference between the frictional forces of the two lubricant types. This difference in frictional force is attributed to the difference in the coefficients of friction of the two lubricants. Assuming a linear relationship between coefficient of friction and frictional force (based on Equation 7); if the difference in frictional force is plotted against the difference in coefficient of friction, then a relationship is created between the change in coefficient of friction and the change in frictional force. From the linear assumption, this can be expanded to compare coefficient of friction and frictional force for a single lubricant type. To support this, the differences in average penetration forces between every type of needle lubrication are plotted against the corresponding changes in coefficients of friction. The plot of this for the four gages of needle tested is shown in Figure 40. Only data for steel needles are included in this plot, as they are the only group of needles that are assumed to have the same penetration mechanism and thus an equivalent normal force. This assumption is described in Section 4.1.2.

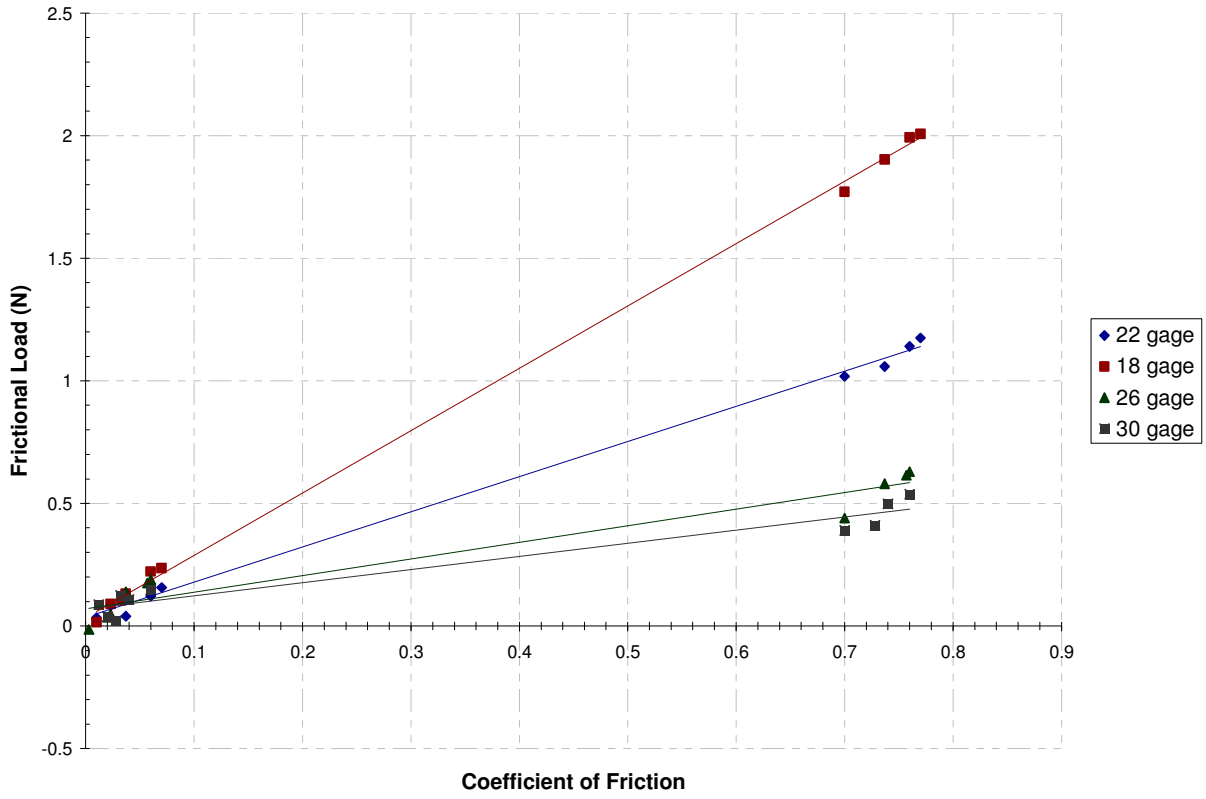

Figure 40 - Plot of change in coefficient of friction vs. change in average load for steel needles

The linear relationship is evident in Figure 40. It is also obvious that larger diameter needles require a larger penetration force as the coefficient of friction is increased. The effect of diameter can be accounted for by multiplying the coefficient of friction by the diameter of the specific needle then plotting that against the corresponding change in load. The force of friction is a result of the normal force that the polyurethane is imparting on the needle, which is attributed to the resistance to deformation of the polyurethane. Scaling by the diameter of the needle is sensible, as it scales with the perimeter of the needle which relates to contact area between the needle and the film, as well as the stretching of the film. This scaling allows a linear regression relating

coefficient of friction, needle diameter, and frictional force to be developed. This plot is shown in Figure 41.

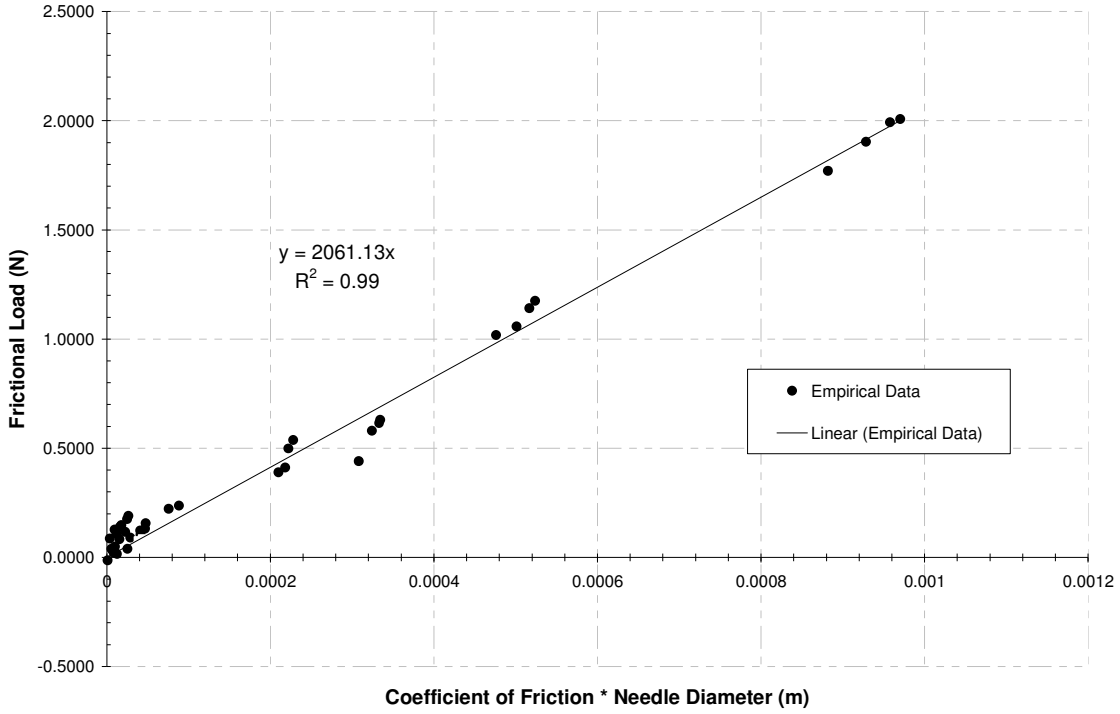

Figure 41 - Coefficient of friction * diameter versus frictional load plot

From this plot, an equation which estimates frictional force based upon needle diameter (perimeter) and coefficient of friction is developed. The equation fits the data well with an R^2 value of 0.99. This is shown as Equation 21.

$$F_f = 2061\mu d \qquad (21)$$

In Equation 20 F_f is the estimated frictional force in Newtons, μ is the coefficient of friction, and d is the outer diameter of the needle in meters. A good test of the validity of this equation is to compare the similarity of the cutting forces of the different lubrication types that is extracted from subtracting the estimated frictional force from the average penetration force. The average estimated frictional force, cutting force, average

cutting force, and standard deviation are all shown in Table 22. As can be seen in Table 23, the standard deviation of the averaged cutting forces is low for each group, which supports the accuracy of the model.

Table 23 - Estimated frictional forces and resulting cutting forces on steel needles

	Bare	Silicone	TriboGlide	MDX	As Received	Average Cutting Force (N)	Standard Deviation (N)
18 gage							
Average Penetration Force (N)	2.927	1.156	1.024	0.934	0.920		
Estimated Frictional Force (N)	2.259	0.441	0.345	0.286	0.260		
Resulting Cutting Force (N)	0.668	0.715	0.679	0.649	0.660	0.674	0.025
22 gage							
Average Penetration Force (N)	1.767	0.749	0.709	0.627	0.593		
Estimated Frictional Force (N)	1.219	0.238	0.186	0.154	0.140		
Resulting Cutting Force (N)	0.548	0.511	0.523	0.472	0.452	0.501	0.039
26 gage							
Average Penetration Force (N)	1.120	0.680	0.540	0.491	0.505		
Estimated Frictional Force (N)	0.789	0.1542	0.1206	0.1	0.102		
Resulting Cutting Force (N)	0.331	0.526	0.419	0.391	0.403	0.414	0.071
30 gage							
Average Penetration Force (N)	0.920	0.530	0.422	0.383	0.509		
Estimated Frictional Force (N)	0.547	0.107	0.082	0.069	0.089		
Resulting Cutting Force (N)	0.373	0.423	0.340	0.313	0.419	0.374	0.048

The slope of the equation (2061 N/m) is likely attributed to both the thickness and the elastic modulus of the material. The elastic modulus defines the elasticity of the

material, and thus the amount of force it will apply to the needle as it is being stretched. The thickness defines how much of the material will be deformed. It is found that Equation 21 can be generalized further to include the elastic modulus of the polyurethane film as well as the thickness. The elastic modulus of the material is 5 MPa, and the thickness is 0.381 mm. Multiplying these values together returns a value of 1905 N/m, which is only 7.5% different than the estimated slope of 2061 N/m. It is reasonable that this difference is a result of the variation of the material's elastic modulus from the measured value. This makes sense physically, as the variables represent the amount that the material must stretch (needle diameter), the thickness of material displaced (material thickness), and the resistance to stretching (modulus of elasticity). When combined, the dimensions of the variables reduce to force. The generalized equation which eliminates the Y-intercept and includes the elastic modulus and thickness of material is shown as Equation 22.

$$F_f = \mu E_f t_f d \tag{22}$$

In Equation 22, F_f is the estimated frictional force in Newtons, μ is the coefficient of friction, E_f is the elastic modulus of the material (Pa), t_f is the thickness of the film (m), and d is the diameter of the needle (m). While this equation was found to estimate the maximum frictional force that polyurethane film imparts on a needle during penetration, further exploration comparing the behavior of other penetration media is necessary for validation outside of this particular case. In order to provide a visualization of Equation 21 compared to Equation 22, the two are compared. This plot is shown in Figure 42.

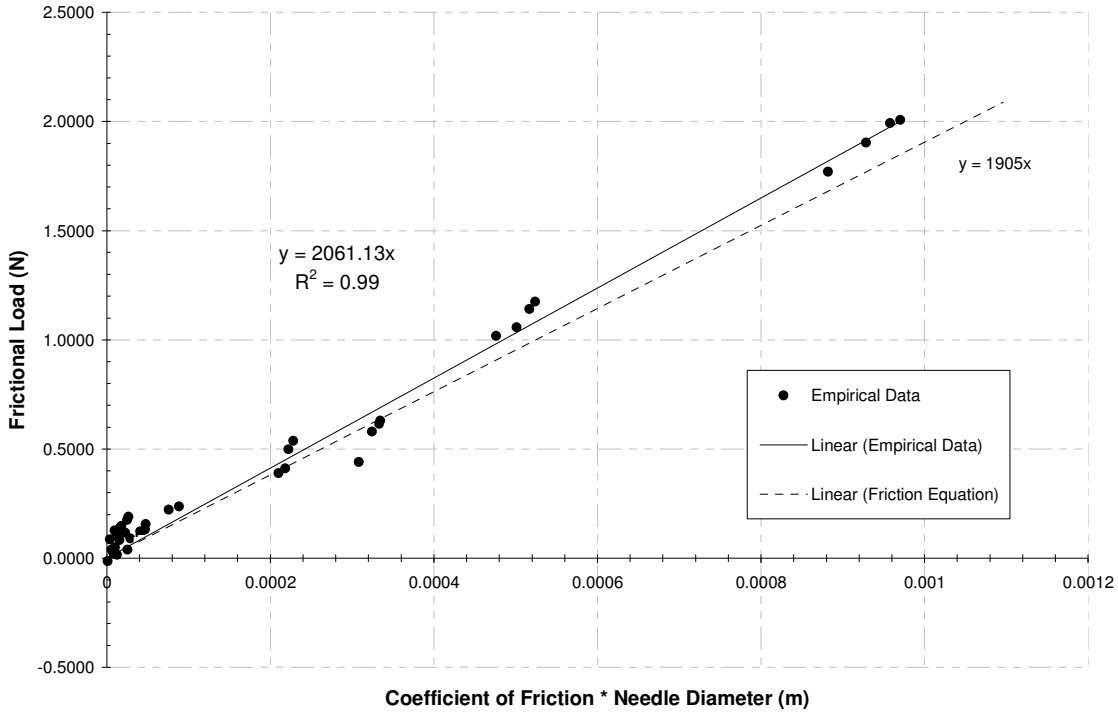

Figure 42 - Comparison of empirical data and friction force equation

The new equation corresponds closely to the empirical data, as can be seen in Figure 42. Equation 22 is used in the following section to develop an equation predicting cutting force.

5.1.2 Estimation of cutting force

Once the frictional forces were isolated, the cutting force was determined by subtracting the calculated frictional force from the total force. These data are presented in Table 22. In order to determine the effect of tip radius and diameter on the cutting force for steel hypodermic needles, the data presented in Tables 16, 17, 18, and 19 are used. The cutting forces for each tip radius range are averaged across the different lubricant types. This is done based on the assumption that cutting force is not dependent

upon lubricant. Previous studies have shown that penetration force is related to the tip radius by a linear relationship between the cutting force and the tip area (as determined from tip radius) [36]. It was determined this relationship is applicable to these data as well. To determine this relationship, the tip contact area is estimated using the tip angle and tip radius. The contact tip area increases as the tip angle increases. Likewise, the tip contact area increases as the tip radius increases. The tip contact area is simplified as being the surface area of the cap of a sphere. This is represented in Figure 43.

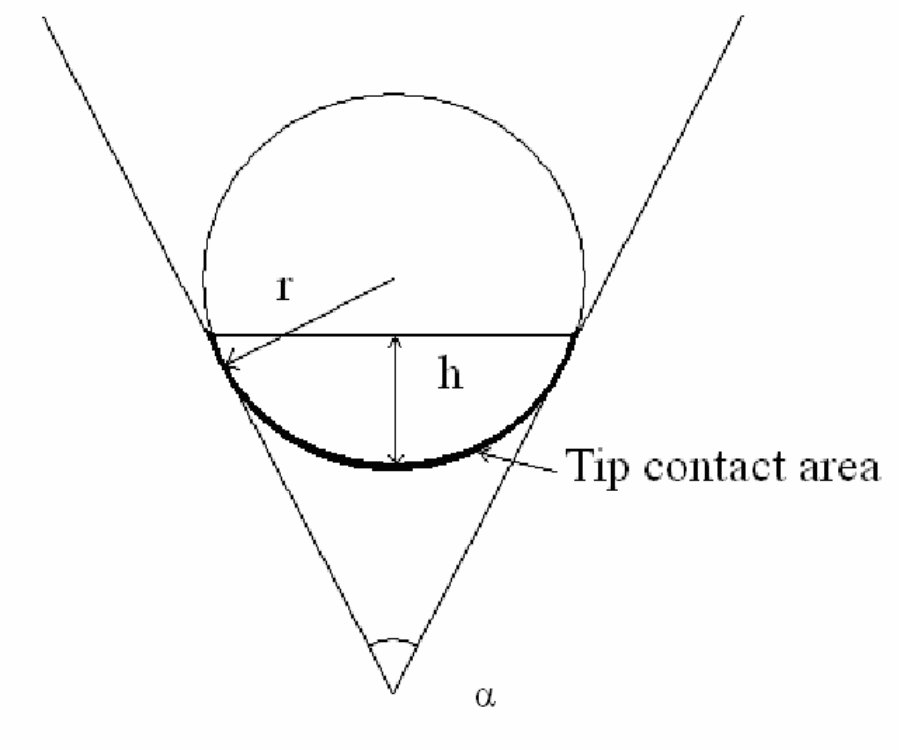

Figure 43 - Representation of tip contact area

From Figure 43, the percentage of the sphere surface area is based upon h, which is the vertical distance from the point where the tip angle intercepts the outer edges of the tip to the point of the needle. This relationship can be described by Equation 23.

$$A_t = 2\pi r^2\left[1-\sin\left(\frac{\alpha}{2}\right)\right] \tag{23}$$

From Equation 23, A_t is the tip contact area (m^2), r is the tip radius (m), and α is the tip angle. The tip contact area is then plotted against the cutting force to determine their relationship. This is shown in Figure 44. The data are grouped by needle gage.

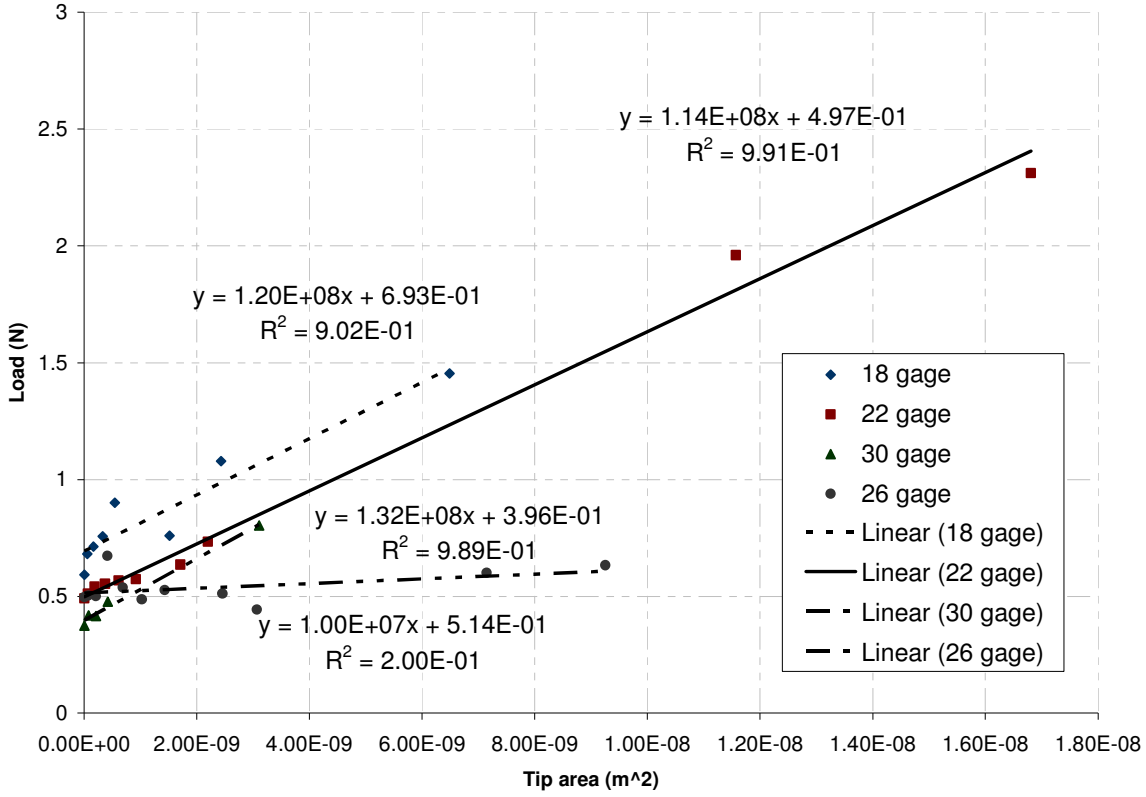

Figure 44 – Tip contact area vs. cutting force, steel hypodermic needles

There is an evident increase in cutting force that corresponds to an increase in tip contact area. This increase is fit with a linear regression for the separate gages, which is shown in Figure 44. The regression fits all data sets well, except for the 26 gage needles. This leads to the belief that the 26 gage needles were damaged between penetration force measurement and tip measurement, which would explain why the larger tip area do not correspond to higher penetration forces. It is also evident that the cutting forces increase as the needle gage increases. The significant factor that changes between gages is the

needle diameter. In order to determine the effect of diameter, the separate equations from Figure 44 are inspected. They are shown below as Equations 24, 25, and 26 for 18 gage, 22 gage, and 30 gage, respectively.

$$F_c = 120 * 10^6 A_t + 0.693 \quad (24)$$

$$F_c = 114 * 10^6 A_t + 0.497 \quad (25)$$

$$F_c = 132 * 10^6 A_t + 0.396 \quad (26)$$

By inspecting Equations 24, 25, and 26, it is evident that the slopes of the equations are relatively constant for the different gages, while the y-intercepts increase as needle diameter increases. In order to interpret these constants, an understanding of the energy required to penetrate a membrane is necessary. There are two phases that occur during a sharp needle penetration, the initiation of puncture and the opening of the tear. The force that is required to initiate and continue the puncture is proportional to the contact area at the point of penetration and the penetration resistance of the material being penetrated, and the force required to open the material is proportional to the change in surface area of the new opening and the tear resistance of the material [37].

This previous study also determined that the force required to initiate a puncture had a linear relationship to tip area, which is supported by Figure 44. Based upon this, the slopes of Equations 24, 25, and 26 are assumed to be related to the force required to initiate and continue the puncture, as they are directly related to tip area. As needle diameter has nothing to do with tip contact area, it is assumed to have no influence on the slope of the equations, i.e., the force required to initiate and continue a puncture. It is found that by subtracting the load represented by the y-intercept from the cutting force data and plotting the result for each gage versus the tip contact area, a linear relationship

can be derived relating tip contact area to force for all gages. This is represented by Figure 45.

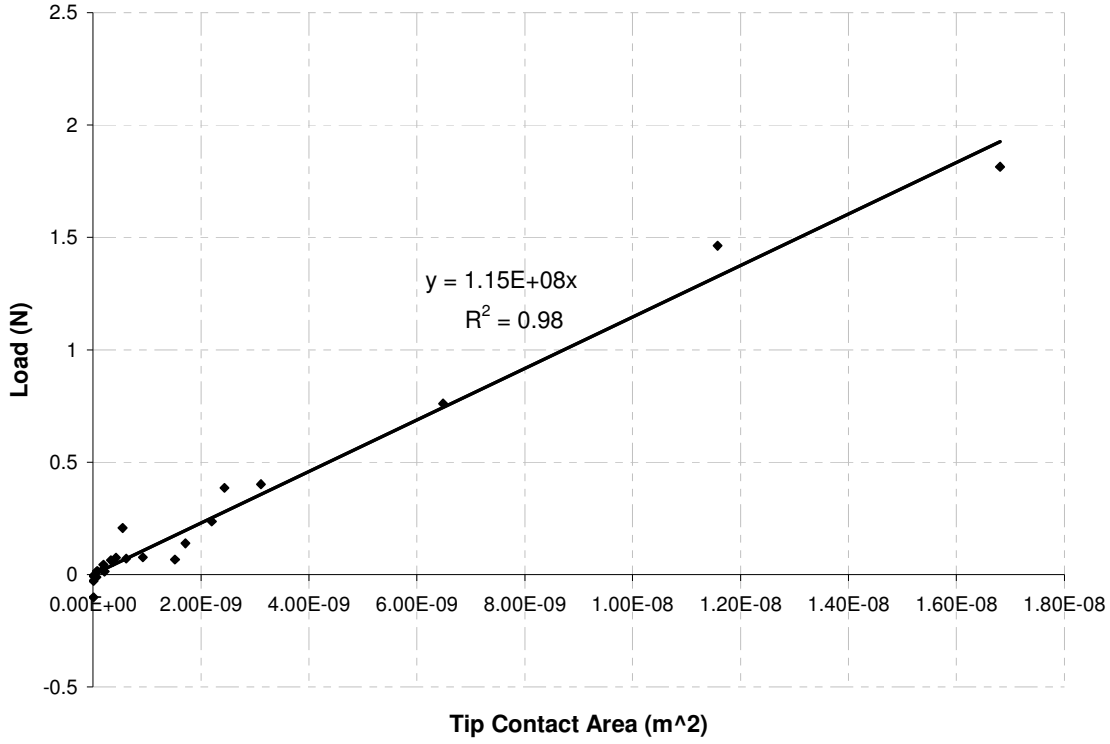

Figure 45 – Force required to initiate puncture vs. tip area

From Figure 45, an equation is developed relating the force required to initiate a puncture and tip contact area. This is shown as Equation 27.

$$F_i = 115 * 10^6 A_t \tag{27}$$

From Equation 27, F_i is the force required to initiate and continue a puncture (N) and A_t is the area of the tip (m^2). The force required to initiate a puncture is known to be related to the puncture resistance of a material which maintains units of work per unit area. Using this, along with the material thickness of the polyurethane, Equation 27 can be further generalized. This generalization is shown as Equation 28.

$$F_i = \frac{G_p A_t}{t_{field}} \tag{28}$$

From Equation 28, F_i is the force required to initiate the crack (N), G_p is the puncture fracture toughness of the material (Nm/m^2), A_t is the tip contact area (m^2), and t_{field} is the material thickness (m). The variable t_{field} is believed to be a numerical constant that is dependent upon the thickness of the material, and should reach an equilibrium level as the thickness approaches infinity. Further testing into thicker media is necessary to fully evaluate this constant. This generalization is only theoretical and needs further testing to support the influence of the material properties (G_p and t_{field}). The remainder of the analysis is conducted with G_p being equal to 43,662 Nm/m^2, which is the slope of Equation 27 multiplied by the thickness of the material (0.381 mm). The actual puncture resistance of the polyurethane is not known, however this value is on the same order of magnitude as other polymers that have been tested, so the assumption is not unreasonable. These known values ranged from 20 – 40 kJ/m^2 [38].

The influence of force required to open the tear is now assumed to be contained within the y-intercepts of Equations 24, 25, and 26. It is known that the work that is required to open a cut, the surface area of the cut, and the tear resistance are related. The relationship is defined by Equation 29 [36].

$$G_c = \frac{\delta W}{\delta A} \tag{29}$$

In Equation 29, G_c is the tear resistance (crack growth resistance) and is in the units of Joules per meter squared, δW is the work input to open the tear, and δA is the change in tear surface area. Equation 29 can be rearranged to solve for the work required to open a tear by multiplying the tear resistance by the change in surface area of the tear.

By assuming that the work is equal to the force required to open the tear multiplied by the displacement of the needle that is necessary to open the tear, the equation can be reduced to solve for maximum opening force. This is shown as Equation 30.

$$F_p = \frac{G_c A_c}{d_f} \tag{30}$$

From Equation 30, F_p is the force required to open the tear (N), G_c is the tear resistance (Nm/m^2), A_c is the surface area of the tear (m), and d_f is the displacement of the needle during the tear opening (m). G_c is the only variable not known in this equation. F_p is estimated by the y-intercepts from Equations 24, 25, and 26. A_c is estimated by assuming it is equal to the circumference of the needle cannula multiplied by the thickness of the film. This assumption is made assuming that the maximum opening force occurs at the widest point of opening. This point on the needle is at the end of the first bevel, where the diameter of the needle becomes constant. Therefore, the tear area would be equal to the diameter of the needle multiplied by the thickness of the material. The variable d_f is estimated by measuring the distance from the tip to the end of the first bevel on the needle. This is the point of the needle where the diameter stops increasing and remains equal to the cannula diameter. For Equation 30 to be accurate, inputting the known variables in to the equation should return a constant value for the tear resistance. This calculation is conducted, and the results are shown in Table 24.

Table 24 – Estimation of tear resistance

Needle Size	Needle Diameter (m)	Displacement Length (m)	Opening Force (N)	Estimated Tear Resistance (Nm/m^2)
18 gage	0.00126	0.002	0.693	2887.2
22 gage	0.00068	0.0015	0.497	2877.5
30 gage	0.0003	0.00082	0.397	2848.1
			Average	2870.9
			Standard Deviation	20.3

From Table 24, the output values are reasonably close to one another, which supports Equation 30. The estimated tear resistance is 2870 Nm/m^2. No literature could be found on the crack fracture toughness of polyurethane to support this value. However, information on values for other polymers could be found, and this estimate falls within range of those values. Table 25 lists crack fracture toughness for various polymers. Further testing with materials of known crack fracture toughness, as well as materials with varying thicknesses and material properties, would be useful in furthering the validity of this equation.

Table 25 - List of known crack fracture toughness for polymers

Material	Crack Fracture Toughness (Nm/m^2)
Polyarylene Ether Film (PAE) [39]	4 - 7
Polyethylene Pipe [40]	2,000 – 6,000
Linear Low Density Polyethylene Film (LLDPE) [41]	9,500 – 11,000

The previous description is outlined to define the maximum penetration force. This analysis is extended to cover the entire penetration process and explained by the following figures.

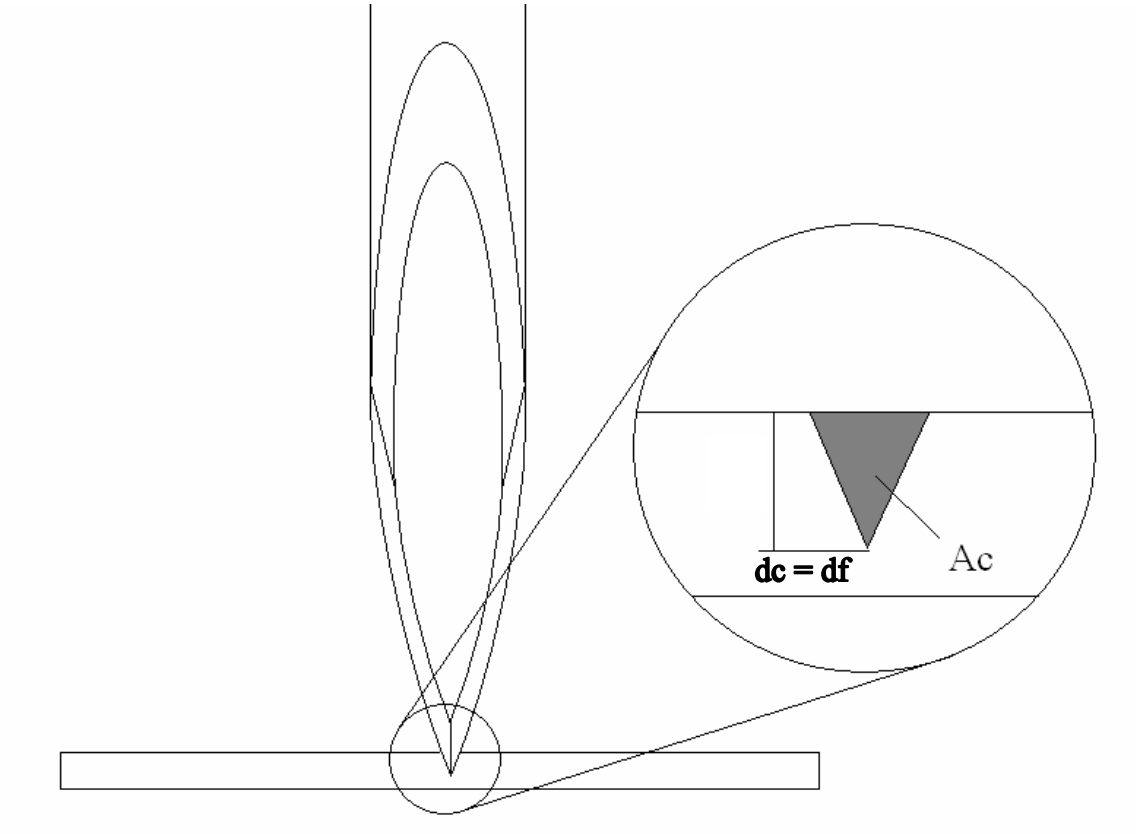

Figure 46 - Cutting area after puncture

Figure 46 shows the cutting area after the initial puncture. The cutting area is estimated by using the tip angle and the depth of the cut. The d_f term is represented by the depth of the cut. The same estimate is valid as the tip passes through the back side of the penetration media, except the area must be estimated by subtracting the portion of the needle that has passed through the media. This is shown in Figure 47.

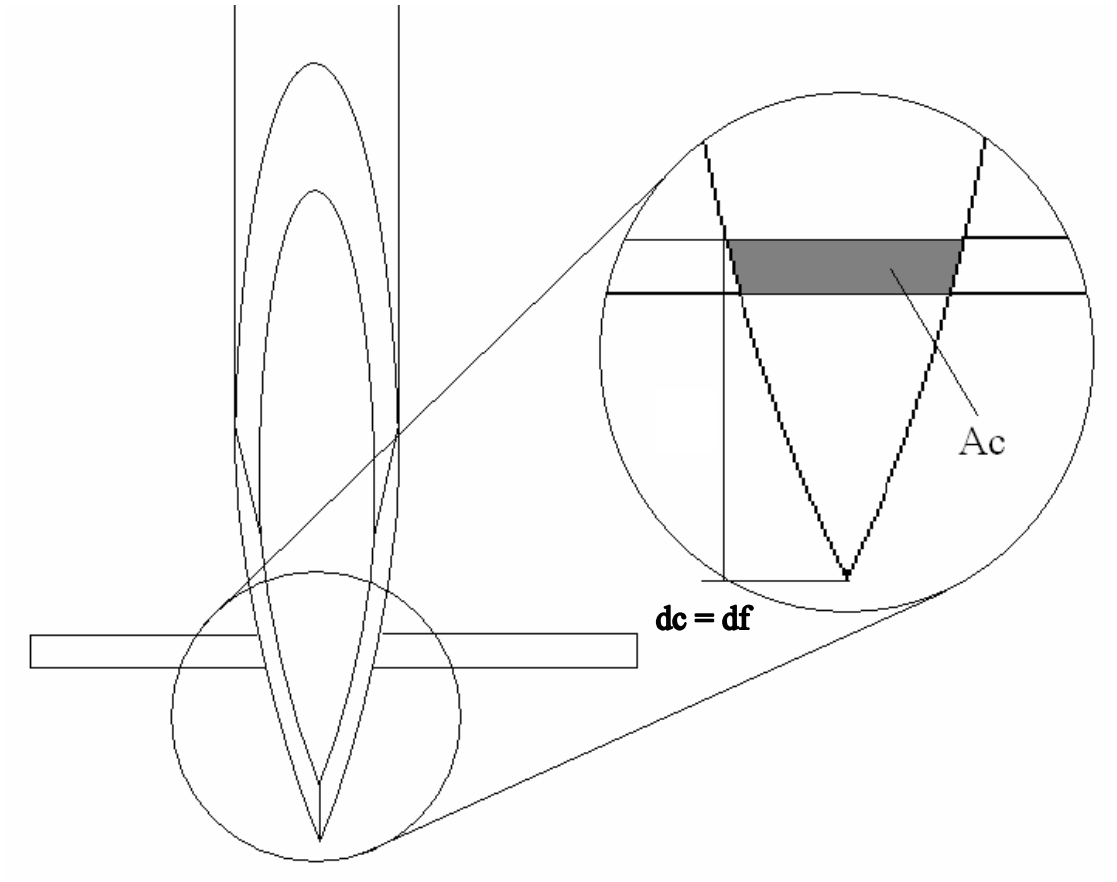

Figure 47 - Cutting area after tip passes through media

The crack area can be seen in Figure 47. The d_f term is still equal to the depth of cut at this stage of penetration. Once the depth of cut is equal to the bevel height, then the d_f term remains constant, until the beveled edges have passed completely through the penetration media. This is shown in Figure 48.

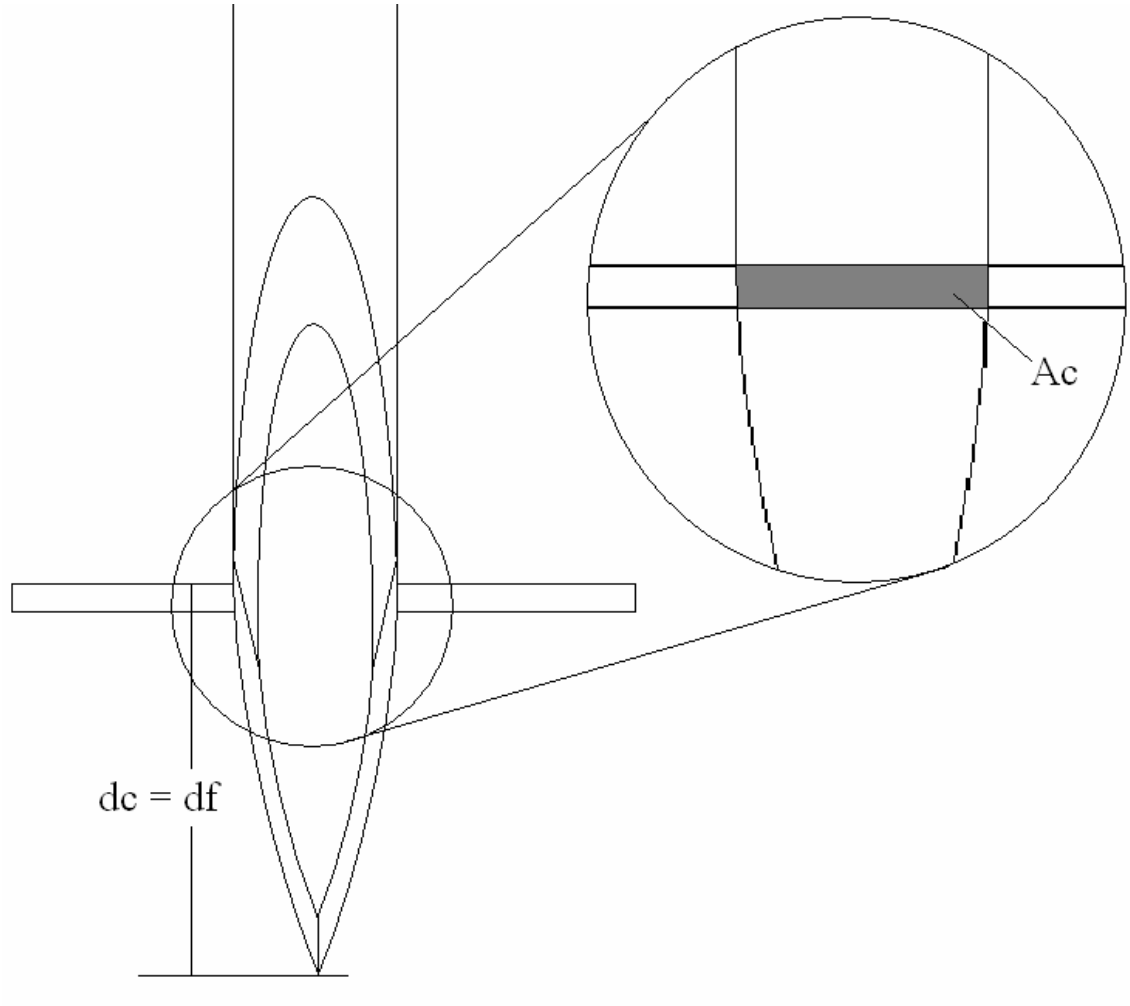

Figure 48 - Cutting area after beveled edge passes through media

Once the beveled edge clears the top surface of the media, the d_f term remains constant and equal to the bevel height of that needle. The cutting force is determined by the area of the crack, which is equivalent to the distance from the end of the beveled edge to the bottom of the penetration media. In a semi-infinite media, this term would remain constant once the beveled edge passed completely into the media; in penetration through film, this term goes to zero as the beveled edge passes through the bottom surface of the film. The cutting area is not assumed to include the area directly under the tip, which is the portion of material that is assumed to be punctured as opposed to cut. This area

would be estimated by multiplying the tip diameter by the thickness of the material; however this value is very small in comparison to the remaining cutting area, so it is excluded from these estimates. For example, the total area in 0.381 mm film under a 22 gage needle with a 10 μm tip diameter is 3.81 nm^2, while the corresponding crack area is 27 μm^2. Further generalizations outlining the entire penetration process are provided in Section 5.1.3.

Combining Equations 28 and 30 produces an equation that defines the maximum total cutting force of a steel hypodermic needle through polyurethane film. This is shown as Equation 31.

$$F_c = \frac{G_p A_t}{t_{field}} + \frac{G_c A_c}{d_f} \tag{31}$$

From Equation 31, F_c is the total cutting force in Newtons, G_c (2870 Nm/m^2) is the tear resistance, A_c is the surface area of the tear (m^2), which is equivalent to the diameter of the needle multiplied by the needle depth in the media, d_f is the distance over which the crack force is applied (m), G_p (43,700 Nm/m^2) is the puncture resistance of the material, A_t is the tip contact area (m^2), and t_{field} is the numerical constantly currently associated with material thickness (m). This is supported by penetration data of needles with diameters ranging from 0.30 mm to 1.26 mm and tip angles ranging from 0.803 – 1.274 rad. Other studies have predicted the puncture force of flat-bottomed and sharp-tipped punches and show that the mechanism of penetration changes as the punch geometry changes [42-44]. The analysis outlined in this thesis varies from these studies as it predicts penetration forces based of the specific tip area properties for the sharp-tipped punches (hypodermic needles). Equation 31 is fully reduced to base values for the assumed maximum values of force in Equation 32.

$$F_c = \frac{G_p\left(2\pi r_t^2\left(1-\sin\frac{\alpha}{2}\right)\right)}{t_{field}} + \frac{G_c d t_f}{d_f} \tag{32}$$

From Equation 32, F_c is the total cutting force in Newtons, G_p is the puncture resistance (Nm/m^2), r_t is the tip radius (m), α is the tip angle, t_{field} is the constant relating material stiffness and the thickness of the film (m), G_c is the tear resistance of the material (Nm/m^2), d is the needle diameter (m), and d_f is the distance which the crack force is applied, which is equivalent to the distance on a needle from the tip to the end of the first bevel (m).

The cutting force equation is plotted against the empirical data in order to provide a visual representation of the equation. This is shown in Figures 49, 50, 51, and 52 for 18 gage, 22 gage, 28 gage, and 30 gage needles, respectively.

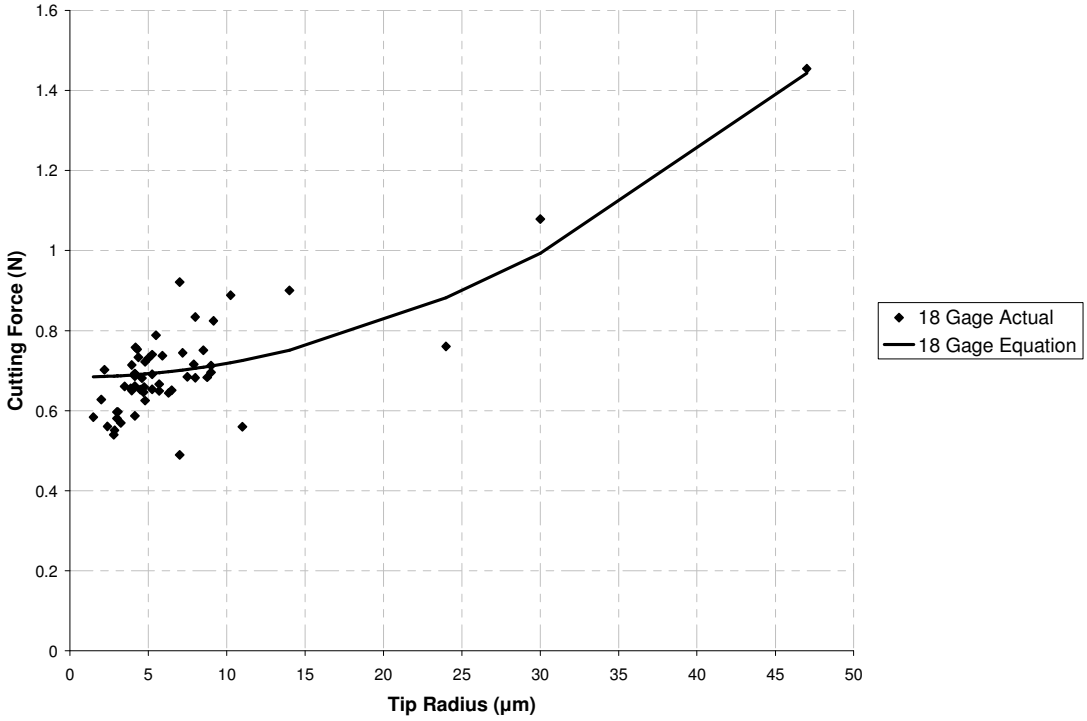

Figure 49 - 18 gage cutting force equation comparison

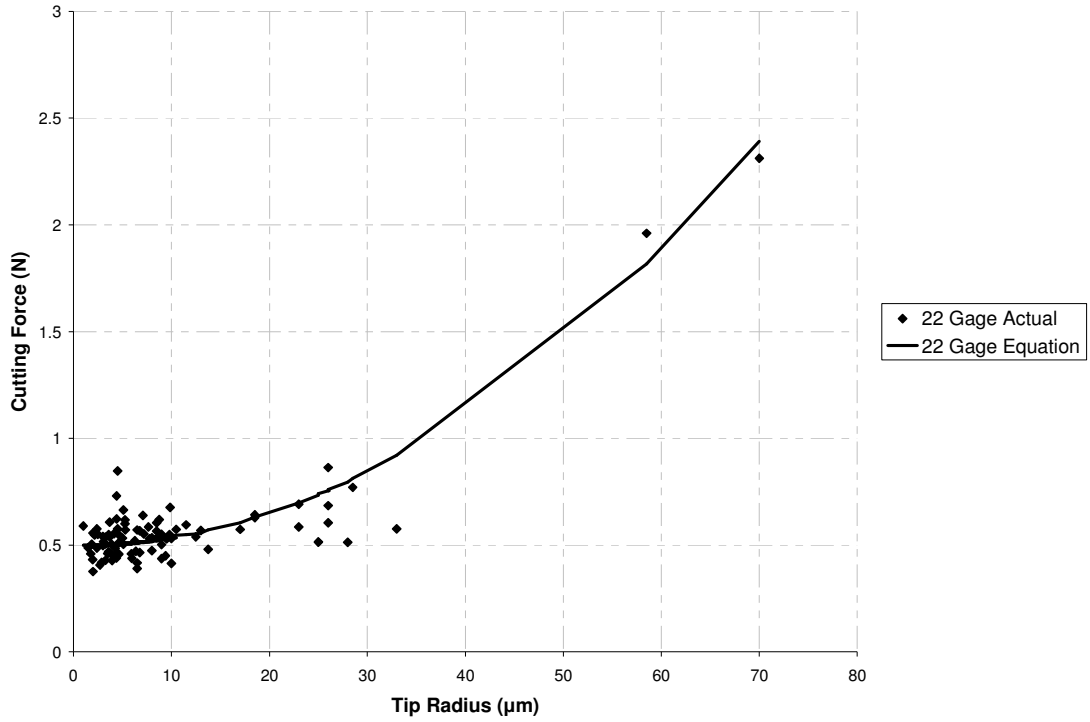

Figure 50 - 22 gage cutting force equation comparison

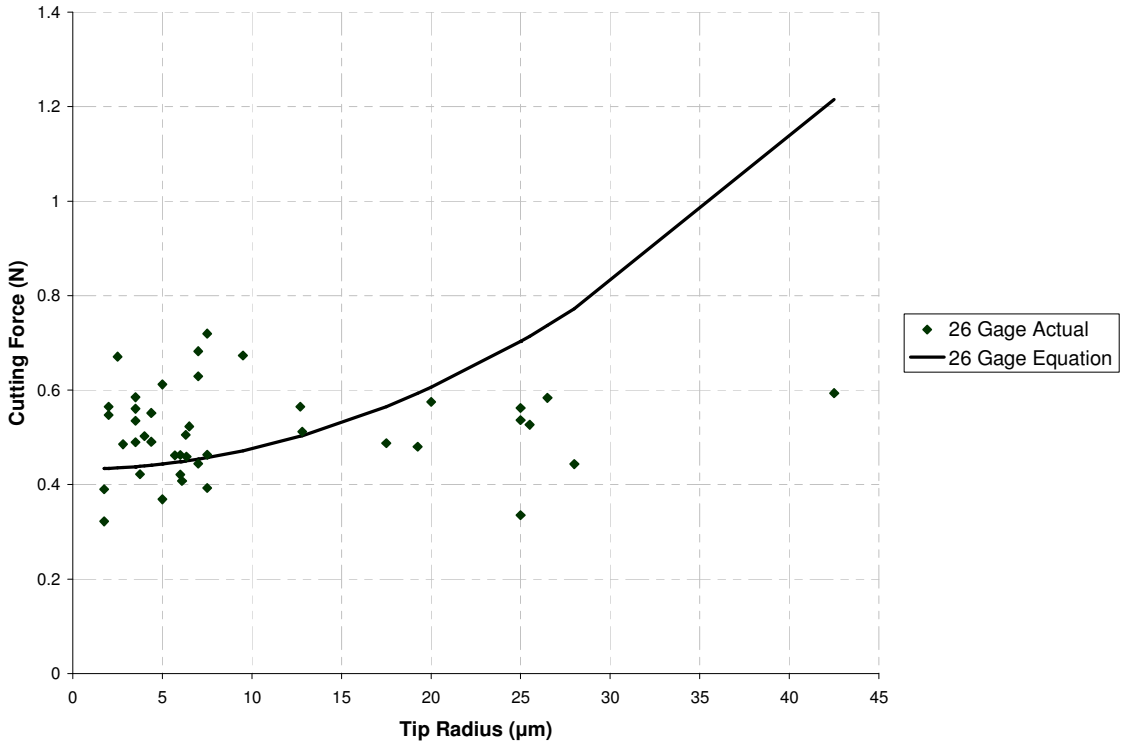

Figure 51 - 26 gage cutting force equation comparison

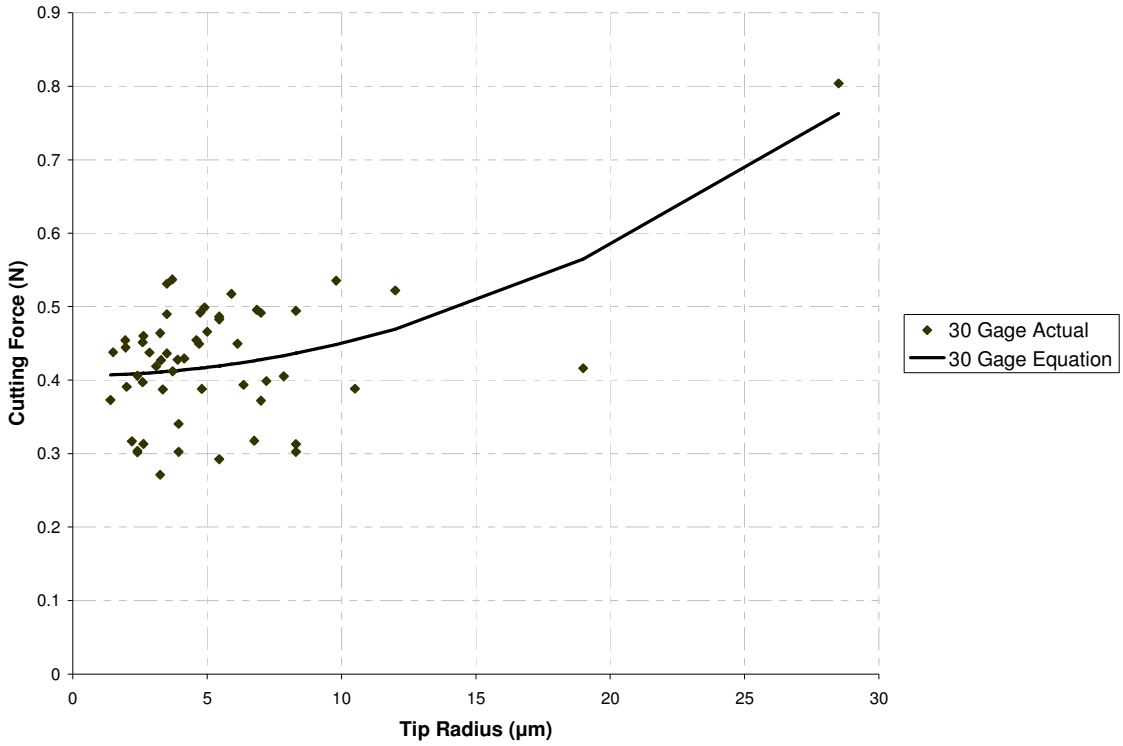

Figure 52 - 30 gage cutting force equation comparison

The averaged empirical data used to determine the cutting force equation and the estimation acquired by using Equation 33 are compared in Table 26.

Table 26 - Comparison of actual and predicted cutting forces

	Tip Radius	Actual Cutting Force (N)	Estimated Cutting Force (N)	Percent Difference
18 Gage	1.5	0.592	0.684	-15.54%
	4.5	0.682	0.690	-1.30%
	7.5	0.713	0.703	1.37%
	10.5	0.757	0.721	4.75%
	13.5	0.900	0.746	17.13%
	22.5	0.760	0.858	-12.83%
	28.5	1.079	0.963	10.75%
	46.5	1.454	1.427	1.86%
22 Gage	1.5	0.492	0.492	-0.12%
	4.5	0.512	0.499	2.45%
	7.5	0.541	0.513	5.23%
	10.5	0.554	0.534	3.53%
	13.5	0.568	0.562	1.07%
	16.5	0.573	0.597	-4.09%
	22.5	0.636	0.688	-8.15%
	25.5	0.734	0.743	-1.33%
	58.5	1.960	1.818	7.27%
	70.5	2.311	2.418	-4.60%
30 Gage	1.5	0.374	0.401	-7.33%
	4.5	0.418	0.409	1.98%
	7.5	0.415	0.425	-2.31%
	10.5	0.477	0.449	5.88%
	28.5	0.804	0.757	5.86%

As can be seen in Table 26, most of the estimated cutting forces are close to the actual forces. This supports the validity of Equation 26 as a predictor of penetration force of a steel hypodermic needle based upon tip radius, tip angle, and needle diameter. The estimation of total force is made by adding the cutting force and the frictional force equations. This prediction is outlined in Section 5.1.3.

5.1.3 Total penetration force equation

Equations 22 and 26 are developed to predict the maximum frictional force and cutting force of a steel needle penetrating polyurethane film. Based upon the assumption that the total force can be estimated by adding the frictional force and the cutting force, the two equations can be combined to develop a single equation that predicts maximum penetration force through polyurethane film based on the inputs coefficient of friction, needle diameter, tip angle, and tip radius. This equation is based upon data for steel hypodermic needles. This is shown as Equation 27.

$$F_f = \mu E_f t_f d$$

$$F_c = \frac{G_p A_t}{t_{field}} + \frac{G_c A_c}{d_f}$$

$$F_t = F_f + F_c$$

$$F_t = \mu E_f t_f d + \frac{G_p A_t}{t_{field}} + \frac{G_c A_c}{d_f} \tag{33}$$

From Equation 33, F_t is the total penetration force in Newtons, μ is the coefficient of friction, E_f is the elastic modulus of the material (5 MPa), t_{field} is the numerical constant associated with the thickness of the material (m), d is the needle diameter (m), G_c (2870 Nm/m^2) is the tear resistance, A_c is the surface area of the tear (m^2), d_f is the distance over which the crack force is applied (m), G_p (43,700 Nm/m^2) is the puncture resistance of the material, and A_t is the tip contact area (m^2). Equation 33 is fully expanded into base units and shown as Equation 34.

$$F_t = \mu E_f t_f d + \frac{G_p\left(2\pi r_t^2\left(1-\sin\frac{\alpha}{2}\right)\right)}{t_{field}} + \frac{G_c d t_f}{d_f} \quad (34)$$

From Equation 34, F_t is the total penetration force in Newtons, μ is the coefficient of friction, E_f is the elastic modulus of the material (5 MPa), t_{field} is the thickness of the material (m), d is the needle diameter (m), G_p is the puncture resistance (43,700 Nm/m^2), r_t is the tip radius (m), α is the tip angle, G_c is the tear of the material (2870 Nm/m^2), and d_f is the distance which the crack force is applied, which is equivalent to the distance on a needle from the tip to the end of the first bevel (m). Ranges for the variables tested are 0.1 – 0.87 for the coefficient of friction, 0.30 – 1.26 mm for the needle diameters, and 1.5 – 70 μm for tip radius. Equation 34 is based on data from steel hypodermic needles and is arranged to solve for maximum force; its application toward other tip designs could be explored through future testing. The actual penetration data are compared to the penetration force estimated by Equation 34 in Tables 27, 28, 29, 30, and 31.

Table 27 - 18 gage Inviro Medical penetration equation comparison

	Tip Radius (µm)	µ	Actual Force (N)	Estimated Force (N)	Percent Difference
As-received	8	0.1	0.942	0.965	-2.47%
	9	0.1	0.955	0.971	-1.69%
	4.15	0.1	0.921	0.949	-3.00%
	7.5	0.1	0.944	0.963	-2.00%
	2	0.1	0.887	0.945	-6.45%
	3	0.1	0.856	0.946	-10.55%
	4.3	0.1	1.013	0.950	6.23%
	5	0.1	0.990	0.952	3.88%
	8.5	0.1	1.011	0.968	4.22%
	2.4	0.1	0.820	0.945	-15.23%
	10.25	0.1	1.148	0.979	14.69%
	3.89	0.1	0.915	0.948	-3.62%
TriboGlide	14	0.133	1.246	1.096	12.00%
	47	0.133	1.799	1.788	0.61%
	24	0.133	1.105	1.227	-10.99%
	11	0.133	0.905	1.070	-18.27%
	5.7	0.133	1.011	1.040	-2.83%
	30	0.133	1.424	1.338	6.02%
	1.5	0.133	0.929	1.030	-10.86%
Silicone	7.2	0.17	1.186	1.143	3.65%
	5.9	0.17	1.179	1.137	3.53%
	8	0.17	1.275	1.147	10.06%
	3.06	0.17	1.038	1.128	-8.67%
	5.5	0.17	1.229	1.135	7.64%
	5.25	0.17	1.181	1.134	3.96%
	4.15	0.17	1.128	1.131	-0.30%
	4.15	0.17	1.134	1.131	0.25%
	3.95	0.17	1.155	1.130	2.18%
	4.5	0.17	1.094	1.132	-3.49%
	5.25	0.17	1.095	1.134	-3.63%
	9.15	0.17	1.266	1.154	8.84%
MDX	9	0.11	0.998	0.997	0.12%
	5.7	0.11	0.934	0.980	-4.92%
	4.8	0.11	0.911	0.977	-7.31%
	3.25	0.11	0.855	0.973	-13.84%
	4.74	0.11	0.944	0.977	-3.47%
	6.3	0.11	0.930	0.983	-5.72%
	4.6	0.11	0.967	0.976	-1.01%
	8.75	0.11	0.969	0.995	-2.76%
	4.7	0.11	0.931	0.977	-4.87%
	3	0.11	0.866	0.972	-12.30%
	3.95	0.11	0.936	0.975	-4.17%
	7.9	0.11	1.001	0.991	1.06%
	5.25	0.11	0.976	0.979	-0.26%
	2.85	0.11	0.836	0.972	-16.19%

Bare	4.18	0.87	3.017	2.949	2.25%
	7	0.87	3.180	2.960	6.94%
	4.15	0.87	2.951	2.949	0.09%
	2.2	0.87	2.961	2.944	0.56%
	4.375	0.87	2.992	2.949	1.43%
	2.8	0.87	2.799	2.945	-5.24%
	4.8	0.87	2.981	2.951	1.03%
	4.15	0.87	2.846	2.949	-3.59%
	6.5	0.87	2.910	2.957	-1.63%
	3.5	0.87	2.920	2.947	-0.94%

Table 28 - 22 gage Myco Medical penetration equation comparison

	Tip Radius (µm)	µ	Actual Force (N)	Estimated Force (N)	Percent Difference
As-received	7.78	0.1	0.676	0.684	-1.22%
	3.25	0.1	0.569	0.636	-11.79%
	4.6	0.1	0.596	0.640	-7.28%
	1.75	0.1	0.599	0.633	-5.59%
	6.5	0.1	0.530	0.648	-22.28%
	6.5	0.1	0.556	0.648	-16.43%
	26	0.1	0.744	0.893	-20.05%
	5.9	0.1	0.600	0.645	-7.51%
	3.5	0.1	0.600	0.636	-6.00%
	26	0.1	1.003	0.893	10.93%
TriboGlide	3	0.13	0.722	0.677	6.22%
	3.9	0.13	0.686	0.679	0.95%
	2.4	0.13	0.758	0.676	10.87%
	10.5	0.13	0.755	0.716	5.18%
	4.6	0.13	0.642	0.682	-6.26%
	23	0.13	0.873	0.879	-0.62%
	2.4	0.13	0.667	0.676	-1.33%
	2.15	0.13	0.729	0.675	7.36%
	8.5	0.13	0.747	0.702	6.07%
	7.1	0.13	0.821	0.693	15.59%
	4.15	0.13	0.735	0.680	7.46%
	3.7	0.13	0.720	0.679	5.70%
Silicone	8	0.17	0.772	0.754	2.25%
	23	0.17	0.823	0.935	-13.56%
	5.25	0.17	0.837	0.740	11.58%
	13	0.17	0.806	0.795	1.39%
	3.25	0.17	0.744	0.734	1.37%
	6.75	0.17	0.805	0.747	7.16%
	5.3	0.17	0.809	0.740	8.49%
	3.06	0.17	0.754	0.733	2.77%
	17	0.17	0.812	0.842	-3.69%
	6.5	0.17	0.809	0.746	7.81%
	3.7	0.17	0.846	0.735	13.13%
	6.25	0.17	0.759	0.745	1.87%
	8.75	0.17	0.857	0.759	11.44%
	58.5	0.17	2.198	2.056	6.48%

MDX	7.2	0.11	0.706	0.666	5.75%
	2.85	0.11	0.572	0.649	-13.31%
	4.595	0.11	0.664	0.654	1.59%
	8	0.11	0.628	0.670	-6.72%
	5.1	0.11	0.658	0.656	0.31%
	5.95	0.11	0.591	0.659	-11.52%
	1.95	0.11	0.586	0.647	-10.35%
	7.65	0.11	0.738	0.668	9.52%
	3.6	0.11	0.623	0.651	-4.47%
	4.265	0.11	0.639	0.653	-2.20%
	2.7	0.11	0.560	0.648	-15.71%
	9	0.11	0.656	0.677	-3.14%
	4.15	0.11	0.602	0.652	-8.33%
	4.375	0.11	0.593	0.653	-10.05%
	9.5	0.11	0.682	0.680	0.28%
Bare	25	0.87	1.733	1.953	-12.70%
	9.4	0.87	1.669	1.745	-4.55%
	5.1	0.87	1.883	1.721	8.63%
	9.8	0.87	1.768	1.748	1.13%
	28	0.87	1.732	2.014	-16.32%
	9.85	0.87	1.895	1.748	7.76%
	4	0.87	1.670	1.717	-2.79%
	3.25	0.87	1.757	1.715	2.41%
	70	0.87	3.531	3.610	-2.24%

Table 29 - 22 gage Inviro Medical penetration equation comparison

	Tip Radius (μm)	μ	Actual Force (N)	Estimated Force (N)	Percent Difference
As-received	4.5	0.1	0.989	0.649	34.41%
	1	0.1	0.731	0.641	12.32%
	4.4	0.1	0.872	0.648	25.67%
	2.5	0.1	0.692	0.643	7.09%
	2	0.1	0.698	0.642	7.94%
	28.5	0.1	0.912	0.956	-4.73%
	1.85	0.1	0.646	0.642	0.64%
	3.6	0.1	0.690	0.646	6.46%
	10	0.1	0.679	0.680	-0.09%
	10	0.1	0.672	0.680	-1.06%
	1.5	0.1	0.629	0.642	-1.93%
Silicone	5.25	0.17	0.859	0.751	12.61%
	11.5	0.17	0.836	0.792	5.33%
	4.4	0.17	0.864	0.748	13.46%
	18.5	0.17	0.884	0.873	1.24%
	4.5	0.17	0.817	0.748	8.42%
	9	0.17	0.793	0.772	2.62%
	5	0.17	0.774	0.750	3.16%
	4.7	0.17	0.786	0.749	4.74%
	26	0.17	0.927	1.002	-8.18%
	18.5	0.17	0.870	0.873	-0.38%
MDX	10	0.11	0.570	0.694	-21.61%
	6.35	0.11	0.626	0.671	-7.06%
	2	0.11	0.532	0.657	-23.42%
	9	0.11	0.593	0.686	-15.71%
	3.935	0.11	0.584	0.661	-13.19%
	25	0.11	0.671	0.897	-33.63%
	3	0.11	0.653	0.658	-0.78%
	13.75	0.11	0.636	0.728	-14.46%
	33	0.11	0.731	1.077	-47.26%
	6.75	0.11	0.622	0.673	-8.23%

Table 30 - 26 gage Myco Medical penetration equation comparison

	Tip Radius (μm)	μ	Actual Force (N)	Estimated Force (N)	Percent Difference
As-received	25	0.113	0.665	0.806	-21.19%
	3.5	0.113	0.638	0.540	15.27%
	17.5	0.113	0.590	0.668	-13.19%
	19.25	0.113	0.583	0.696	-19.36%
	7	0.113	0.547	0.556	-1.72%
	26.5	0.113	0.686	0.839	-22.27%
	6.3	0.113	0.608	0.552	9.13%
	4.375	0.113	0.593	0.543	8.35%
	6	0.113	0.565	0.551	2.59%
TriboGlide	12.8	0.133	0.633	0.624	1.33%
	25.5	0.133	0.647	0.835	-28.94%
	3.5	0.133	0.610	0.559	8.50%
	4	0.133	0.623	0.560	10.13%
	2	0.133	0.685	0.555	19.03%
	6.5	0.133	0.644	0.572	11.20%
	7.5	0.133	0.584	0.578	1.06%
	20	0.133	0.696	0.726	-4.43%
	2.8	0.133	0.606	0.557	8.17%
Silicone	2.5	0.17	0.825	0.589	28.54%
	7.5	0.17	0.874	0.611	30.06%
	7	0.17	0.783	0.608	22.36%
	5	0.17	0.766	0.598	22.00%
	7	0.17	0.836	0.608	27.31%
	2	0.17	0.701	0.589	16.06%
	9.5	0.17	0.828	0.626	24.37%
MDX	7.5	0.11	0.493	0.557	-13.01%
	1.75	0.11	0.490	0.534	-8.94%
	28	0.11	0.543	0.872	-60.54%
	1.75	0.11	0.422	0.534	-26.53%
	42.5	0.11	0.693	1.314	-89.65%
	5	0.11	0.469	0.543	-15.92%
	6.1	0.11	0.508	0.548	-8.07%
	6	0.11	0.521	0.548	-5.22%
	48.5	0.11	0.493	0.557	-13.01%
Bare	25	0.87	1.124	1.492	-32.73%
	3.75	0.87	1.211	1.228	-1.40%
	12.7	0.87	1.354	1.291	4.60%
	3.5	0.87	1.349	1.227	9.09%
	4.375	0.87	1.340	1.230	8.25%
	25	0.87	1.325	1.492	-12.60%
	5.7	0.87	1.251	1.236	1.20%
	3.5	0.87	1.374	1.227	10.69%
	6.35	0.87	1.248	1.239	0.74%

Table 31 - 30 gage Inviro Medical penetration equation comparison

	Tip Radius (µm)	µ	Actual Force (N)	Estimated Force (N)	Percent Difference
As-received	3.5	0.117	0.562	0.484	13.91%
	12	0.117	0.595	0.542	8.86%
	4.7	0.117	0.522	0.488	6.38%
	2	0.117	0.463	0.480	-3.74%
	4.6	0.117	0.527	0.488	7.37%
	1.965	0.117	0.517	0.480	7.04%
	2.625	0.117	0.532	0.482	9.54%
	4.8	0.117	0.460	0.489	-6.18%
	3.5	0.117	0.509	0.484	4.86%
	3.28	0.117	0.500	0.483	3.22%
	1.95	0.117	0.527	0.480	8.78%
	1.5	0.117	0.510	0.480	6.00%
	4.15	0.117	0.502	0.486	3.09%
	7.85	0.117	0.477	0.506	-5.93%
	2.6	0.117	0.469	0.482	-2.61%
TriboGlide	2.625	0.13	0.394	0.490	-24.41%
	10.5	0.13	0.469	0.535	-14.15%
	7.2	0.13	0.479	0.509	-6.33%
	6.35	0.13	0.474	0.504	-6.40%
	19	0.13	0.497	0.645	-29.93%
	28.5	0.13	0.884	0.843	4.66%
Silicone	9.8	0.17	0.641	0.554	13.57%
	3.7	0.17	0.642	0.517	19.40%
	3.5	0.17	0.636	0.517	18.78%
	2.6	0.17	0.557	0.514	7.59%
	5.45	0.17	0.588	0.524	10.76%
	7	0.17	0.596	0.533	10.65%
	3.9	0.17	0.533	0.518	2.77%
	6.85	0.17	0.601	0.532	11.45%
	2.85	0.17	0.543	0.515	5.07%
	3.25	0.17	0.569	0.516	9.31%
	5.9	0.17	0.622	0.527	15.38%
MDX	8.3	0.11	0.381	0.505	-32.49%
	8.3	0.11	0.370	0.505	-36.25%
	5.45	0.11	0.361	0.487	-35.17%
	2.4	0.11	0.372	0.477	-28.26%
	3.935	0.11	0.408	0.481	-17.79%
	3.935	0.11	0.370	0.481	-29.92%
	7	0.11	0.440	0.496	-12.67%
	3.25	0.11	0.339	0.479	-41.17%
	6.75	0.11	0.386	0.494	-28.20%
	2.4	0.11	0.370	0.477	-28.89%
	2.2	0.11	0.385	0.476	-23.85%

Bare	8.3	0.87	1.032	0.974	5.58%
	3.1	0.87	0.957	0.948	0.87%
	3.72	0.87	0.950	0.950	-0.03%
	4.9	0.87	1.037	0.955	7.92%
	1.4	0.87	0.911	0.945	-3.75%
	2.4	0.87	0.944	0.947	-0.31%
	6.125	0.87	0.988	0.961	2.72%
	3.35	0.87	0.925	0.949	-2.59%
	4.74	0.87	1.030	0.954	7.34%
	5	0.87	1.004	0.955	4.84%
	5.45	0.87	1.024	0.957	6.54%

As can be seen in Tables 27, 28, 29, 30, and 31, a majority of the estimated data falls within 10% of the measured penetration forces. As mentioned earlier one area of low accuracy is the 26 gage needle group. Based upon the accuracy of the other data points, it is believed that something adversely affected this data group during testing. In addition, the multiple penetration testing suggests that the 26 gage needle group was damaged between tests. Another area of low accuracy is the 30 gage MDX group, as all of these values were beyond 15% of the actual penetration force. This can be explained by the fact that the estimated cutting force for this group is higher than the cutting force of the MDX group. So while the estimation fits the average value well, the MDX group becomes slightly over estimated. In order to visualize the effectiveness of the penetration force estimation equation, a histogram is created which groups data by percent accuracy with a range of five percent. This histogram is shown as Figure 53.

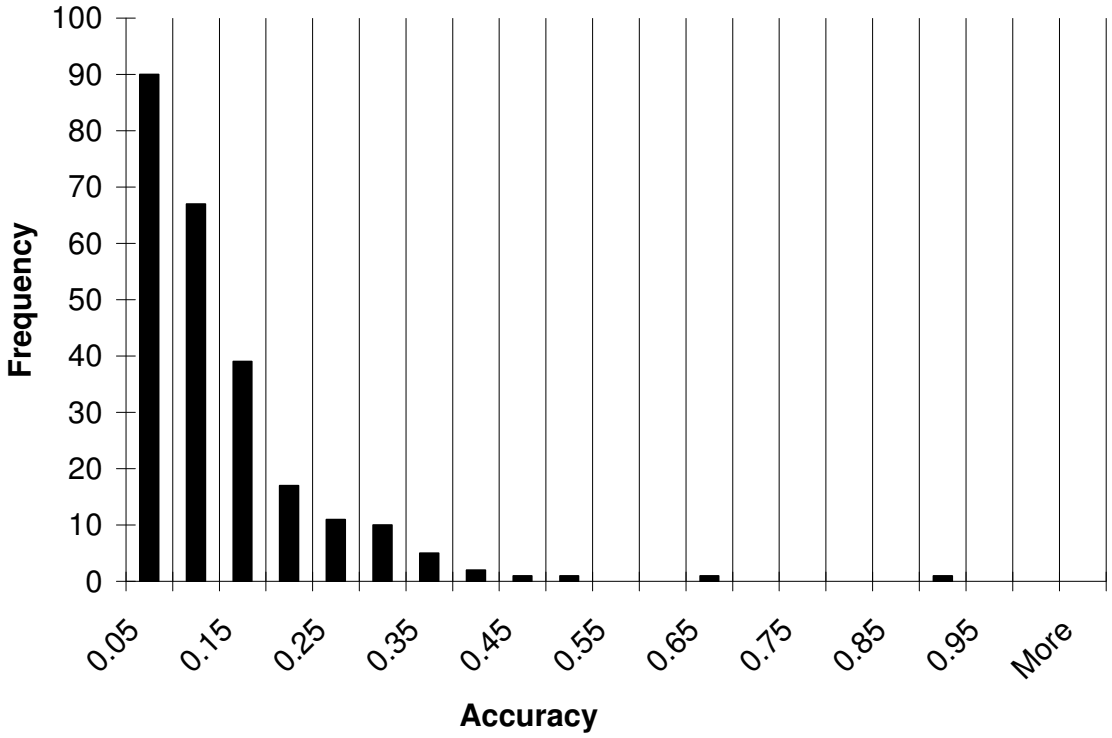

Figure 53 - Equation accuracy histogram

As can be seen in Figure 53, of the 245 data points evaluated, 90 estimated values are within five percent of the actual value. Sixty four percent of the data points are within 10% accuracy, and 80% fall within 15% accuracy. The outliers are to be expected in a model of this size, and are likely attributed to the needle tips being damaged between penetration and tip measurements. The development of the penetration equation along with the buckling data outlined in the following section is used to analyze the plastic needles that are tested in Section 5.4.

The previously explained equations are setup to determine the maximum penetration force of a hypodermic needle through film. These events theoretically should occur separately based upon the thickness of the material that is being penetrated; however the following observations are made. It is determined that at low tip radii, the force required to initiate and continue the puncture is small in comparison to the other

force components, so its calculation is insignificant. It is also observed that at high tip radii, the events occur simultaneously. This is because the increased tip radius requires more deflection of the material for puncture to initiate, which in turn stores more energy in the film. This increased energy increases the rate of the puncture which causes the puncture and opening to occur virtually instantaneously and in turn supports the addition of the puncture and opening terms in the maximum penetration force prediction. Based upon this observation, varying the velocity of puncture is an area of future exploration.

For an ideal penetration, the penetration equation is modified to define the penetration force at the various stages of penetration. This model is for an ideally sharp needle, which allows for the separate penetration events to be separately visualized. The penetration stages are as follows:

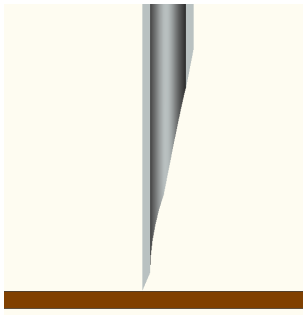

$$\delta_t = 0$$

δ_t is the total displacement (displacement of needle tip)

Figure 54 - Stage 1: Tip contacts penetration media

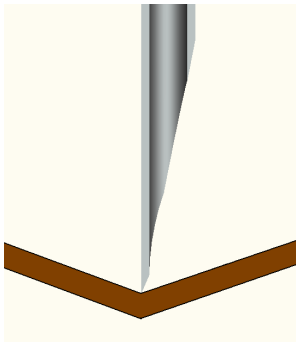

$$\delta_t = \delta_m$$
$$F_t = F_{stiffness}$$

$F_{stiffness}$ is the stiffness force of the material
k is the material stiffness
δ_m is the displacement of the media

Figure 55 - Stage 2: Movement of tip displaces penetration media

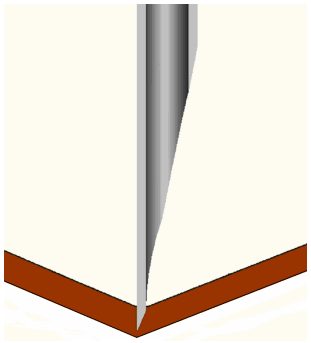

$$\delta_t = \delta_m + \delta_c$$

$$F_t = \mu E_m d_m \delta_c + \frac{G_p A_t}{t_{field}} + \frac{G_c A_c}{d_f}$$

δ_c is the depth of cut (distance from needle tip to top media surface)
μ is the coefficient of friction
E_m is the elastic modulus of the material
d_m is the horizontal distance of the opening
G_p is the resistance to puncture of the media
A_t is the tip contact area
t_{field} is the field thickness (further testing necessary)
G_c is the resistance to tearing of the material
A_c is the surface area of the crack
d_f is the tearing force distance which is equal to the depth of cut until the bevel height is reached, then remains constant at the value of the bevel height.

Figure 56 - Stage3: Stiffness force exceeds the force required to tear the penetration media.

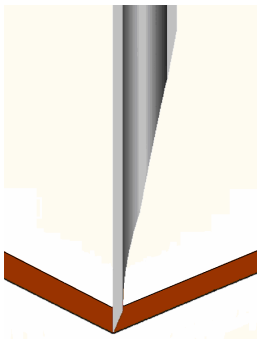

$$\delta_t = \delta_m + \delta_c$$

$$F_t = \mu E_m d_m t_m + \frac{G_c A_c}{d_f}$$

t_m is the material thickness

Figure 57 - Stage 4: Tip breaches opposite side of penetration media, force required to puncture no longer accounted for

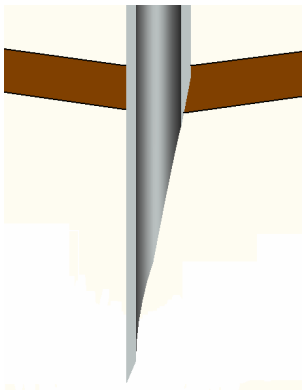

$F_t = \mu E_m d_n t_m$

d_n is the needle diameter

Figure 58 -Stage 5: Transition of media over final bevel, force required to cut the media is no longer accounted for

The stages of penetration shown in Figures 54, 55, 56, 57, and 58 are based on the special situation of penetration through film, which correlates to the work in this thesis. It could be expanded to cover penetration into semi-infinite media by altering the depth and contact area parameters. Future work is necessary to determine the values of the field thickness variables which are influenced by the material stiffness as the penetration media thickness increases. The equations are used to develop a plot of the complete penetration force as the depth of the cut is increased. This is shown in Figure 56.

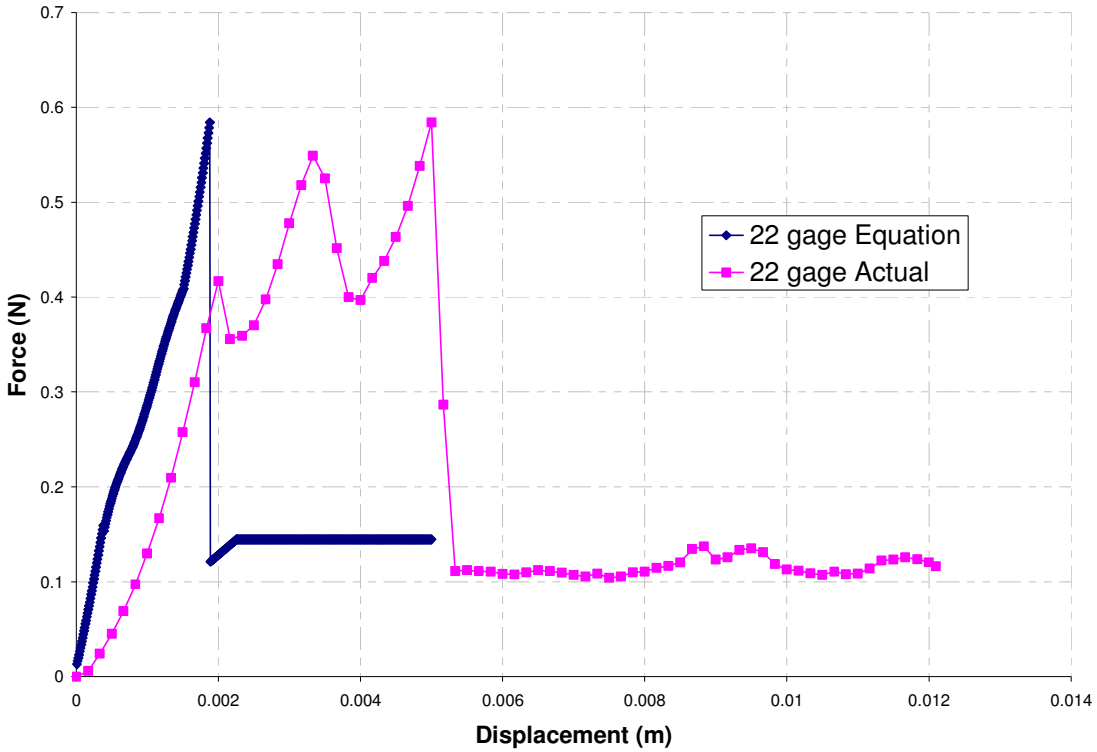

Figure 59 - Comparison of actual and estimated load vs. displacement

As can be seen in Figure 59, the equation results are close to the actual penetration force data. The variation is attributed to fact that only cutting depth is being plotted in the estimation, while the actual data includes the material deflection in the displacement data. Also, the various peaks in the empirical data are attributed to the film passing over geometries in the needle (bevel transitions, inner channels, etc.) which are not accounted for in the simplified model. In addition, the material is assumed to be merely tearing and opening and not deforming in any way.

5.2 Discussion of buckling load

The buckling data developed in Chapter 4 provide information on the strength requirements for materials used to make plastic hypodermic needles. The calculations of tip strength provide insight to pre-puncture strength requirements. The calculations of

cannula critical buckling load provide insight to material strength after puncture occurs, as the tip strength is no longer an issue because the tip has passed the point of loading once penetration occurs.

As pointed out in Figure 39, a significant portion of loading occurs prior to puncture of the polyurethane film. Therefore, the tip must be capable of withstanding this load in order to ensure that penetration will occur. In addition, the tip could deform and the penetration would still occur because penetration force is related to tip radius and tip deformation would result in an increase of the tip radius. To determine a minimum acceptable value for material strength, Equation 12 (developed by finite element models in Chapter 4) is used. Equation 12 relates critical tip buckling load to a corresponding elastic modulus for 22 gage steel needles. Only 22 gage steel needles were evaluated, as this was the only gage of plastic needle that was tested. Equation 12 is valid for needles with a tip geometry that is the same as a steel needle, which includes the Vectra A130 needles.

$$E = 17.627 P_{cr} - 0.0003 \tag{12}$$

In Equation 12, E is the critical elastic modulus (GPa) and P_{cr} is the critical buckling load (N). A finite element model is used to determine the tip strength of a 22 gage steel needle, as the geometry is quite complex and difficult to analyze through the use of equations. The puncture force for a 22 gage needle is determined to be in the range of 0.35 – 0.45 N. This value is determined by evaluating the penetration plots generated from penetration testing. Using the larger force value and Equation 12, the minimum elastic modulus for a material used for making hypodermic needles is 7.93 GPa, assuming the needle has the same geometry as a steel 22 gage hypodermic needle.

This eliminates any material having an elastic modulus below this value, and does not include any factor of safety. A material with an elastic modulus of 10 GPa would provide a factor of safety of 1.26. This elastic modulus corresponds to that of Vectra MT1300 (10.5 GPa), which has proven to be capable of producing needles that will puncture polyurethane film.

The cannula strength is evaluated using finite element and analytical models. An equation similar to the tip strength equation is developed from these finite element models to determine the minimum acceptable material strength for a hollow 22 gage needle based upon the critical buckling load of the cannula. Equation 9, presented earlier in Chapter 4, is restated below.

$$E = 3.091P_{cr} - 1.959*10^{-5} \quad (9)$$

In Equation 9, E is the critical elastic modulus (GPa), and P_{cr} is the critical buckling load (N). The generalization of cannula buckling load to apply to any diameter and length needle is outlined in Section 3.2.3. Using this equation along with the minimum average penetration force seen in a group of plastic needles (1.62 N which corresponds to MDX coated Vectra A130 needles) the lowest acceptable elastic modulus is calculated. This value is 5.0 GPa.

As both tip and cannula strengths are critical to successful penetration, the highest elastic modulus requirement should be taken to be the minimal acceptable material elastic modulus. Therefore the minimum elastic modulus derived from the tip strength equations should be taken to be the lowest acceptable material elastic modulus for a needle that is based off a 22 gage hypodermic needle. This value is 7.9 GPa, therefore the use of plastic for hypodermic needles is possible. This also is supported by the results

of the plastic needle testing, as needles made of materials with an elastic modulus lower than 7.9 GPa were not successful (polystyrene, Lexan, and COC), and needles tested with an elastic modulus larger than 7.9 GPa were successful (Vectra A130, Vectra MT1300). These values correspond to an idealized situation presented by the testing setup. In practice, these requirements may be higher, as an individual holding a needle may not represent a perfectly fixed end condition. In addition, the patient may move which would create additional instability in the needle. This movement is not accounted for in these estimations.

5.3 Discussion of multiple penetration testing

Most of the needle groups showed decreased penetration forces after multiple penetrations. This leads to two observations. First, the coefficient of friction between the needles and the polyurethane film decreases after a penetration. This is reasonable as the polyurethane tends to clean the needle in a manor that does not tend to remove lubrication as it passes through which smoothes the surface and reduces friction. Secondly, the needle structure is not affected by penetration through the polyurethane. This is reasonable as the elastic modulus of the steel needles is 200 GPa, while the elastic modulus of the polyurethane is 5 MPa. It is safe to assume that all deformation will occur in the film. This is supported by the multiple penetration data. The plastic needles were not tested for multiple penetrations, as none of the plastic needle test groups showed a 100% penetration success rate. It was desired to have a reliable and repeatable needle design before multiple penetration tests were conducted. None of the needles measured, however, had a noticeable change in tip radius before and after penetration. Therefore, it is assumed that the difference in elastic modulus between the plastic and polyurethane

(10.5 – 15 GPa for plastic and 5 MPa for polyurethane) is significant enough to transfer all deformation to the polyurethane.

Three of the 26 gage needle groups had increased penetration forces after multiple penetrations, as seen in Figure 34 (Section 4.1.3). The increased penetration loads are likely attributed to mishandling of the needles between penetration tests. It is likely that this occurred in the 26 gage needles and not the larger diameter needles because the 26 gage needles are significantly smaller in diameter than the larger needles and therefore more delicate. In addition, the needles were removed from and then replaced into their protective covers at least seven times in order to test the needles and document any damage by taking pictures of the tip. It is not unreasonable to assume that something could have happened to the needle tips during this process.

5.4 Relation of data to plastic needles

5.4.1 Buckling correlation

The buckling tests provide straight forward information for the material properties necessary to create plastic needles. Based on the data, any material with an elastic modulus less than 8 GPa would be unable to successfully penetrate the polyurethane membrane. This lower limit of elastic modulus does not include any safety factor, and a higher elastic modulus would eliminate uncertainty in tip integrity. It is safe to say that the higher elastic modulus, the less likely tip failure becomes.

5.4.2 Tip radius measurements

The development of the cutting force equation emphasizes the importance that small tip radius has on needle design. The needle that produced the lowest penetration

force (1.06 N) was a MDX coated Vectra A130 needle that has the same tip design as a steel 22 gage needle. It also has the lowest post-penetration tip radius of the plastic needles which is 14 μm. The post penetration tip radii of the Vectra A130 needles range from 14 μm as the lowest measured tip radius to 80 μm as the highest measured tip radius that allowed for penetration through the polyurethane film. The tips of the plastic needles are capable of withstanding the puncture forces without significant deformation, as the needle which had a 14 μm post-penetration tip radius had an estimated 12 μm pre-penetration tip radius. However the needles are very delicate and require careful handling to prevent damage. Exploration into alternate tip designs could prove to provide more durable needles with lower penetration forces.

The average tip radius of the SSB MT1300 needles is 52 μm with the smallest measured tip radius being 50 μm. They do not present a measurable change in tip radius between pre and post-penetration measurements. This design varies significantly from a steel hypodermic needle. Figure 60 shows a comparison of a 22 gage steel and SSB MT1300 needle.

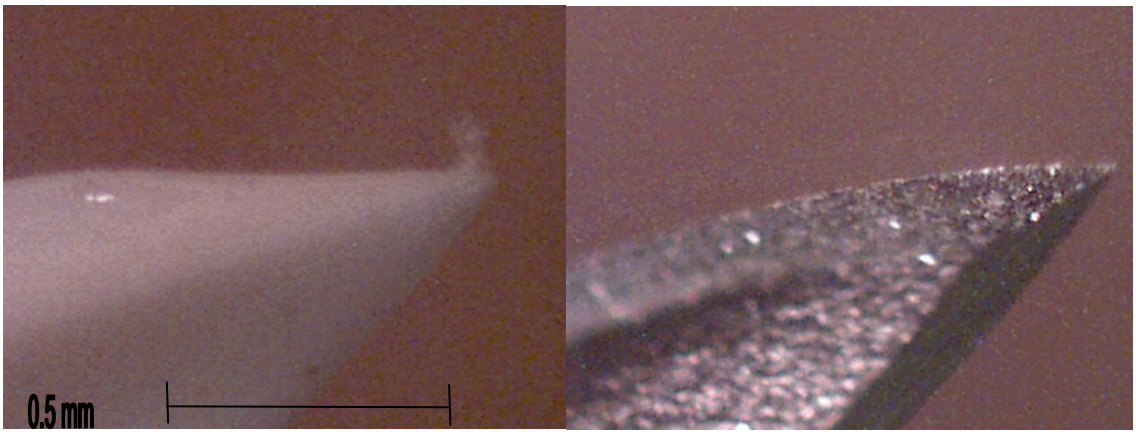

Figure 60 - Comparison of SSB MT1300 (left) and steel (right) 22 gage hypodermic needles

The tip radius of a plastic needle is essential in determining what penetration mechanism occurs. As pointed out earlier in Section 4.1.2, a noticeable change in the shape of the penetration plot occurs for the plastic needles. Some needles actually cut through the polyurethane film as a steel needle does, while others tore through the polyurethane as would a blunt object. By inspecting the Vectra A130 needle data, it was determined that this transition from cutting to tearing occurs as the needle's tip radius approaches 55 μm. The estimated tip contact area for a Vectra A130 needle with a 55 μm tip radius is $1*10^{-8}$ m^2. As pointed out in Figure 45, the slope of the line relating tip contact area to force necessary to initiate a crack is $1.14*10^{8}$. It is sensible that once the combination of the two exponents become greater than or equal to one the total force equation will become dominated by the force necessary to initiate a crack, which would translate to tearing of the film. The tip contact area of the SSB MT1300 needles is estimated to be $2.69*10^{-8}$ m^2, which is well above the largest tip contact areas of the steel needles. That explains the higher penetration forces that the SSB MT1300 needles require, and also explains why the penetration mechanism is primarily tearing.

As the penetration mechanism transitions to tearing, all of the loading is applied to the tip, which in turn requires higher tip strength. This is not the case with cutting, as the load transitions to the cannula once the initial puncture occurs. Based upon this observation, plastic needle tip designs should be limited to 50 μm as a maximum tip radius, although Equation 34 supports that even lower tip radii are essential for minimal penetration forces.

5.4.3 Coefficient of friction estimations

The frictional force equation supports the importance that coefficient of friction has on the total penetration force. It is important to understand what lubrication processes produce lower frictional forces in the plastic needles so that the methods can be further refined. The lubricants that produced the most successful penetrations in plastic needles were MDX and TriboGlide. SSB MT1300 needles that had no lubricant had a 0% penetration rate, and the same variety with silicone lubricant only produced a 10% penetration rate. The MDX and TriboGlide lubricants are compared using the equations developed for total penetration force.

For the comparison of friction coefficients between plastic needles, the tip radii of the Vectra A130 needles MDX lubricant are measured and are shown in Table 20. These measured radii and the corresponding penetration forces are put into Equation 27, the equation for estimating total penetration force, and the unknown coefficient of friction is solved for. The Vectra A130 needles with MDX coating returned the lowest average coefficient of friction, which is 0.32. This value is based on the assumption that because the tip geometry is the same as a 22 gage steel needle the cutting and deformation of the polyurethane is also the same. Therefore, as the cutting force among steel needles is assumed equal, then so are the cutting forces for plastic needles with the same tip geometry. With these assumptions made, the use of Equation 27 is considered to be valid for a comparison of Vectra A130 needle friction coefficients.

As the penetration load of a plastic needle is much higher than that of a steel needle (1.06 N for a MDX coated plastic needle versus 0.63 N for a MDX coated steel needle both with a 14 μm tip radius), it is reasonable that the estimate of coefficient of

friction is much higher for a plastic needle then for a steel needle. As mentioned earlier, the estimated coefficient for a MDX-coated A130 needle is 0.32, which is three times the coefficient of MDX on steel (0.11). This coefficient of friction is used to determine the frictional force acting on that needle, and thus the cutting force can be estimated because total force is a summation of frictional and cutting forces. This cutting force, which is assumed the same for needles of the same geometry, is subtracted from the lowest penetration forces of needles from the other two types of lubricant, silicone and TriboGlide. This isolates the frictional forces of the two lubrication types so that the unknown coefficients of friction can be estimated using Equation 22. The same is done for the SSB MT1300 needles; however no comparison to steel needles could be safely made due to the varying tip geometries. Therefore an estimated value for MDX was made based on physical observations of the needles. They felt to be well lubricated, as they were difficult to hold once the lubrication was applied, so a coefficient for excellent lubrication was chosen. This coefficient is 0.1 [45]. These calculations are summarized in Table 32.

Table 32 - Estimates of plastic needle coefficients of friction

Vectra A130	Total Force (N)	Frictional Force (N)	Estimated Coefficient of Friction
MDX	1.064	0.479	0.323
TriboGlide	1.322	0.737	0.497
Silicone	1.666	1.081	0.728
MT1300			
MDX	5.393	0.154	0.1
Silicone	7.951	2.712	1.75

From Table 32, the estimated coefficient of friction for TriboGlide on Vectra A130 is 0.5, and that of silicone on Vectra A130 is 0.73. Known values for non-metal on

non-metal coefficients of friction range from 0.12 for excellent lubrication to 0.5 for no lubrication [45], so the estimates are reasonable. The high value for the silicone-coated A130 needles suggests that increased deformation occurs as a result of poor lubrication, which would affect the equivalent cutting force assumption. In addition, the extremely high coefficient for silicone-coated SSB MT1300 needles suggests that the friction for this group of needles cannot be safely analyzed by the same method as the A130 needles. Future coefficient testing on the interaction between Vectra MT1300 and polyurethane would be beneficial in better understanding the frictional force. This was not conducted in this study because no material was available for friction testing. Regardless, reduction in coefficient of friction for a plastic needle is essential for reducing the penetration force. This could possibly be achieved through improvement of the surface finish of the plastic, as the tips of the plastic needles tended to be rougher in comparison to a steel needle. This roughness is evident in Figure 61 which compares pictures taken at 200x of a plastic and steel needle.

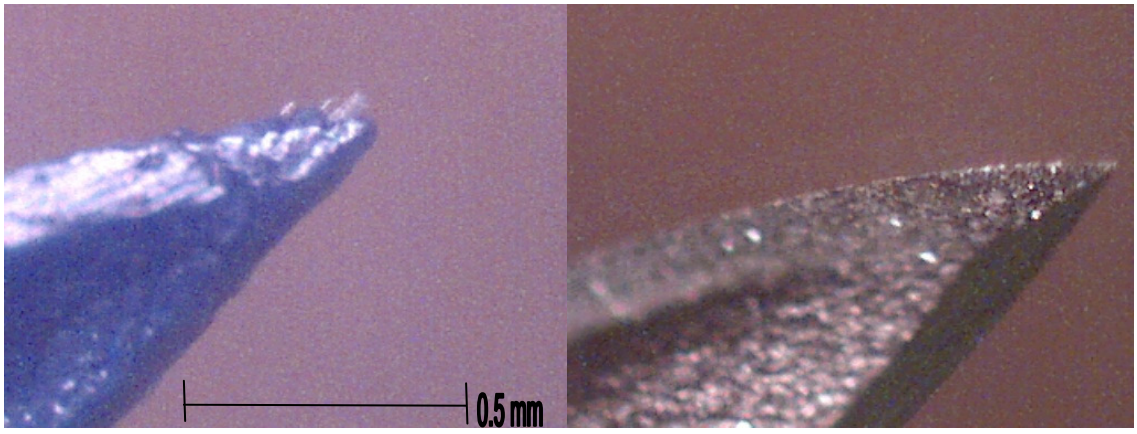

Figure 61 - Comparison of plastic and steel surface finish, 200x

5.4.4 Estimation of plastic needle penetration force

The penetration forces of the Vectra A130 needles are estimated using Equation 34. The tip radius measurements from Table 20 (Section 4.3) as well as the coefficient of friction estimated from Table 32 are used. These data, along with the actual penetration force and percent difference, are presented in Table 33.

Table 33 - Vectra A130 penetration force estimates

	Tip Radius	Actual Force (N)	Estimated Force (N)	Percent Difference
TriboGlide	21	1.382	1.416	-2.40%
	75	2.546	3.425	-34.51%
	33.5	1.341	1.680	-25.26%
	46	1.734	2.065	-19.09%
	32.5	1.626	1.654	-1.75%
	20	1.617	1.400	13.45%
	75	3.401	3.425	-0.71%
	27	1.661	1.527	8.03%
	20	1.710	1.400	18.12%
Silicone	55	2.465	2.827	-14.69%
	32.5	1.849	2.064	-11.63%
	35	2.256	2.129	5.62%
	103	5.170	5.766	-11.54%
	30	1.934	2.003	-3.56%
	15	1.672	1.742	-4.17%
	35	1.667	2.129	-27.75%
MDX	31	2.296	1.343	41.50%
	45	1.311	1.732	-32.12%
	19	1.471	1.113	24.30%
	17	1.236	1.085	12.16%
	34	1.146	1.391	-21.40%
	21	1.065	1.135	-6.61%
	19	1.444	1.105	23.45%
	67	2.624	2.501	4.69%
	30	1.762	1.281	27.28%
	73	2.152	2.729	-26.78%
	84	2.364	3.258	-37.82%
	54	2.695	1.907	29.24%
	49	2.305	1.731	24.92%
	20	1.308	1.104	15.57%

	26	1.216	1.185	2.48%

The application of Equation 34 to the plastic needle data produces reasonable results. Most values are predicted within a close range; however, there is more variation than in the steel needle estimates. This could be attributed to the lower consistency of the quality of surface finish of the plastic needles versus that of the steel needles. In addition, many of the measured tip radii are much larger than the tip radii of the steel needles. The penetration force data for the SSB MT1300 needles show that needles with large but essentially equivalent tip radii and contact areas still produce a significant level of deviation between measurements (Table 5, Section 4.1.2). This suggests that in-homogeneities in the polyurethane have more impact on penetration force as the tip contact areas and required forces increase.

Equation 31 is used to evaluate the estimated cutting force of the SSB MT1300 needles. The contact area is calculated in Section 4.3 to be $2.69*10^{-8}$ m^2. Placing this value into Equation 31 returns an estimated cutting force for the needles to be 3.58 N. This is within 3% of the average force of the MDX-coated 16 mm SSB MT1300 needles (3.48 N). This suggests that Equation 31 is a reasonable predictor of cutting force for the SSB MT1300 needles. Table 34 compares estimated total forces and actual forces for SSB MT1300 needles.

Table 34 - Estimation of SSB MT1300 penetration forces

SSB MT1300	Actual	Estimated
25.4 mm		
MDX	5.393	3.735
Silicone	7.951	6.293
16 mm		
MDX	3.486	3.735
Silicone	10.687	6.293

As can be seen in Table 34, there is variation in the force predictions. This could be explained by the fact that the friction equations are developed for steel needles. The frictional force of the SSB MT1300 needles cannot be accurately determined by Equation 22, as no coefficients of friction between MT1300 and polyurethane are known. Also, the penetration mechanism of these needles is different than that of the other needles tested so the same assumption relating cutting forces that was made for the Vectra A130 needles cannot be made. It is believed that the frictional force has a much greater impact on the penetration force for the SSB MT1300 needles than the steel needles because of the significantly larger tip contact area of the SSB MT1300 needles. This is supported by the penetration data shown in Table 5, as no bare SSB MT1300 needles produced successful penetrations, and only 25% of the silicone coated needles penetrated.

5.5 Penetration prediction

Equations are developed in Section 5.1 and Section 5.2 which predict the penetration force of a needle through polyurethane film (Equation 34) and the critical buckling load of a needle (Equation 4). It is known that the penetration force must not exceed the critical buckling load in order to have a successful penetration. This assumption and Equations 4 and 34 are used to develop a prediction of the success of a penetration, based on the tip contact area of the needle, coefficient of friction of the needle, and elastic modulus of the needle. Equation 35 represents this assumption.

$$\frac{\pi^3 E_m \left(r_o{}^4 - r^4{}_i\right)}{(KL)^2} \geq \mu E_f t_f d + \frac{G_p \left(2\pi r_t{}^2 \left(1 - \sin\frac{\alpha}{2}\right)\right)}{t_{field}} + \frac{G_c d t_f}{d_f} \tag{35}$$

From Equation 35, E_m is the elastic modulus of the needle material (Pa), r_o is the outer radius of the needle cannula (m), r_i is the inner radius of the needle cannula (m), L is the length of the needle (m), K is the effective length factor and depends upon the end conditions of the column (0.699 for a needle penetration using the current experimental setup), μ is the coefficient of friction, E_f is the elastic modulus of the material (5 MPa), t_f is the thickness of the material (m), d is the needle diameter (m), G_p is the puncture resistance (43,700 Nm/m^2), r_t is the tip radius (m), α is the tip angle, G_c is the tear resistance of the material (2870 Nm/m^2), and d_f is the distance which the tearing force is applied, which is equivalent to the distance on a needle from the tip to the end of the first bevel (m). The variables that change with needle gage are fixed to the values for 22 gage needles, as all of the plastic needles are 22 gage. This equation for 22 gage needles with a 25.4 mm cannula length is shown as Equation 36.

$$\frac{E_m}{3.091} \geq \mu E_f t_f d + \frac{G_p\left(2\pi r_t^2\left(1-\sin\frac{\alpha}{2}\right)\right)}{t_{field}} + \frac{G_c \pi d t_f}{d_f} \tag{36}$$

Coefficient of friction and tip radius are the only variables that can vary for a 22 gage needle. These two variables are plotted against one another by incrementing the needle material elastic modulus. In addition, actual penetration data for steel, GT A130 and SSB MT1300 needles are plotted to serve as a comparison. This is shown as Figure 60, which shows only successful penetrations of GT A130 needles, all steel penetrations, and all MT1300 penetrations. Figure 63 includes all Vectra A130 penetrations as well as the other groups.

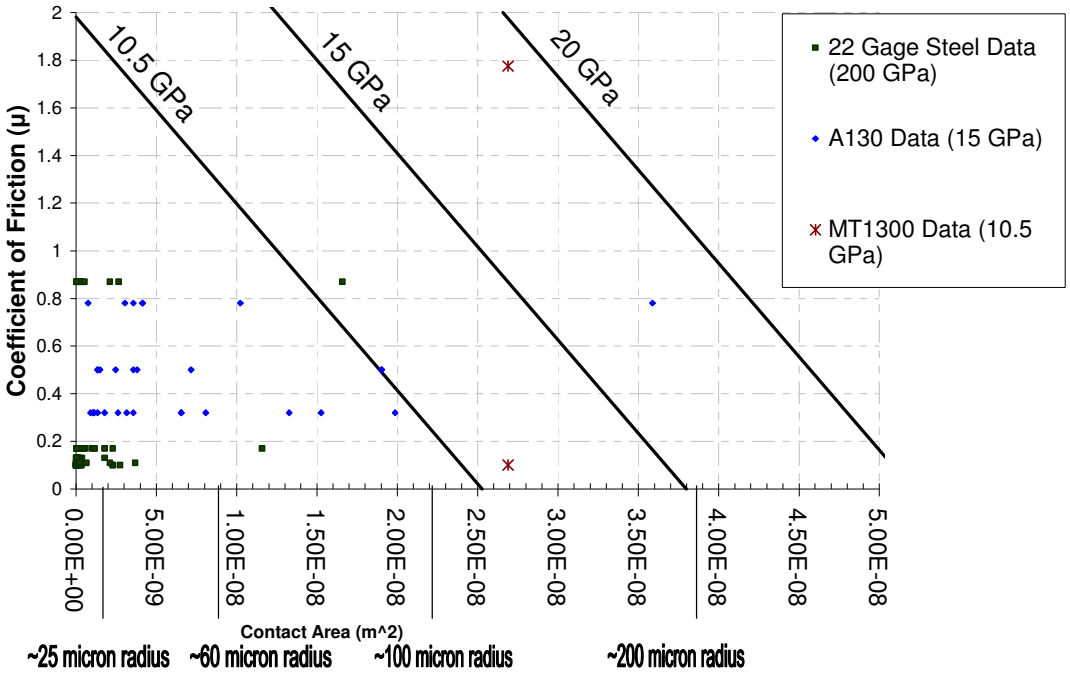

Figure 62 - Penetration prediction for 22 gage needle through polyurethane film

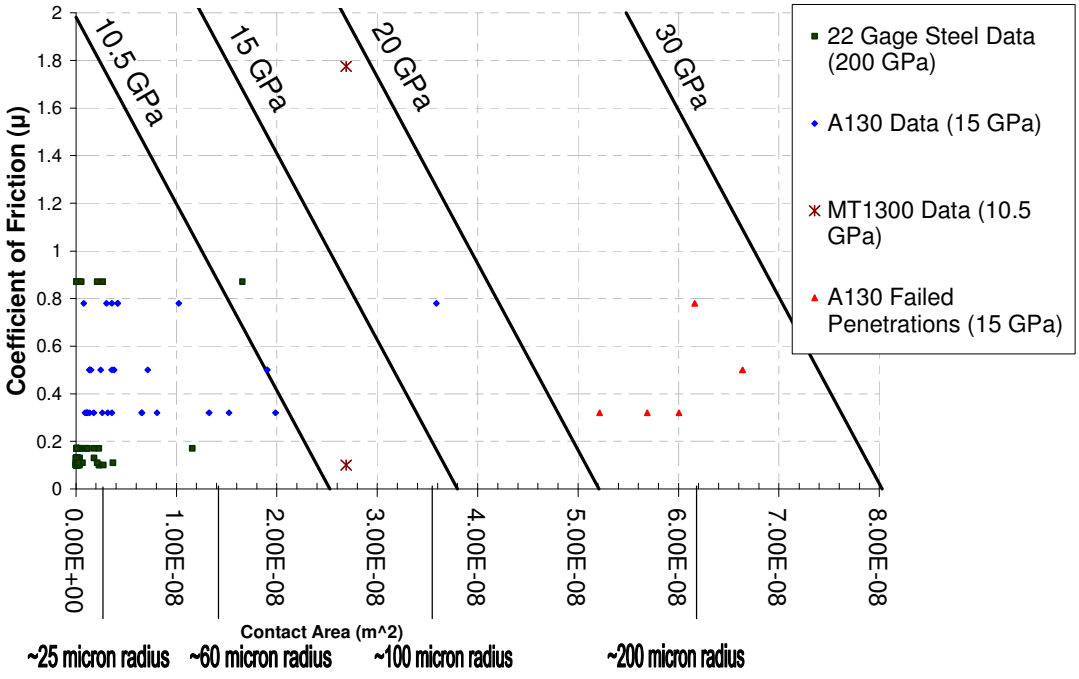

Figure 63 - Penetration prediction for 22 gage needle through polyurethane film

Figures 62 and 63 graphically predict the success of the penetration of a needle with the of a 25.4 mm 22 gage hypodermic needle based upon the variables coefficient of friction, needle tip contact area, and elastic modulus of the needle. The data point (contact area serving as the X-variable and coefficient of friction as the Y-variable) is predicted to be a combination of variables that will produce a successful penetration through polyurethane film for any needle material elastic modulus for which the variable falls beneath. The graph does not include the elastic modulus for steel (200 GPa), as it is far beyond the scale of the data. From Figure 59 it is evident that the steel and a majority of the Vectra A130 needles fall below the corresponding modulus datum. From Figure 60 it is evident that the Vectra A130 needles with tip contact areas that were too large failed to penetrate. The silicone-coated SSB MT1300 needles are well above the 10.5 GPa datum, which is supported by the fact that there was only a single successful penetration for that group. The MDX-coated SSB MT1300 needles were closer to the corresponding datum, but still were slightly above. This is reasonable, as they had an 80% success rate. In addition, the diameters of these needles are slightly larger than a steel hypodermic needle (0.75 mm versus 0.71 mm), so they will have a slightly higher critical buckling load than what is represented by the chart. An ideal 22 gage SSB MT1300 needle, however, would have a 0.71 mm diameter. It is important to note that the penetration prediction is based on an ideal situation similar to the test setup for this study. In practice, the buckling force could be influenced affected by variations in patient or injector movement. This is a possible area of further study.

5.6 Summary

This chapter summarizes the results of the testing conducted, as well as explains the relevance of the results. The development of equations relating tip radius, needle diameter, and coefficient of friction to the penetration force of a steel needle through polyurethane film are developed based upon the penetration and coefficient of friction tests. In addition, the importance that material strength has on the critical buckling loads of the tip and cannula of the needle is highlighted. A lower limit of modulus of elasticity for materials used in making plastic needles is developed based upon these results. Finally, the importance of tip radius and coefficient of friction are emphasized by the analysis of plastic needles. Conclusions developed based upon these findings are presented in Chapter 6.

CHAPTER 6

CONCLUSIONS AND RECOMENDATIONS FOR FUTURE WORK

6.1 Conclusions

The first notable portion of this study is the development of a process for manufacturing 22 gage plastic needles with geometries and penetration forces similar to steel needles. The needles are injection molded using a Sumitomo 75 ton injection molding machine. The unique portion of this process is the development of the tip insert for the molds used to form the plastic needles. The tip is formed by forging a piece of copper wire using a steel needle as the forging mold. While only tips that resembled steel hypodermic needles were manufactured, it is believed that this process could be expanded to a multitude of tip designs. The best performance of needles molded from this design was by needles made from Vectra A130 and coated in MDX lubricant. The average penetration force of this group of needles is 1.62 N, which is lower than the average penetration force for a bare 22 gage steel needle.

In addition, penetration testing consisting of five types of needle lubricant and eight different types of needles was used to draw conclusions on the affect that tip radius, needle diameter, tip angle, and coefficient of friction have on the penetration force through polyurethane film. While the penetration tests are not intended to mimic penetration force through human skin, they do allow for conclusions to be drawn about needle characteristics as well as serve as a means of comparison for plastic and steel needles. It is concluded that penetration force increases as each of these different parameters increase. Equations are developed using the results of the penetration testing

and coefficient of friction testing which relate the four variables to the maximum penetration force through polyurethane film. These equations are combined to create a single equation which predicts penetration force through polyurethane film, which is shown below.

$$F_t = \mu E_f t_f d + \frac{G_p A_t}{t_{field}} + \frac{G_c A_c}{d_f} \tag{33}$$

From Equation 33, F_t is the total penetration force in Newtons, μ is the coefficient of friction, E_f is the elastic modulus of the material (5 MPa), t_{field} is the field thickness, which is currently assumed equal to the thickness of the material (m), d is the needle diameter (m), G_c (920 Nm/m^2) is the tear resistance, A_c is the surface area of the tear (m^2), which is simplified to be equal to the diameter of the needle cannula multiplied by the film thickness, d_f is the distance over which the tearing force is applied (m), G_p (43,700 Nm/m^2) is the puncture fracture toughness of the material, and A_t is the tip contact area (m^2). Equation 33 is fully expanded into base units and shown as Equation 34.

$$F_t = \mu E_f t_f d + \frac{G_p\left(2\pi r_t^2\left(1-\sin\frac{\alpha}{2}\right)\right)}{t_{field}} + \frac{G_c d t_f}{d_f} \tag{34}$$

From Equation 34, F_t is the total penetration force in Newtons, μ is the coefficient of friction, E_f is the elastic modulus of the material (5 MPa), t_f is the thickness of the material (m), d is the needle diameter (m), G_p is the puncture resistance (43,700 Nm/m^2), r_t is the tip radius (m), α is the tip angle, G_c is the tear resistance of the material (920 Nm/m^2), and d_f is the distance which the tear force is applied, which is equivalent to the distance on a needle from the tip to the end of the first bevel (m).

Ranges for the variables tested are 0.1 – 0.87 for the coefficient of friction, 0.30 – 1.26 mm for the needle diameters, and 1.5 – 70 μm for tip radius. Equation 34 is based on data from steel hypodermic needles penetrating polyurethane film; its application toward other tip designs penetrating different media could be explored through future testing. In addition, testing at varied speeds might further explain the penetration problem.

Buckling tests are also conducted to determine limits for the elastic modulus of materials used for making plastic needles. Physical tests are conducted and buckling equations are solved to serve as a validation of finite element models. The finite element models separate the requirements for tip strength and cannula strength. It is determined that based upon a 22 gage steel hypodermic needle the tip strength is more critical than the cannula strength, as it requires a higher material elastic modulus to prevent failure. The tip model is used to develop a linear equation relating critical tip load to modulus of elasticity. Using the average puncture force derived from the needle penetration plots, it is determined that the minimum useful elastic modulus is 8 GPa. The buckling and penetration data are used develop a chart which predicts the success of a 25.4 mm 22 gage needle penetration through polyurethane film based on material strength, tip contact area, and coefficient of friction. This chart is shown as Figure 54 in Section 5.5.

Finally, multiple penetration tests are conducted to determine the affect that repeated penetrations have on penetration force. It is determined that the penetration force tends to decrease after multiple penetrations. It is concluded that because the steel needles have a significantly higher elastic modulus than the polyurethane, the tips will not deform as a result of penetration. The more likely affect on penetration force is mishandling of the needles between penetrations.

All of the testing can be used to draw conclusions about plastic needle design. The two most important ways of minimizing the penetration force of plastic needles is to minimize the tip radius and minimize the coefficient of friction. The effect of diameter is noted; however this is a variable that cannot be changed. In addition, it is important handle the needles carefully as plastic needles tend be quite delicate. These conclusions are used to develop suggestions on future areas of study. All conclusions are summarized in Table 35.

Table 35 - Summary of conclusions for plastic needles

Optimal Lubricant	MDX
Lowest Average Penetration Forces	
22 gage steel: MDX	0.60 N
22 gage plastic: Vectra A130 MDX	1.62 N
Minimum Penetration Force	
22 gage steel: MDX	0.55 N
22 gage plastic: Vectra A130 MDX	1.06 N
Minimum Material Elastic Modulus	8.0 GPa

6.2 Recommendations for future work

One primary focus for future work should be the implementation of a hollow core in the Vectra A130 needles. A hollow core is a necessity for a hypodermic needle. Every aspect of the tip of the existing design is the same as a hollow needle. The variation does not occur until the tip transitions to the cannula, therefore the tip strength should not be affected by the addition of a hollow core. It was concluded that the tip is the critical region for failure so an addition of a hollow core should not affect the penetration success of the design.

In addition, different tip designs should be explored. It is concluded that a small tip radius is a necessity for minimal penetration force. The current design produced small tip radii; however it has room for improvement. Also, exploring other aspects of the tip such as thickness, bevel angle, and shape could result in lower penetration forces. Based upon the findings of this study, an optimal needle plastic needle tip mimics a steel needle tip in geometry and has a tip radius as close to 0 μm as possible. The needles manufactured by SS&B technology have a promising design; however it is difficult to compare the tip design with the other needles tested because the tip radius is significantly higher than the other designs. This resulted in significantly higher penetration forces. This design could be significantly improved by reducing the tip radius, as this is the variable that has the most influence in penetration force.

The Georgia Tech manufacturing process of the needles could be improved upon. One alteration that is believed to be beneficial to the manufacturing process is the addition of a heating element to the mold. Increasing the mold temperature would create a less drastic change in temperature between the melt and the mold, which would allow for increased flow into the mold. This could allow more accurate replication of the details of the mold, as well as a smoother surface finish. Also it would increase the amount of resins that could be tested and used for plastic needles. Materials such as Ixef 1022 have promising material properties, as the elastic modulus is 20 GPa which is 33% higher than Vectra A130; however needles made of this resin were not able to be created due to the lack of flow of the plastic in the mold. Materials with the strongest material properties are better than those with weaker properties, and further decisions on material selection should be based upon this. At the same time, the material must be flexible

enough not to break in the event of eccentric axial loading. An ideal material is a material that is as strong as possible, yet maintains sufficient flexibility.

The coefficient of friction between the plastic needles and the material being penetrated can be reduced. Possibilities for lowering the friction coefficient include producing a smoother surface finish in the needles and exploring the lubrication process. The needle surface finish can be improved by improving the molds. Polishing the molds to a mirror-like finish would increase the surface finish of the needles. Heating the molds would also improve the flow characteristics of the plastic and allow for heightened replication of the mold cavity. An ideal lubricant is one that minimizes the coefficient of friction. At this point of the study, the MDX lubricant is an ideal choice.

In addition to the alteration of needle design and lubrication, the testing method could be expanded to include biological materials or other suitable skin mimics. One study explores the suitability of pig skin and artificial chamois for skin simulants during penetration testing [46]. Animal organs or cuts of meat such as chicken breasts or beef steaks would also be effective test media. These materials could be expanded to the study of plastic hypodermic needle testing. The addition of different materials could be used to further explain the equations developed for cutting and frictional force to include the effect of the difference in material properties of the objects being penetrated. The actual effectiveness of plastic hypodermic needles can be determined by human analogues however the best judge of effectiveness is testing in humans, which would be the ideal test specimen.

All of these improvements would further the knowledge on hypodermic needle penetration, as well as increase the effectiveness of plastic hypodermic needles. The next

step in the design process should be the exploration of alternate tip designs. The process developed for making the molds can be easily expanded to include other designs by simply replacing the steel needle, which is the current forging mold, with a wire that is machined to the specifications of the new design. This could be easily achieved, as making a positive replication of a needle is significantly less difficult than trying to machine the inverse pattern. Therefore multiple designs could be attempted without a significant time investment.

With sufficient effort the necessary changes to plastic needles can be made, and they will serve as a suitable substitute for steel needles. The implementation of plastic hypodermic needles into society is an attainable goal that would prove to be beneficial for millions.

APPENDIX A – LUBRICATION METHODS

MDX4-4159 Dispersion Solution Application

1. Clean needle by wiping with isopropyl alcohol*

2. Allow alcohol to evaporate from surface of needle

3. Dilute MDX4-4159 to desired silicone concentration. The solution is bottled at a 50% silicone concentration. To dilute to 5% silicone add 1 ml MDX4-4159 to 6.3 ml mineral spirits and 2.7 ml isopropyl alcohol

4. Wipe lubricant onto the needle using a lent-free cloth*

5. Place needle in oven. Avoid contacting the needle cannula of tip to any surface

6. Bake in oven for three days at 70°C

7. Allow needles to cool, and then remove from oven

8. Test needle as presctibed

Silicone Fluid Application

1. Dip needle into silicone fluid then remove

2. Allow excess fluid to drip off

3. Wipe remaining fluid off needle using a lent-free cloth*

4. Test needle as prescribed

* It is important to only wipe the needles in the direction going from the hub to the tip. Doing so prevents damage to the needle and to your fingers.

APPENDIX B – NEEDLE TESTING PROTOCOL

Single Needle Testing Protocol

1) Attach the 25 N load cell to the crosshead of Instron Model 33R4466.

2) Position and secure the polyurethane clamping device directly beneath and perpendicular to the needle mount on the load cell making sure that the center of the 1 inch diameter hole aligns with the needle.

3) Attach the needle so it is vertically suspended from the load cell.

4) Secure the polyurethane skin mimic within the aluminum clamp which is secured to the base of the Instron.

5) Run the Instron “needle penetration” program, in a compression setup, at a speed of 100 mm/min.

6) Analyze the results, specifically the penetration and friction forces acting on the needle.

7) For buckling tests, align the needle with an aluminum plate in place of the skin mimic.

APPENDIX C – EXPERIMENTAL DATA

*Yellow or red filled cell represents failed penetration					
Compiled Data	**18 Gage**				
Needle	As-Received	TriboGlide	Silicone	MDX	Bare
1	0.94195	1.2458	1.18606	0.99815	3.10401
2	0.95488	1.79942221	1.17853	0.93437	2.96325
3	0.92145	0.96997575	1.27519	0.9068	3.01675
4	0.94366	1.10540559	1.03817	0.91055	3.18021
5	1.00335	0.9051538	1.22922	0.95354	2.95134
6	0.93925	1.01145788	1.18126	0.8545	2.82399
7	0.88734	1.42412171	1.12754	0.9441	2.96106
8	0.85599	1.38293378	1.08646	0.92959	2.87303
9	0.87464	1.00272996	1.1337	0.93498	2.97249
10	0.86142	0.92878782	1.15549	0.96664	2.99219
11	0.96314	0	1.20072	0.94276	2.98825
12	1.01264	0	1.12987	0.9687	3.04608
13	0.87947	0	1.07711	0.93143	2.79893
14	0.98462	0	1.09372	0.86577	2.92029
15	0.99018	0	1.09468	0.93551	2.96811
16	0.88832	0	1.15696	1.00118	2.797
17	1.01066	0	1.12738	0.97605	2.77101
18	0.93391	0	1.18451	0.83649	2.88606
19	0.84867	0	1.20755	0.96337	2.8749
20	0.85135	0	1.26562	0.9325	2.98132
21	0.82025	0	0	0	2.84644
22	0.91635	0	0	0	2.86544
23	0.90908	0	0	0	2.87907
24	0.86054	0	0	0	2.85078
25	1.14793	0	0	0	2.95656
26	0.80169	0	0	0	2.94953
27	0.91554	0	0	0	2.90993
28	0.89229	0	0	0	3.01857
29	0.86614	0	0	0	2.91954
30	0.91529	0	0	0	2.74822

Compiled Data	**22 Gage Myco 1st Penetration**				
Needle	As-received	TriboGlide	Silicone	MDX	Bare
1	0.73926	0.77989	0.84216	0.67333	1.74227
2	0.65645	0.72393	0.837	0.69302	1.71737
3	0.5332	0.80896	0.91529	0.61402	1.88258
4	0.56978	0.75658	0.94757	0.55826	1.85464
5	0.61516	0.70395	0.89971	0.6611	1.8712
6	0.56867	0.68875	0.86941	0.59415	1.93629
7	0.64834	0.74751	0.85513	0.60586	1.65338
8	0.71149	0.75964	0.99986	0.63605	1.77896
9	0.63014	0.78509	0.81772	0.58307	1.76006
10	0.59437	0.7846	0.82088	0.5536	1.88097
11	0.94271	0.81526	0.9166	0.7082	1.75828
12	0	0.83591	0.85907	0.61574	0
13	0	0.7675	0.83683	0.62003	0
14	0	0.76399	0.88716	0.61683	0
15	0	0.72743	0.8867	0.65249	0
16	0	0	0.82351	0.58402	0
17	0	0	0.93422	0.64897	0
18	0	0	0.81382	0.6154	0
19	0	0	0.89372	0.57968	0
20	0	0	1.0532	0.62065	0
21	0	0	0	0	0
22	0	0	0	0	0
23	0	0	0	0	0
24	0	0	0	0	0
25	0	0	0	0	0
26	0	0	0	0	0
27	0	0	0	0	0
28	0	0	0	0	0
29	0	0	0	0	0
30	0	0	0	0	0

Compiled Data	**22 Gage Myco 2nd Penetration**				
Needle	As-received	TriboGlide	Silicone	MDX	Bare
1	0.72424	0.73865	0.80967	0.70498	1.77266
2	0.66842	0.65967	0.79499	0.67765	1.65587
3	0.58212	0.75275	0.88775	0.62522	1.85593
4	0.57362	0.75162	0.86714	0.55876	1.74121
5	0.58699	0.64759	0.83356	0.63976	1.71535
6	0.53833	0.83144	0.7914	0.58808	1.89925
7	0.61272	0.69717	0.81062	0.63788	1.60315
8	0.73386	0.72373	0.98525	0.64924	1.80739
9	0.61171	0.75037	0.82666	0.56198	1.72725
10	0.61217	0.7463	0.83684	0.56189	1.90068
11	0.9245	0.80245	0.82893	0.69979	1.65673
12		0.80461	0.78409	0.6	
13		0.75091	0.79045	0.67982	
14	0	0.73134	0.81079	0.63901	0
15	0	0.71465	0.81113	0.70407	0
16	0		0.78196	0.54356	0
17	0		0.89843	0.63948	0
18	0	0	0.77551	0.61414	0
19	0	0	0.8612	0.57849	0
20	0	0	2.32167	0.67669	0
21	0	0	0	0	0
22	0	0	0	0	0
23	0	0	0	0	0
24	0	0	0	0	0
25	0	0	0	0	0
26	0	0	0	0	0
27	0	0	0	0	0
28	0	0	0	0	0
29	0	0	0	0	0
30	0	0	0	0	0

Compiled Data	**22 Gage Myco 3rd Penetration**				
Needle	As-received	TriboGlide	Silicone	MDX	Bare
1	0.71508	0.7219	0.77179	0.71687	1.73275
2	0.67567	0.68595	0.75359	0.70621	1.66902
3	0.56855	0.75822	0.82304	0.66727	1.88321
4	0.59629	0.75536	0.83722	0.57248	1.76779
5	0.59916	0.64156	0.80633	0.66425	1.73192
6	0.52982	0.87313	0.76973	0.62809	1.89537
7	0.55644	0.66692	0.73382	0.6593	1.67016
8	0.74428	0.72317	0.87776	0.6576	1.75711
9	0.59994	0.72899	0.74388	0.59114	1.75411
10	0.6002	0.74687	0.80486	0.58631	3.53059
11	1.00317	0.82104	0.80917	0.73849	1.75753
12		0.73508	0.75456	0.6227	
13		0.74308	0.75414	0.70405	
14	0	0.71984	0.81165	0.63852	0
15	0	0.71499	0.80915	0.68361	0
16	0		1.02593	0.56029	0
17	0		0.84596	0.65629	0
18	0	0	0.75892	0.60201	0
19	0	0	0.85736	0.59328	0
20	0	0	2.1984	0.68241	0
21	0	0	0	0	0
22	0	0	0	0	0
23	0	0	0	0	0
24	0	0	0	0	0
25	0	0	0	0	0
26	0	0	0	0	0
27	0	0	0	0	0
28	0	0	0	0	0
29	0	0	0	0	0
30	0	0	0	0	0

Compiled Data	**22 Gage Inviro Medical**				
Needle	As-received	TriboGlide	Silicone	MDX	Bare
1	0.562	0.697743148	0.92062	0.66286	1.83049
2	0.69589	0.912410716	1.01403	0.60485	1.85391
3	0.74078	0.654103555	0.96728	0.65215	1.82651
4	0.65567	0.646258235	0.91008	0.54424	1.77713
5	0.60605	0.69038816	0.88998	0.59615	1.8745
6	0.69373	0.714806719	0.85774	0.58728	1.71337
7	0.98898	0.67891438	0.81431	0.54484	1.59493
8	0.81024	0.686269367	0.86326	0.63684	1.53732
9	0.73125	0.672441991	0.90225	0.5963	1.78898
10	0.8722	0.629488864	0.89929	0.61355	1.78138
11	0.54081	0	0.88082	0.59499	1.69535
12	0.61037	0	0.84674	0.59504	1.77827
13	0.77176	0	0.82215	0.64622	1.59267
14	0.5823	0	0.88327	0.66092	1.81411
15	0.71537	0	0.83367	0.55196	1.78341
16	0.58253	0	0.82159	0.61018	1.78291
17	0.68978	0	0.7433	0.63525	1.78838
18	0.73028	0	0.82264	0.64102	1.85651
19	0.6923	0	0.84598	0.69232	1.73691
20	0.57595	0	0.90425	0.73388	1.75121
21	0.60288	0	0.97206	0	1.77647
22	0.57475	0	0.91663	0	1.69779
23	0.7365	0	0.82789	0	1.81747
24	0.56864	0	0.88027	0	1.80141
25	0.65956	0	0.83049	0	1.77748
26	0.72833	0	0.88624	0	1.84648
27	0.75703	0	0.91584	0	1.7352
28	0.57481	0	0.88803	0	1.6722
29	0.59306	0	0.79916	0	1.83676
30	0.8448	0	0.93204	0	1.80177

	Vectra SSB MT1300 16 mm MDX Hollow	Vectra SSB MT1300 16 mm MDX Solid	Vectra A130 MDX
	Max Load (N)	Max Load 1 (N)	Max Load (N)
Needle	(Through Polyurethane)	(Through Polyurethane)	(Through Polyurethane)
1	3.93233	3.50879	failed to penetrate
2	3.67898	4.8317	2.29588
3	3.30765	3.01215	1.31129
4	3.21544	Failed to Penetrate	1.4706
5	4.57426	4.73658	1.23559
6	2.72655	2.42467	1.14593
7	3.40592	3.71401	1.06488
8	2.99653	4.78266	1.44394
9	3.65659	2.65876	2.62366
10	3.37007	4.33633	1.7617
11			2.15214
12			2.36369
13			2.69483
14			2.30539
15			1.30775
16			1.21558
17			failed to penetrate
18			failed to penetrate

	Vectra A130 Triboglide Solvent	Vectra A130 Triboglide No Solvent	Vectra A130 Non Plasma
	Max Load 1 (N)	Max Load 1 (N)	Max Load 1 (N)
Needle	(Through Polyurethane)	(Through Polyurethane)	(Through Polyurethane)
1	1.38236	1.32217	2.46474
2	2.54619	1.70323	1.84873
3	1.34092	Failed to Penetrate	2.25585
4	1.73385	1.76613	5.16979
5	1.62566	1.40666	1.9344
6	1.61715	1.78704	Failed to Penetrate
7	3.4006	1.70824	1.67183
8	Failed to Penetrate	1.42158	1.66666
9	1.66058	2.63917	
10	1.70954	1.89562	
11			
12			
13			
14			
15			
16			
17			
18			

	MT 1300 1" MDX	MT 1300 16 mm MDX	MT 1300 1" Silicone
	Max Load 1 (N)	Max Load 1 (N)	Max Load 1 (N)
Needle	(Through Polyurethane)	(Through Polyurethane)	(Through Polyurethane)
1	5.35893	5.54787	Failed to Penetrate
2	5.59886	2.94	Failed to Penetrate
3	Failed to Penetrate	5.8281	Failed to Penetrate
4	Failed to Penetrate	5.61612	Failed to Penetrate
5	6.97505	6.43824	Failed to Penetrate
6	4.81567	4.61487	Failed to Penetrate
7	7.44592	4.0499	Failed to Penetrate
8	3.64757	3.33221	7.95103
9	4.03608	7.14355	Failed to Penetrate
10	5.26507		Failed to Penetrate
11			
12			
13			
14			
15			
16			
17			
18			

	MT 1300 16 mm Silicone	MT 1300 1" Bare	MT 1300 16 mm Bare
	Max Load 1 (N)	Max Load 1 (N)	Max Load 1 (N)
Needle	(Through Polyurethane)	(Through Polyurethane)	(Through Polyurethane)
1	11.7075	Failed to Penetrate	Failed to Penetrate
2	Failed to Penetrate	Failed to Penetrate	Failed to Penetrate
3	10.38605	Failed to Penetrate	Failed to Penetrate
4	Failed to Penetrate	Failed to Penetrate	Failed to Penetrate
5	Failed to Penetrate	Failed to Penetrate	Failed to Penetrate
6	Failed to Penetrate	Failed to Penetrate	Failed to Penetrate
7	Failed to Penetrate	Failed to Penetrate	Failed to Penetrate
8	10.92844	Failed to Penetrate	Failed to Penetrate
9	Failed to Penetrate	Failed to Penetrate	Failed to Penetrate
10	9.72406	Failed to Penetrate	Failed to Penetrate
11			
12			
13			
14			
15			
16			
17			
18			

Compiled Data	**26 Gage**				
Needle	As-received	Teflon	Silicone	MDX	Bare
1	0.59053	0.57892	0.82491	0.58263	1.19284
2	0.59848	0.55829	0.87373	0.49262	1.24343
3	0.57717	1.39818	0.68066	0.48991	1.36493
4	0.5418	0.56511	0.74067	0.54865	1.3441
5	0.4812	0.59705	0.78307	0.50031	1.15772
6	0.50416	0.66123	0.73422	0.54303	1.36592
7	0.46116	0.59883	0.74745	0.50742	1.28465
8	0.50543	0.58689	0.76611	0.4218	1.25149
9	0.51554	0.5393	0.73128	0.69303	1.36678
10	0.5188	0.60035	0.74235	0.53931	1.22726
11	0.54971	0.62662	0.72649	0.87482	1.28796
12	0.531271	0.5718	0.72008	0.48309	1.2806436
13	0.044514	0.57786	0.83642	0.56823	0.073346
14	0	0.57106	0.76623	0.50496	0
15	0	0.59	0.70112	0.48519	0
16	0	0.587379	0.82751	0.46859	0
17	0	0.030024	0.78654	0.50752	0
18	0	0	0.78636	0.47644	0
19	0	0	0.7297	0.52074	0
20	0	0	0.77025	0.72548	0
21	0	0	0	0	0
22	0	0	0	0	0
23	0	0	0	0	0
24	0	0	0	0	0
25	0	0	0	0	0
26	0	0	0	0	0
27	0	0	0	0	0
28	0	0	0	0	0
29	0	0	0	0	0
30	0	0	0	0	0

Compiled Data	**30 Gage**				
Needle	As-received	TriboGlide	Silicone	MDX	Bare
1	0.56225	0.44669291	0.92555	0.38126	0.99882
2	0.52634	0.4493407	0.64054	0.41265	0.97428
3	0.59456	0.39363893	0.64201	0.42207	0.82711
4	0.52164	0.46875787	0.63635	0.38084	1.03203
5	0.46311	0.47915292	0.65903	0.37034	0.95685
6	0.5268	0.47405346	0.55816	0.36056	0.94836
7	0.51674	0.4499291	0.5567	0.37182	0.95004
8	0.53248	0.4724844	0.62005	0.40848	1.03692
9	0.52043	0.49651069	0.57252	0.37033	1.00167
10	0.54251	0.88426563	0.5877	0.42633	0.93288
11	0.5213		0.59647	0.34181	0.91092
12	0.50995		0.62574	0.4401	1.06794
13	0.50077		0.53288	0.37163	0.88171
14	0.5173		0.60082	0.41469	0.94387
15	0.46034		0.54253	0.33929	0.98757
16	0.50879		0.62914	0.3856	0.80646
17	0.49951		0.56909	0.36998	0.85116
18	0.52658		0.62245	0.38473	0.92521
19	0.49396		0.59885	0.34983	0.9422
20	0.51556		0.57862	0.34881	0.97193
21	0.49668				1.02341
22	0.50944				0.96096
23	0.48273				1.02966
24	0.51272				1.00384
25	0.51028				0.97618
26	0.50176				0.96557
27	0.47743				0.87378
28	0.46942				0.89899
29	0.48947				0.95958
30	0.53229				1.02432

REFERENCES

[1] Hutin, Y.J.F. and R.T. Chen, Injection safety: a global challenge, *Bulletin of the World Health Organization*, 1999, 77(10), pp. 787-788.

[2] Simonsen, L. et al, Unsafe injections in the developing world and transmission of bloodborne pathogens: a review, *Bulletin of the World Health Organization*, 1999, 77(10), pp. 789-800.

[3] Kane, A et al, Transmission of hepatitis B, hepatitis c and human immunodeficiency viruses through unsafe injections in the developing world: model-based regional estimates, *Bulletin of the World Health Organization*, 1999, 77(10) pp. 801-807.

[4] Hauri, Anja M et al, The global burden of disease attributable to contaminated injections given in health care settings, *International Journal of STD & AIDS*, 2004, 15, pp. 7-16.

[5] Miller, M.A. and E. Pisani, The cost of unsafe injections, *Bulletin of the World Health Organization*, 1999, 77(10), pg. 808.

[6] ISO 7864:1993(E) Sterile Hypodermic Needles for Single Use.

[7] Ekwueme, Donatus U. et al, Model based risks of disease transmission and economic costs of seven injection devices in sub-Saharan Africa, *Bulletin of the World Health Organization*, 2002, 80(11), pp. 859-870.

[8] Brown, Phyllida, Putting injection waste out of harm's way, *GAVI Immunization Focus*, March 2002, pp. 6-8.

[9] Mujeeb, Syed Abdul et al, Recycling of Injection Equipment in Pakistan. *Infection Control and Hospital Epidemiology*, 2003, 24:2, pp.145-146.

[10] Tamplin, S.A. et al, Issues and options for the safe destruction and disposal of used injection materials, *Waste Management*, 2005, 25, pp. 655-665.

[11] Busillo, Eric, Characterization of Plastic Hypodermic Needles, Masters of Science Thesis, Georgia Institute of Technology, December 2008.

[12] Kim, H. and J.S. Colton, Fabrication and Analysis of Plastic Hypodermic Needles, *SPE-ANTEC Tech. Papers*, 2004, 3727.

[13] Kim, H. and J.S. Colton, Fabrication and Analysis of Plastic Hypodermic Needles, *J. Medical Eng. and Tech.,* 2005, 29(4), pp. 181-186.

[14] ISO 9626: 1991(E) Stainless Steel Tubing for Manufacture of Medical Devices.

[15] Dow Corning, Dow Corning MDX4-4159, 50% Medical Grade Dispersion, Frequently Asked Questions, 52-1039-01. 2002.

[16] TriboGlide Silicone Free Research Systems, TriboFilm Research Inc., http://www.triboglide.com/ February 10, 2009.

[17] Stevens, John F., Smith, Trevor G., and Bartlett, Jack H. US Patent 5620639. 1997.

[18] Small Parts, Inc., *Niagara Cutter 059872 Ball End Mill.028 Flute, 1 1/2" L, 1/8" Shank, Carbide, 4 Flts,* 2008, http://www.smallparts.com/Niagara-Cutter-059872-Mill-028-Carbide/dp/B001DNJUP4?ie=UTF8&qid=1234191480&pf_rd_r=0Y31W294CH860X3FSD6C&pf_rd_p=467590031&pf_rd_i=0&sr=1-1&pf_rd_s=center-3&pf_rd_m=AIUBT5HP6PMAF&pf_rd_t=301. February 10, 2009.

[19] Hibbeler, R.C., *Mechanics of Materials 5th edition*, Pearson Education, Inc., Upper Saddle River, NJ, 2003, pp. 649-659.

[20] Solvay Advanced Polymers L.L.C., *IXEF polyarylamide data sheet*, 2005, http://www.solvayadvancedpolymers.com/static/wma/pdf/9/7/0/2/IXEF_1022.pdf. February 16, 2009.

[21] Solvay Advanced Polymers L.L.C., *KetaSpire polyetheretherketone data sheet*, 2005, http://www.solvayadvancedpolymers.com/static/wma/pdf/8/6/7/4/KetaSpire_KT880CF30.pdf., February 16, 2009.

[22] Celanese Ticona – A business of Celanese, *Product Data Sheets*, 2005, http://tools.ticona.com/tools/mcbasei/product-tools.php?sPolymer=&sProduct=. February 17, 2009.

[23] Sabic Innovative Plastics IP BV, *Lexan Resin 3413R Product Data Sheet*, 2008, http://www.matweb.com/search/datasheet.aspx?matguid=2ac88f3836144bb293630db0dbfd54bf&ckck=1. February 17, 2009.

[24] Unigel Plásticos, *Durolon VR-2500 Product Data Sheet,* 2008, http://www.ides.com/grades/ds/E23368.htm. February 17, 2009.

[25] TOPAS Advanced Polymers, *Processing Conditions for Injection Molding TOPAS 8007X10*, 2006, http://www.topas.com/tds_8007x10_e-3.pdf. February 10, 2009.

[26] Ides, *Polystyrene Typical Properties*, 2009, http://www.ides.com/generics/PS/PS_typical_properties.htm February 20, 2009.

[27] Johnson L, Olley P, Coates PD, Gas assisted injection moulding - Finite element modelling and experimental validation, *Plastics Rubber and Composites*, 2000, 29:1, pp. 31-37.

[28] DIN 13097 (09/2002) Medical Needles – Point Designs and Testing.

[29] Mak, A.F.T. and M. Zhang, Skin and Muscle, *Handbook of Biomaterial Properties,* Chapman & Hall, London, 1998, ISBN 0 412 60330 6.

[30] Hendriks, F.M. et al, A numerical experimental method to characterize the non-linear mechanical behaviour of human skin, *Skin Research and Technology,* 2003, 9, pp. 274-283.

[31] Test Protocol – Insulin Needle Penetration, Sherwood Medical, St. Louis, MO.

[32] Wu, Jeff, Hamada, Michael, *Experiments: Planning, Analysis, and Parameter Design Optimization,* Jon Wiley & Sons, Inc, New York, NY, 2000, pp. 1-14.

[33] Okamura, Allison et al, Force Modeling for Needle Insertion Into Soft Tissue, *IEEE Transactions on Biomedical Engineering*, 2004, 10, pp. 1707-1716.

[34] Abolhassani, Kiki et al, Needle Insertion into soft tissue: A survey, *Medical Engineering & Physics*, 2007, 29, pp. 413-431.

[35] Kataoka, Hiroyuki et al, Measurement of the Tip and Friction Force Acting on a Needle During Penetration, National Institute of Advanced Industrial Science and Technology, Ibaraki, Japan.

[36] Davis, Shan P. et al, Insertion of microneedles into skin: measurement and prediction of insertion force and needle fracture force, *Journal of Biomechanics*, 2004, 37, pp. 1155-1163.

[37] Barbé, L. et al, Needle insertions modeling: Identifiability and limitations, *Biomedical Signal Processing and Control*, 2007, 2, pp. 191-198.

[38] Marchal Y. et al, Characterization of the fracture toughness of rubber-toughened polypropylene thin plates, *POLYMER ENGINEERING AND SCIENCE,* 1998, 38:12, pp. 2063-2071.

[39] Kearney, A.V. et al, Pore size scaling for enhanced fracture resistance of nanoporous polymer thin films, *Acta Materialia*, 2008, 56:20, pp. 5946-5953.

[40] Anderson, T.L., *Fracture Mechanics Fundamentals and Applications*, CRC Press, New York, NY, 1995, pg. 441.

[41] Tielking, J.T., A Fracture Toughness Test for Polymer Film, *Polymer Testing*, 1993, 12, pp. 207 – 220.

[42] Shergold, Oliver A. and Fleck, Norman A., Mechanisms of deep penetration of soft solids, with application to the injection and wounding of skin, *Proc. R. Soc. Lond.* A, 2004, 460, pp. 3042, 3048–3050.

[43] Shergold, Oliver A., Fleck, Norman A., and Radford, Darren, The uniaxial stress versus strain response of pig skin and silicone rubber at low and high strain rates, *International Journal of Impact Engineering*, 2006, 32(9), pg. 1395.

[44] Shergold, Oliver A. and Fleck, Norman A., Experimental Investigation Into the Deep Penetration of Soft Solids by Sharp and Blunt Punches, With Application to the Piercing of Skin, *Journal of Biomechanical Engineering*, 2005, 127(5), pg. 839.

[45] Rabinowicz, Ernest, *Friction and Wear of Materials*, John Wiley & Sons, Inc., New York, NY, 1995, pg. 118.

[46] Ankersen, J. et al, Puncture resistance and tensile strength of skin simulants, Proc Instn Mech Engrs, 1999, 213, part H.